Simulations and parameterisation of volcanic plumes observed in La Reunion Island, Piton de la Fournaise

Sandra Gurwinder Sivia

THÈSE

En vue de l'obtention du

DOCTORAT DE L'UNIVERSITÉ DE TOULOUSE

Délivré par : *l'Université Toulouse 3 Paul Sabatier (UT3 Paul Sabatier)*

Présentée et soutenue le *13/11/2014* **par :**

Sandra Gurwinder Sivia

Simulations and parameterisation of volcanic plumes observed in La Réunion Island, Piton de la Fournaise

---

JURY

Frank Roux	Président du Jury
Peter Bechtold	Rapporteur
Frédéric Hourdin	Rapporteur
Edouard Kaminski	Rapporteur
Andrea DiMuro	Examinateur
Céline Mari	Directrice de thèse
François Gheusi	Co-Directeur de thèse

École doctorale et spécialité :
SDU2E : Océan, Atmosphère et Surfaces Continentales
Unité de Recherche :
Laboratoire d'Aérologie (UMR 5560)
Directeur(s) de Thèse :
François Gheusi et *Céline Mari*
Rapporteurs :
Peter Bechtold, *Frédéric Hourdin* et *Edouard Kaminski*

Acknowledgements

Firstly, I want to thank both my supervisors, Céline Mari and François Gheusi. Thank you very much for supporting me and guiding me during my research. Thank you for being very patient and always receiving me with a smile! Your support, feedback, corrections, motivation and teacher-like approach are invaluable. I also thank Pierre Tulet and Andrea DiMuro for the opportunity to visit this famous Island. Thank you for always replying to my Emails even if the questions I asked were sometimes repetitive.

I would also like to thank Juan Escobar and Didier Gazen, always available to answer my many questions with patience and kindness. A big thank you to Soline Bielli for helping me with the complexities of NCL even when you moved far far away! I thank Frank Roux and everyone at Laboratoire dAérologie for welcoming me so warmly. Thank you very much to the jury members for agreeing to delve into my manuscript and for taking their time to provide very useful insight and comments on work undertaken during this PhD.

Flore Tocquer and Alexandre Berger, merci beaucoup for listening me moan when 'my' Meso-NH was not 'working'. Flore, I can not thank you enough for always remaining positive (well, for the most of it) and it was an immense pleasure to share the office with you, I wouldn't have it any other way ;) !

To say some final words, I want to thank my family. My parents and my sisters for helping their always 'broke' elder daughter/sister, for all your love and for feeling proud of all my achievements thus far! My 'in-laws'

for their continuous support and tremendous kindness. Thank you Kiko for showering me with all your love and warmth during the last six years and for keeping me company during my sleepless nights. And of course, thank you Fabrice Andrzejczak for supporting me from the last 13 odd years! A super thanks (especially) for the last 5 months when you continuously cooked and cleaned so that I could complete this manuscript :) .

Contents

CONTENTS

Introduction en français

Les éruptions volcaniques sont des phénomènes complexes qui lient étroitement:

- la dynamique du transfert et le stockage du magma dans la croûte supérieure,
- le déclenchement de l'activité volcanique,
- les processus de transport de magma et leur interaction avec l'édifice volcanique,
- la dynamique et le budget des éruptions (magma et de gaz),
- le transport atmosphérique et
- l'impact des gaz et les aérosols volcaniques.

L'activité volcanique a de nombreuses caractéristiques en commun avec d'autres catastrophes naturelles, comme des conditions météorologiques extrêmes, tremblements de terre, glissements de terrain et en particulier les incendies de forêt (un risque naturel très similaire aux volcans). Les risques naturels sont typiquement complexes et impliquent de nombreux paramètres et processus. Certains des processus de contrôle sont fortement non-linéaires, de sorte que dans certaines circonstances, des changements brusques de comportement peuvent se produire, tels que la transition soudaine d'une éruption effusive à une éruption explosive.

Sur terre, on compte approximativement 550 volcans en activité, à proximité desquels au moins 500 millions de personnes vivent exposées à un danger potentiel. Parmi les principaux dangers et inconvénients associés aux émissions volcaniques, on peut citer leur impact sur le trafic aérien, la qualité de lair et le climat, du fait des émissions de gaz volcaniques et daérosols. Les éruptions volcaniques éjectent de nombreux gaz volatiles par example,

- la vapeur deau (H_2O représente 50 90 % du volume de la phase gazeuse)
- le dioxyde de carbone (CO_2, 1 à 40 % du volume)
- les espèces soufrées (2 à 35 % du volume), dont les plus abondantes sont le dioxyde de soufre (SO_2) et le sulfure dhydrogène (H_2S), et
- relativement récemment découvert le monoxyde de brome (BrO) (Bobrowski *et al.* (2003), entre autres).

Les émissions volcaniques qui atteignent la stratosphère, telles que le SO_2 sont principalement issues d'éruptions explosives et ont des effets avérés sur le climat en contribuant à la formation d'aérosols de sulfate (Robock, 2000). Cependant, le sort des émissions troposphériques (de éruptions effusives) et leurs impacts environnementaux et atmosphériques ont été beaucoup moins étudiés (Delmelle *et al.*, 2002, Mather *et al.*, 2003). Les éruptions de type effusif et leurs émissions sont plus fréquentes que les rares et grandes éruptions. Mather *et al.* (2003) montre que la quantité de SO_2 d'origine volcanique, libérée par des éruptions continues, est aussi importante voire supérieure à celle des éruptions explosives sporadiques. Andres & Kasgnoc (1998) ont estimé que l'activité sporadique ne contribue que'à 1 % (en moyenne sur des échelles de temps longues, par exemple 1 an) au flux total de soufre troposphèrique. Le dégazage permanent par les volcans contribue donc de façon significative au bilan global du SO2.

Situé dans la partie sud-est de l'île de la Réunion (21 °S; 55,5 ° E), le Piton de la Fournaise (PdF ci-dessous) est l'un des volcans les plus actifs au monde (Lenat & Bachelery, 1988) avec une moyenne d'une éruption tous les huit mois dans les cinquante dernières années (Peltier *et al.*, 2009). En dépit de l'importante activité du PdF, les émissions de gaz, la composition chimique, la distribution en taille et les propriétés optiques des aérosols issus de l'activité volcanique sont peu ou pas documentées. Au contraire, les gaz et les flux d'aérosols ont été bien étudiés et pour un certain nombre d'autres volcans tels que l'Etna et le Kilauea. En outre, l'impact radiatif et chimique des gaz volcaniques et des aérosols sur l'atmosphère et les écosystèmes de la Réunion sont totalement inconnus (Lesouëf, 2010).

Bien que les éruptions de PdF peuvent ne pas être aussi spectaculaires (sauf dans le cas de Avril 2007) que le volcan Eyjafjallajokull de l'Islande, par contre, une telle

activité volcanique représente l'une des sources naturelles les plus importantes de polluants dans l'atmosphère (à la fois pendant et entre les éruptions sous formes de fumerolles)(Mather *et al.*, 2003). Parmi d'autres gaz, le dioxyde de soufre (SO_2) émis lors de l'activité volcanique est la plus préoccupante. Le SO_2 dans l'atmosphére réagit chimiquement avec la lumière du soleil, l'oxygène, les particules de poussière et de l'eau pour former un mélange d'aérosols sulfatés (d'acide sulfurique (H_2SO_4), et d'autres espèces de soufre oxydé). Par exemple, Bhugwant *et al.* (2009) montre que pendant la majeure éruption d'Avril 2007 du PDF, les normes de qualité de l'air pour SO_2 (seuil d'information: 300 $\mu g/m^3$; seuil d'alerte: 500 $\mu g/m^3$) ont été dépassés à plusieurs reprises dans les différents stations de surveillance (y compris les parties les plus reculées de l'île). La concentration maximale de SO_2 relevée pendant cet épisode d'Avril 2007 est de 2486 $\mu g/m^3$ (Viane *et al.*, 2009). De plus, on a observé durant cette éruption volcanique

- un smog volcanique (également appelé 'vog') résultant de la réaction photochimique du SO_2 avec O_2 et H_2O en présence de radiation solaire,
- une pluie acide résultant de la dissolution du SO_2 dans leau liquide nuageuse (dépôt humide), et
- un brouillard volcanique (également appelée 'laze') résultant de lécoulement de lave dans locéan, créant un dense nuage dacide chlorhydrique.

La surveillance et la prévision des cendres et des gaz volcaniques est essentielle en terme de sécurité aérienne, de qualité de l'air et d'étude du climat. Une question centrale à cet objectif est la détermination au plus juste des altitudes atteintes par les panaches volcaniques. Cette hauteur, dite hauteur d'injection, correspond à l'altitude à laquelle le panache commence à être advecté sous le vent de la source volcanique. Cette hauteur est contrainte par la stabilité verticale de l'atmosphère (Bursik, 2001, Glaze & Baloga, 1996, Graf *et al.*, 1999, Tupper *et al.*, 2009). Déterminer correctement la hauteur du panache a des influences directes sur

- la dispersion du panache, affectée par la rotation et le cisaillement vertical du vent,

- le vieillissement chimique du panache, affecté par les conditions atmosphériques ambiantes : température, humidité, concentrations en aérosols, radiation solaire, etc., et

- les impacts du panache, en terme de pollution de lair, de dégâts pour lenvironnement, etc.

L'amélioration de la prévision est étroitement liée aux progrès dans la compréhension des processus dynamiques. La modélisation numérique est devenue un outil incontournable pour la prévision et l'évaluation des risques (Sparks, 2003b, Sparks & Aspinall, 2013). Aidé par le développement de l'outil informatique ainsi que l'amélioration de la compréhension de la physique impliquée, ces modèles sont de plus en plus sophistiqués (Melnik & Sparks, 1999, Neri & Macedonio, 1996). En effet, ces dernières années, les simulations numériques d'éruptions volcaniques se sont fortement améliorées. En raison de la complexité des processus et les différentes échelles impliquées depuis les flux de conduit jusqu'au panache volcanique aux échelles régionale et globale, tous les processus ne peuvent être abordés aujourd'hui par un seul modèle.

Les modèles découlement de conduit sintéressent au rôle des espèces volatiles, des bulles de gaz, et de la fragmentation du gaz et de la lave, parmi beaucoup dautres aspects. De tels modèles peuvent renseigner sur la géométrie de la bouche éruptive, la vitesse déjection, et les flux de chaleur et de masse. Cependant, ils sont numériquement trop coûteux en terme de temps d calcul et de mémoire pour entrer dans le cadre dun modèle de prévision du développement du panache et de sa dispersion atmosphérique.

Les modèles de panache de haute énergie traitent des processus rapides et hors équilibre qui règnent dans la région proche du jet volcanique. Ces modèles, focalisés surtout sur la partie basse du panache, étudient entre autres aspects les panaches à flottabilité négative (au caractère instable), la génération et la propagation découlements pyroclastiques, et la dynamique déjection des pyroclastes. Lusage de tels modèle est également limité par le coût de calcul et la mémoire requise, car simuler la colonne éruptive et sa dispersion demande des échelles de temps plus longues, ainsi que de prendre en compte des processus tels que la micro-physique nuageuse et les transformations chimiques au sein de la colonne.

Le modèle ATHAM (Active Tracer High Resolution Atmospheric Model) est un modèle extrêmement sophistiqué capable non seulement de simuler une colonne convective et sa dispersion (de particules et de gaz), mais aussi prend en compte des processus tels que le lessivage de gaz solubles et lagrégation de cendres. Cependant, ce modèle a été jusquici principalement appliqué au volcanisme explosif, et comme il sagit dun modèle de convection explicite, son coût numérique est trop élevé pour simuler la dispersion sur une région étendue.

Dans une autre catégorie de modèle, on trouve ceux utilisé par les VAAC (Volcanic Ash Advisory Centers), chargés de prévoir la dispersion atmosphérique des panaches de cendres pour prévenir des rencontres (dangereuses) avec les avions. Ces modèles ne résolvent pas la dynamique de la colonne éruptive, mais les caractéristiques de celle-ci sont estimées à partir de certains paramètres de la source volcanique selon des méthodes empiriques.

Il existe donc un manque clair en terme de modèle de prévision de la qualité de lair à échelle locale et régionale, ce qui nous amène à lobjet principal de cette thèse. Lobjectif de cette étude est de préparer la voie à un système de prévision numérique capable de simuler une colonne éruptive et sa dispersion de manière pronostique et non diagnostique. Ce modèle régional, dune résolution horizontale typiquement de 1 km, serait activé en cas déruption, et chose essentielle doit être rapidement exécutable. Dans les modèles globaux ou à mésoéchelle utilisés pour la simulation de la qualité de l'air, la source de chaleur intense que représente le volcan est instantanément diluée dans la grille du modèle ne permettant pas de générer de la convection. Ces sources de chaleur tout comme les mouvements convectifs ou les émissions de gaz et aérosols par les volcans sont des processus sous-maille qui requièrent d'être paramétrés aux résolutions considérées.

Dans le but de modéliser des injections démissions volcaniques en profondeur dans la troposphère au sein dun système rapidement exécutable, la stratégie de cette étude est de modifier une paramétrisation sous-maille de nuages convectifs peu profonds, déjà existante dans le modèle Méso-NH. Ce manuscrit a été développé en deux grandes parties, chapitres 1 & 2 et les chapitres 3 & 4. Le Chapitre 1 est un prélude qui reprend les connaissances fondamentales sur les éruptions volcaniques. Il donne une vision globale des éruptions volcaniques passées en se concentrant principalement sur la dynamique de ces éruptions et celle de la colonne convective. Le Chapitre 2 expose

les impacts climatiques et environnementaux des éruptions et leur représentation dans les modèles. Le Chapitre 3 se présente sous la forme d'un article récemment soumis à la revue "Geoscientific Model Development" (GMD). Cet article décrit le modèle utilisé, Meso-NH, et la nouvelle paramétrisation issue de la modification du schéma de convection peu profonde. La paramétrisation est testée sur la version unidimensionnelle du modèle et validée par des simulations à l'échelle des grands tourbillons turbulents (LES). Inspiré par les résultats des simulations idéalisées, la paramétrisation est testée dans la version tri-dimensionnelle du modèle pour l'éruption de Janvier 2010. Les premiers résultats sont présentés dans le chapitre 4. Le manuscrit se termine avec les conclusions et les perspectives de ces travaux.

Introduction

Volcanic eruptions are complex phenomena, such as;

- the dynamics of magma transfer and storage within the upper crust,
- the initiation of volcanic unrest,
- the processes of magma transport and their interaction with the volcanic edifice,
- the dynamics and budget of eruptions (magma and gases) and
- the atmospheric transport and impact of volcanic gases and aerosols.

These topics are all closely linked and part of an overall single process.

Volcanic activity has many features in common with other natural hazards, such as extreme weather, earthquakes, landslides and especially wildfires (a natural risk with similar processes than volcanoes). Natural hazards are characteristically complex and involve numerous parameters and processes. Some of the controlling processes are highly non-linear, so that in certain circumstances abrupt changes of behaviour can happen, such as the sudden transition from effusive to explosive eruption.

There are approximately 550 active volcanoes in the world and at least 500 million people live within a potential exposure range of a volcano. The primary hazards associated with volcanic activity amongst others are related to impacts on air traffic, pollution and climate through the emitted volcanic gases and aerosols. Volcanic eruptions eject numerous volatiles namely,

- water vapour (H_2O represents 50 - 90 % by volume gas phase),
- carbon dioxide (CO_2 represent 1 - 40 % by volume gas phase),

- sulphur species (represents 2 - 35 % by volume gas phase) whereby sulphur dioxide (SO_2) and hydrogen sulphide (H_2S) are the most abundant, and
- relatively recently discovered bromine monoxide (BrO) (Bobrowski *et al.* (2003) amongst others).

Volcanic emissions into the stratosphere mostly from explosive volcanoes such as SO_2 are widely known to have impacts on our climate through the formation of sulphate aerosols (Robock, 2000). However, the fate of tropospheric emissions from effusive eruptions and their environmental and atmospheric impacts have been far less investigated (Delmelle *et al.*, 2002, Mather *et al.*, 2003). Effusive type eruptions and their emissions are more frequent than the much rare, larger eruptions. Mather *et al.* (2003) report volcanic SO_2 release from continuous eruptions are comparable or even larger than the release by sporadic eruptions. Andres & Kasgnoc (1998) estimates that sporadic activity contributes only 1% (averaged over long time-scales, e.g. 1 year) to the total tropospheric sulphur flux, hence, it is the continuous degassing of volcanoes that contributes the most to the SO_2 budget.

Located in the south-eastern part of Reunion Island (21°S;55,5°E), Piton de la Fournaise (PdF hereafter) is one of the worlds most active volcanoes (Lenat & Bachelery, 1988) with an average of one eruption every eight months in the last fifty years (Peltier *et al.*, 2009). Despite the important activity of PdF, its gas emission and aerosol formation, size distribution, optical properties, and chemical composition of particles have poorly or not been documented. On contrary, gas and aerosols fluxes have been well studied and referenced for a number of others volcanoes such as Etna and Kilauea. Moreover, the radiative and chemical impact of volcanic gases and aerosols on the atmosphere and the Reunion ecosystems are totally unknown (Lesouëf, 2010).

Although eruptions of PdF may not be as dramatic (except for the case of April 2007) as Eyjafjallajokull volcano, Iceland, however, such volcanic activity represent one of the most significant natural sources of pollutants in the atmosphere, both during and between eruptions in forms of fumeroles (Mather *et al.*, 2003). Amongst other gases, sulphur dioxide (SO_2) emitted during volcanic activity is of most concern. Airborne SO_2 reacts chemically with sunlight, oxygen, dust particles, and water in the air to form a mixture of sulphate aerosols, sulphuric acid (H_2SO_4), and other oxidized sulphur species. For instance, Bhugwant *et al.* (2009) showed that during the major April 2007

eruption of PdF, air quality standards for SO_2 (information threshold: 300 $\mu g/m^3$; alert threshold: 500 $\mu g/m^3$) were exceeded many times at various monitoring stations (including the most remote parts of the island with respect to the volcano). The highest record was as high as 2486 $\mu g/m^3$ (Viane *et al.*, 2009). Furthermore, during this eruption period

- volcanic smog termed 'VOG' which is a result of SO_2 reaction with O_2 and H_2O in presence of sunlight,
- acid rain resulting from reaction of SO_2 with H_2O (wet deposition), and
- volcanic haze termed 'laze' resulting from lava-ocean interaction creating a dense hydrochloric acidic plume were also observed.

On the whole, successfully monitoring and forecasting volcanic ash and gases in terms of aviation safety, air quality and climate studies, a central issue is the correct determination of the heights reached by volcanic plume. This height is the vertical zone in which a buoyant plume begins to transport horizontally away from its source affected by environmental factors such as, wind shear and atmospheric vertical stability (Bursik, 2001, Glaze & Baloga, 1996, Graf *et al.*, 1999, Tupper *et al.*, 2009). Correctly determining the height of a plume has direct impacts on the plume

- dispersal affected by wind shear and direction,
- ageing affected by humidity, temperature, aerosol concentrations, solar radiation etc and
- impacts in terms of air pollution, environmental damage etc.

Improvements in forecasting are closely linked to advances in understanding of the underlying dynamical processes. Numerical modelling is becoming an important aspect of forecasting and risk assessment, the evolving approaches have largely focused on numerical simulations (Sparks, 2003b, Sparks & Aspinall, 2013). Aided by increasing computer power as well as improved understanding of the physics involved, such models are becoming increasingly sophisticated (Melnik & Sparks, 1999, Neri & Macedonio, 1996). Indeed in recent years, numerical simulation of volcanic eruptions have greatly improved. However, because of the complexity of the processes and the various scales

involved from the conduit flow to the ash cloud tracking at regional and global scale, not all processes could be addressed so far.

Conduit flow models study the role of volatiles, gas bubbles, fragmentation of gases and lava amongst numerous other aspects. Such models can provide information related to vent geometry, ejection speed, heat fluxes and mass fluxes however, they are too demanding in terms of computer time and memory to simulate volcanic column development and dispersal. High energy plume models deal with the rapid and non-equilibrium processes that occur close to the volcanic jet region. Such models confined to the lower convective region of the eruption study amongst others the negatively buoyant columns (unstable behaviour), pyroclastic flow generation and propagation and the dynamics of clast ejection. These models too are limited in terms computation and memory especially as simulating an eruption column and dispersal needs much longer time scales and one needs to consider a high number of column processes such as micro-physics and/or chemistry. In terms of buoyant column models and dispersion a model such as ATHAM (Active Tracer High resolution Atmospheric Model) exist. ATHAM is a highly sophisticated model which is not only able to simulate the volcanic column and dispersion (particles and gases) but also includes possibilities of gas scavenging and ash aggregation. However, thus far this model has been applied mostly to explosive volcanic events and since it is an explicit model, it would be computationally very expensive to model the plume transport over large areas. In a different class of models there exist operational models such as those used by VAAC (Volcanic Ash Advisory Center). Such models forecast the ash plume dispersion in order to prevent ash-aircraft interaction. Such models do not resolve the eruption column dynamics but instead are prescribed with certain eruption source parameters.

There is a clear lack of forecasting models for air quality on regional to local scale, bringing us to the main focus of this study. The purpose of this study is to pave the way towards a forecast system which is able to simulate a volcanic column and its dispersion in a prognostic way as opposed to a prescribed way. This model is to be implemented into a 1 km resolution model, which is activated in case of an eruption and most importantly is quickly executable. In terms of modelling dynamical processes, in kilometric resolution models used for air quality purposes (simulation or forecasts), the localised heat source is diluted in the model grid and hence no convection is explicitly generated. Several types of atmospheric movements (e.g. heat sources, induced

atmospheric convective motions and volcanic emissions of gases and aerosols) are all sub-grid scale processes and incorporated into atmospheric models through appropriate parameterisation schemes.

With an aim to model deep injections of tropospheric volcanic emissions in a quickly executable system, the strategy of this study is to modify an existing sub-grid parameterisation for shallow convective clouds in a Meso-scale model. This manuscript has been developed into two main parts, chapters 1 & 2 and chapters 3 & 4. Chapter 1 considered as a prelude to the manuscript provides the thematic and fundamental knowledge of volcanic eruptions. It provides an overview of past volcanic eruptions, concentrating primarily on the dynamics of volcanic eruptions (focussing on the convective column). Chapter 2 aims on building on the climatic and environmental impacts of eruptions. Furthermore, it concentrates on the efforts of the scientific community to investigate the impacts through modelling studies. Lastly, the chapter outlines the main aims and objectives of this study. Chapter 3 is largely based on an article accepted by the journal of Geoscientific Model Development - GMD. It describes the research model used throughout this study, proposing a modified formulation of an updraft model, where the volcano induced updrafts are parameterised. Furthermore, it is tested on an idealised 1 dimensional (1-D), single column model (SCM) and validated through Large Eddy Simulation (LES), considered as a reference simulation. Inspired by the results of the idealised simulations, the parameterisation is tested in real case set-up and the first results are presented in chapter 4. Ultimately, the manuscript ends with conclusions, short and long term perspectives of the work undertaken during this thesis.

1

Volcanic eruptions in the Earth's system

Contents

Man has been a witness to volcanic eruptions for centuries. Zeilinga de Boer & Sanders (2004) explains how volcanism has found it's way into certain literatures and

beliefs across Iceland, Greece, Japan (Davis, 1992), Hawaii, amongst others. Furthermore, the associated widespread population migrations due to eruptions, along with how such phenomena spurred scientific debates and discoveries are also discussed. Alongside, Sigurdsson (1999) considers how over centuries philosophers and scientists have attempted to understand volcanic eruptions. On the whole Zeilinga de Boer & Sanders (2004) and Sigurdsson (1999) outline understanding the structure of our earth has greatly aided in our comprehension of volcanic systems. Finally during the 19th and 20th century various fields of sciences (e.g. research in thermodynamics, petrology, geochemistry, plate tectonics and of course volcanology) have contributed to our overall current understanding of volcanic activity.

This chapter aims to introduce the reader to the thematic of volcanic eruptions by firstly introducing certain components that control various eruption styles (section 1.2) and followed by the dynamics behind volcanic eruptions (section 1.3). An overview of certain volcanic eruptions through human history and their impacts are outlined in section (1.4) and lastly, an overview on the chapter is outlined in section (1.5).

1.1 Types of volcanoes: Volcanic eruption variability

According to the Global Volcanism program of the Smithsonian Instituiton there are about 550 geologically active volcanoes on earth (Smithsonian, 2014). From quiescent lava emissions to extremely violent, explosive events, there is a rather large variability of eruption types. Volcanologists classify volcanoes into groups based on the material that form them, their eruption style, their shapes and sizes. Most can be grouped into three main types (Fig.(1.1)) largely based on their eruptive patterns and their general forms (e.g. scoria cone (cinder cone), shield volcano and stratovolcano (composite volcanoes)).

Cinder cones are the smallest of the volcanoes, typically only a couple hundred of meters high. Shield volcanoes are made by numerous successive basaltic lava flows in a given region (rock formed from the rapid cooling of basaltic lava exposed at or very near the Earth's surface), e.g. Piton de la Fournaise volcano in la Réunion Island. Stratovolcanoes are formed through a sometimes explosive and sometimes effusive eruptions. Hence, they are also known as composite volcanoes, as they represent a composite of lava flows and pyroclastic materials (Petersen *et al.*, 2010).

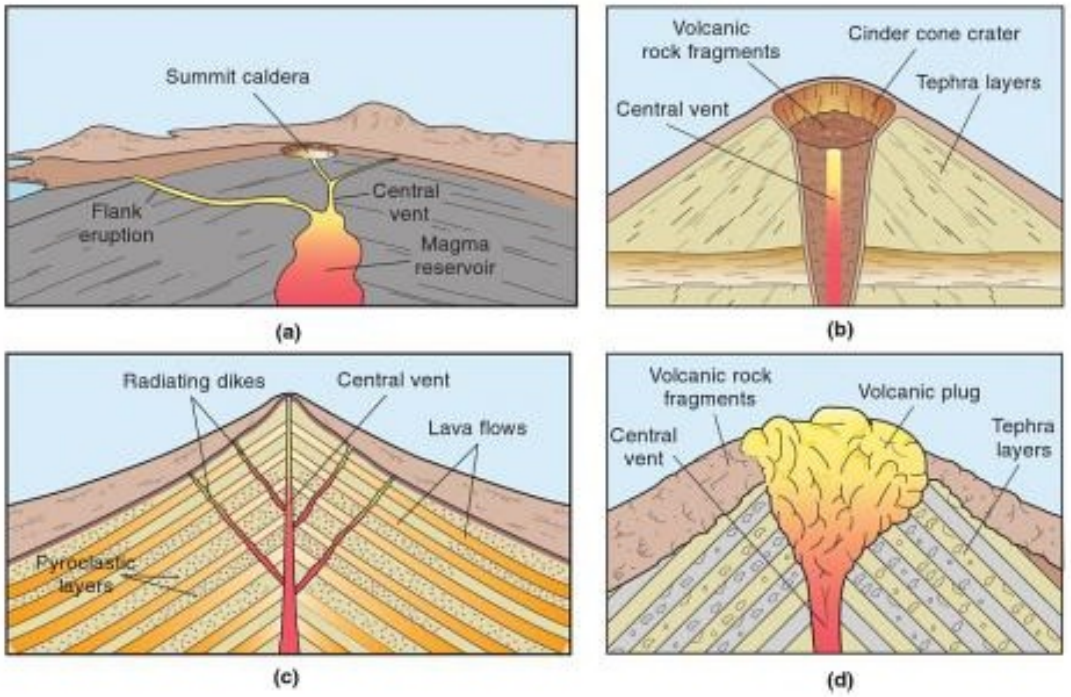

Figure 1.1: Types of volcanoes - The four basic type of volcanoes are: (a) shield volcano, (b) cinder cone, (c) stratovolcano and (d) plug dome. Diagram taken from Petersen *et al.* (2010)

An eruption occurs when magma migrates upward, often driven by expansion of dissolved gas, and is discharged onto the earth's surface. Three main metatypes of eruptions exist, phreatic eruptions, magmatic eruptions and phreatomagmatic eruptions. Generally a phreatic eruption occurs when the ascending magma heats the ground/surface water causing near-instantaneous evaporation to steam and resulting in an explosion of steam, water, ash, rock, and volcanic bombs (Barberi *et al.*, 1992). In contrast to phreatic eruptions, magmatic eruptions mainly eject fragmented magma and the variability in magmatic eruptions depend greatly on the physical and chemical nature of the magma (discussed in greater detail shortly). When magma or lava interacts with the near-surface water, a phreatomagmatic eruption takes place. Such eruptions occur especially in water rich environments (White & Houghton, 2000). Out of the three metatypes of eruptions, magmatic eruptions are the most well observed.

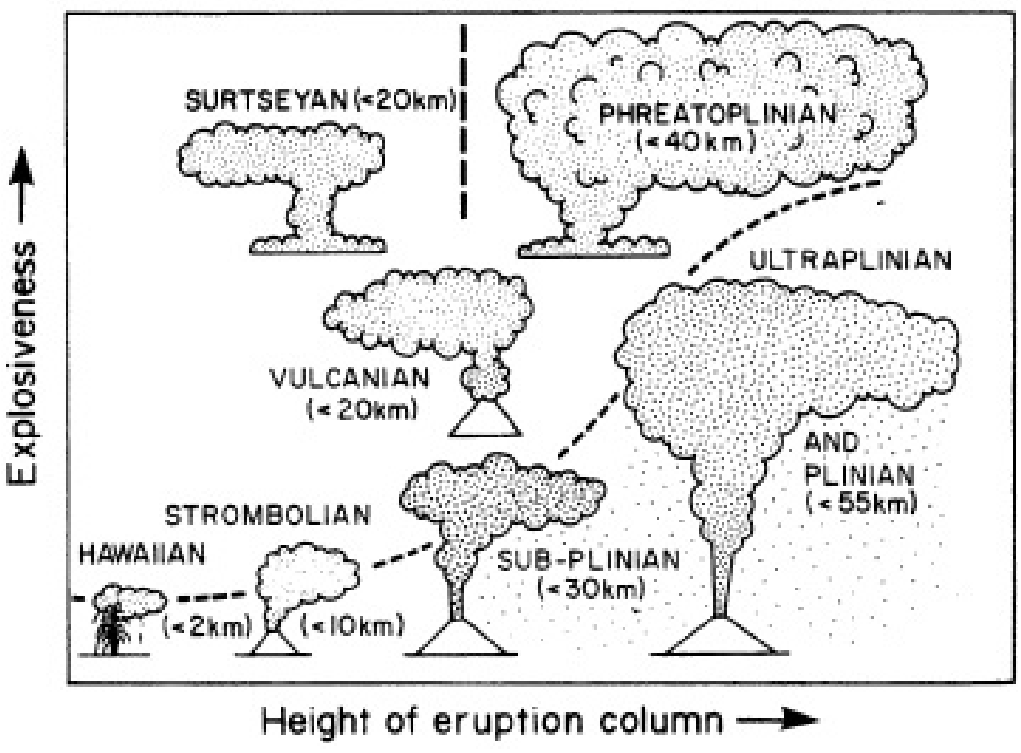

Figure 1.2: Erution column height and "explosiveness" - Various eruption types can be defined by variations in their explosiveness and the height of the eruption plumes (Cas, 1987).

In accordance with the physical properties of magma (density, viscosity, thermal

conductivity, cooling rates etc. discussed in the following sections) and the scale of eruption, explosive eruptions are classified by Cas (1987) as in Fig.(1.2). The 'explosiveness' or explosive power of an eruption is measured through the Volcanic Explosivity Index (VEI) (Newhall & Self, 1982). It can be thought to be similar to the Richter scale used to assign a magnitude number to quantify the energy released by an earthquake. The VEI uses a numerical index ranging from 0 to 8, where each increment represents a 10-fold increase (logarithmic scale) in explosivity. Factors that are taken into account include the volume of pyroclastic material (including ashfall, pyroclastic flows, and other ejecta), the height of the eruption, duration in hours, style of past activity and a number of other qualitative measurements (e.g. "gentle", "effusive", "explosive", "cataclysmic", etc.) (Newhall & Self, 1982). Piton de la Fournaise (PdF) is classified as a Hawaiian type volcano, clearly named after the Hawaiian volcanoes. As for Hawaiian volcanoes, PdF is a typical basaltic shield volcano, mostly characterized by it's effusive eruptions and fire fountaining. Majority of it's eruptions are not centralized at the main summit, they often occur at vents around the summit and from fissures.

1.2 What controls eruption styles?

In order to complete our understanding behind the dynamics of volcanic eruptions, it is necessary to understand magma and its composition. The chemical composition of magma and its cooling and solidification rate is what directly or indirectly controls numerous aspects in volcanism. One such aspect is the range in the explosivity (relatively quiescent to explosive eruptions) of volcanic eruptions.

In this section the basic concept of magma composition and its cooling rate is outlined, followed by a description of the controlling factors on explosivity (i.e. viscosity, temperature, and the amount of dissolved gases in the magma).

1.2.1 Magma composition

Magma is a naturally occurring liquid. About 99% of magmas are made up of 10 main elements, namely, Silicon (Si), Titanium (Ti), Aluminum (Al), Iron (Fe), Magnesium (Mg), Calcium (Ca), Sodium (Na), Potassium (K), Hydrogen (H) and Oxygen (O) (Brophy, 2014, Sen, 2013). Without detailing the chemistry behind how chemical bonds are created, it is simpler to say that, different oxide molecules are formed when the

first nine elements mentioned above bond with Oxygen. Hence, magmas are viewed as a mixture of the nine chemical oxides. The chemical composition of a magma is expressed in terms of the weight percentage of the nine chemical oxides (namely, SiO_2 (silicon dioxide), TiO_2 (titanium dioxide), Al_2O_3 (aluminium oxide), FeO (iron oxide), MgO (magnesium oxide), CaO (calcium oxide), Na_2O (sodium oxide), K_2O (potassium oxide), H_2O (hydrogen oxide)) (Brophy, 2014, Sen, 2013). What makes one 'type' of magma different from another is simply the variation in these nine chemical oxides. It is this fact that largely controls the wide range of volcanic rock types, eruption styles, and types of volcanic cones that characterise global volcanic activity (Brophy, 2014).

The variations in magma compositions are rather organised. For example, Fig.(1.3) from Brophy (2014) depicts the chemical compositions of four volcanic rock types found on Mount St. Helens, United States of America. It is observed that as SiO_2 content of each rock (1 to 4) increases, FeO, MgO and CaO decrease, while, Na_2O and K_2O increase. Such relation is true for most magmas and subsequent igneous rocks around the world (Brophy, 2014).

As oxygen and silicon are the two most abundant elements in magma, the various magma types are described in terms of their silica content (SiO_2), for convenience.

1.2.1.1 Volcanic rocks - mineral composition

Upon the upward migration of magma towards the earth's surface, it begins to cool and eventually solidifies (or crystallises). During the cooling process a magma forms several different substances (called minerals), over a wide range of temperatures (1200°C down to around 800°C) (Brophy, 2014). These solid minerals (formed as crystals) reflect the chemical composition of the magma itself.

The colour of a solidified magma (i.e. the igneous rock) depends on the composition of the magma that formed it. For example, for magmas that are rich in FeO (and in turn low in SiO_2, Na_2O and K_2O while high in MgO and CaO) the different minerals and rock formed when cooled are dark in colour (Brophy, 2014, Jerram & Petford, 2011, Oxlade, 2012, Wicander & Monroe, 2005). Thus, magmas that are low in SiO_2 form dark coloured minerals upon cooling and the resultant volcanic rock is in turn dark. Inversely, light coloured rocks are formed for magmas that are relatively poor in FeO, i.e. high in SiO_2. For intermediate amounts of SiO_2 in magmas, the resulting

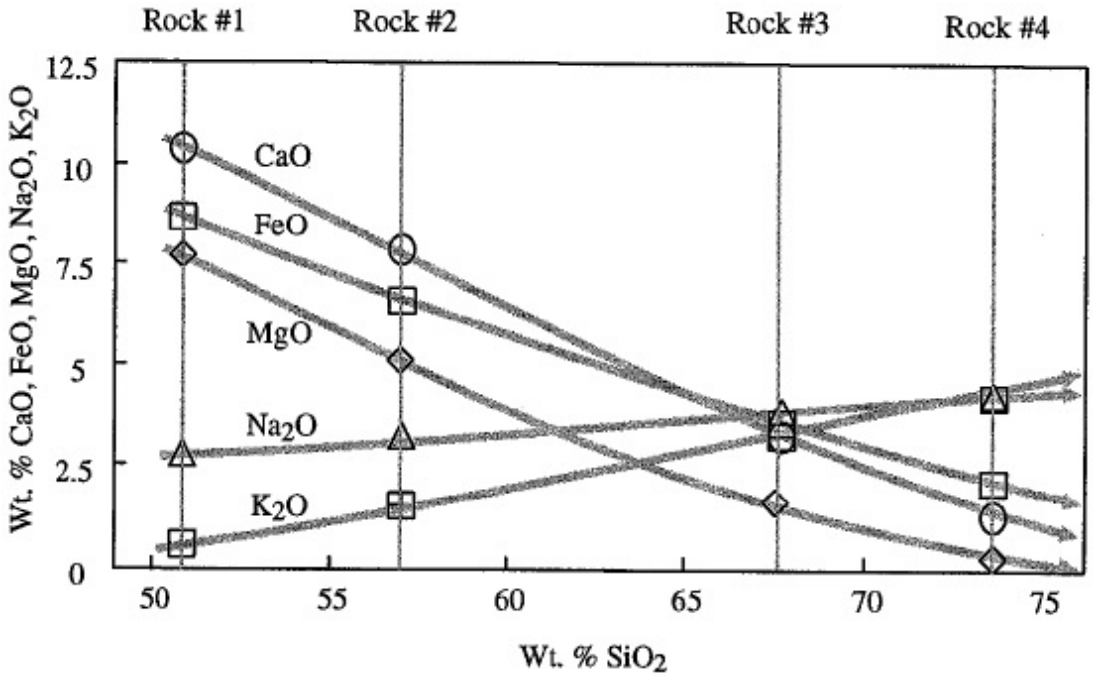

Figure 1.3: Examples of magma composition - Magma composition from 4 different rock types from Mount St. Helens. Weighted percentage of SiO_2 on the x-axis versus the weighted percentage of FeO, MgO, CaO, Na_2O and K_2O on the y-axis. Diagram taken from Brophy (2014)

minerals upon crystallisation are of dark and light coloured. The resulting rock reflects this combination of coloured minerals with a grayish visual (Brophy, 2014, Oxlade, 2012).

1.2.1.2 Volcanic rocks - magma cooling rate

Although magma composition is one factor in determining the visual of a igneous rock, another important factor is the cooling rate of magma (Brophy, 2014, Jerram & Petford, 2011). It determines the texture of the rock (which is a measure of how big the individual minerals are that form during the cooling process, (Brophy, 2014), Sen2013). To understand how the cooling rate controls the size of a crystal, this section briefly delves into the process of crystallisation.

Through experimental studies (Dawson (1992), Gibb (1974), Lofgren (1980), amongst others) a general relationship between cooling rate and the total number of crystal nuclei that form in most fluids (including magmas) have been determined. Generally, slow cooling rates form a small number of crystal nuclei. Furthermore, due to the availability of greater time for these crystals to grow, this results in a rock that is dominated by large crystals. Such rocks are called phaneritic, i.e. coarse grained (Brophy, 2014, Jerram & Petford, 2011, Oxlade, 2012, Wicander & Monroe, 2005). As the cooling rate increases the number of crystal nuclei formed increase. This increased cooling rate means a relatively short amount of time available for crystal growth, hence this results in a fine grained rock, named aphanitic (Brophy, 2014, Jerram & Petford, 2011, Oxlade, 2012, Wicander & Monroe, 2005). A rock texture referred to as porphyritic is created when magma goes through two stages of cooling, i.e. a slow rate followed by a relatively faster rate. Such a textured rock contains large crystals enclosed within a fine-grained rock. Lastly, very fast cooling rate lead to a dark coloured solidified magma (solidified into volcanic glass) that is absent of any crystals. Such a solid is referred to as obsidian (Brophy, 2014).

We now know that cooling rates control the texture of the igneous rocks, but why are cooling rates different? When ascending magma is suspending within the earths crust (known as the plutonic environment in volcanology), due to the insulation provided by the surrounding rocks, magma loses it's heat very slowly. Overall it can be said that in plutonic environment the magma cooling rates are slow creating coarse-grained phaneritic rocks (Brophy, 2014, Jerram & Petford, 2011, Wicander & Monroe,

2005). On the other hand, once magma erupts onto the earth's surface known as the volcanic environment, due to the lack of insulation compared to the plutonic environment, magma cools down relatively quickly. Resulting in a fine-grained aphanitic rock or, in some circumstances, obsidian (Brophy, 2014, Jerram & Petford, 2011, Wicander & Monroe, 2005). An intermediate situation is when magma is suspended for some time within the earth's crust and then erupts onto the surface. This process leads to a volcanic rock that has experienced the two periods of cooling (i.e. first at a slow rate followed by a relatively faster rate). The resultant rock is said to have a porphyritic texture (Brophy, 2014, Jerram & Petford, 2011, Wicander & Monroe, 2005).

1.2.1.3 Volcanic rocks - classifications

Overall, magma composition controls the type of minerals it forms (i.e. mineral composition, light versus dark) and its cooling rate controls what the minerals look like when they form (i.e. rock texture; size, shape and arrangement of the minerals). Igneous rocks can be classified depending upon the information presented in these sub-sections as in Fig.(1.4).

SiO_2 content (approximately)	Magma type	Environnment of crystallisation	Magma cooling rate	Rock category	Rock texture	Rock colour
50%	Mafic	Plutonic	Slow	Gabbro	Phaneritic	Dark
60%	Intermediate			Diorite		Intermediate
65%	Felsic (low Si)			Granodiorite		Intermediate - light
70%	Felsic (high Si)			Granite		Light
50%	Mafic	Volcanic	Fast	Basalt	Aphanitic	Dark
60%	Intermediate			Andesite		Intermediate
65%	Felsic (low Si)			Dacite		Intermediate - light
70%	Felsic (high Si)			Rhyolite		Light
50%	Mafic	Sub-volcanic	2 Stages: Slow followed by fast	Basalt - Porphyritic	Porphyritic	Dark
60%	Intermediate			Andesite - Porphyritic		Intermediate
65%	Felsic (low Si)			Dacite - Porphyritic		Intermediate - light
70%	Felsic (high Si)			Rhyolite - Porphyritic		Light
70%	Felsic (high Si)	Volcanic	Very fast	Obsidian	Volcanic glass	Dark

Figure 1.4: Magma and rock classification - Magma composition and cooling rates classified in terms of various rock textures and categories.

On the whole, from Fig.(1.4) it can be seen that the rock colors (controlled by the color of the minerals) are controlled by the chemical composition of the magma from which they form. Thus, magma composition indirectly controls volcanic rock colours. It is worth noting that the only difference between for example, basalt and gabbro is

the grain size, controlled entirely by the cooling rate. Hence it can be said that various igneous rocks are formed from a given magma composition depending on where and how magma cools and solidifies.

1.2.2 Magma viscosity, temperature and gas content

The viscosity of a substance is defined as it's internal resistance to flow. A magma's viscosity is controlled by its temperature, gas content and most importantly its composition (Sen, 2013). In this summary, the chemical and physical facts as to how the above variables control magma viscoscity will not be discussed in depth. This is to avoid deviation from the basic or minimum facts in order to comprehend basic volcano dynamics.

Temperature plays an important role in lowering the viscosity of most liquids (including magmas) by increasing its fluidity. However, the composition of magma plays a greater role in magma viscosity. It has already been established that SiO_2 is the most abundant oxide in a magma. Hence, the most important factor in determining the viscosity is the number of silicate 'chains' formed (this chemical process is known as polymerisation) (Sen, 2013, Wicander & Monroe, 2005). This is because, as SiO_2 content increases, so does the network of silica tetrahedra-form. If a certain flow is to take place then the strong bonds between SiO_2 must be broken. Hence, magma with greater silica content (felsic) have greater viscosity then those with lower silica content (mafic). Temperature increases further break down the silica bonds, hence lowering viscosity of a magma (Sen, 2013). Lastly, gas content too has an effect on the viscosity. During the process of exsolution (process in which a solution of molten rocks separate into its constituents), the gases that begin to escape the melt exhibit low viscosity. However, the residual melt will exhibit an increased viscosity as gas escapes. Although this too is an important factor in determining the viscosity of a magma, however, exsolving gases play a more important role by providing the driving force for an eruption (discussed next).

1.2.3 Controls on explosivity

Dissolved gases in a magma have been recognised to be the driving force of an eruption. This being said, viscosity of magma too plays an important role in determining the explosive nature of an eruption (Parfitt & Wilson, 2009). The ability of the dissolved

gases to escape magma determines the nature of an eruption and is strongly linked to magma's viscosity. Rhyolitic magmas (see Fig.(1.4)) with high viscosity (related to high polymerization of silicates), prevent gas bubble segregation. This prevention increases the overall pressure exerted onto the magma column and eventually the gas ejects in an explosive manner (Parfitt & Wilson, 2009). For basaltic magmas, the gas bubbles can relatively easily escape the magma due to its low viscosity. Hence, as a general rule, basaltic magmas favour non-explosive eruptions and lower gas content, whereas explosive eruptions are typical of rhyolitic magmas and favour high gas content (Parfitt & Wilson, 2009). Table 1.1 consolidates information from this section regarding magma viscosity, gas content and various eruption styles in terms of magma's silica content.

Table 1.1: Various eruption styles in terms of magma's silica content and viscosity

SiO_2 content	Magma type	Temperature °C	Viscoscity	Gas content	Eruption style
$\sim 50\%$	Mafic	~ 1100	low	low	non explosive
$\sim 60\%$	Intermediate	~ 1000	intermediate	intermediate	intermediate
$\sim 70\%$	Felsic	~ 800	high	high	explosive

1.3 General volcanic eruption dynamics

This section briefly describes the two main columns comprising a volcanic eruption, the magma column and the eruption column as depicted in a cross sectional view of an erupting column of Fig.(1.5).

1.3.1 Magma column

Eruptions are fed from a magma column that mostly exists below the point source of the eruption. In general, magmas rise as they are less dense than the surrounding solid rocks (Sparks, 2003a):

1. The exsolution surface occurs in the magma reservoir beneath the volcano. It separates a zone of magma containing dissolved volatiles from an overlying zone of magma containing exsolved gas bubbles.

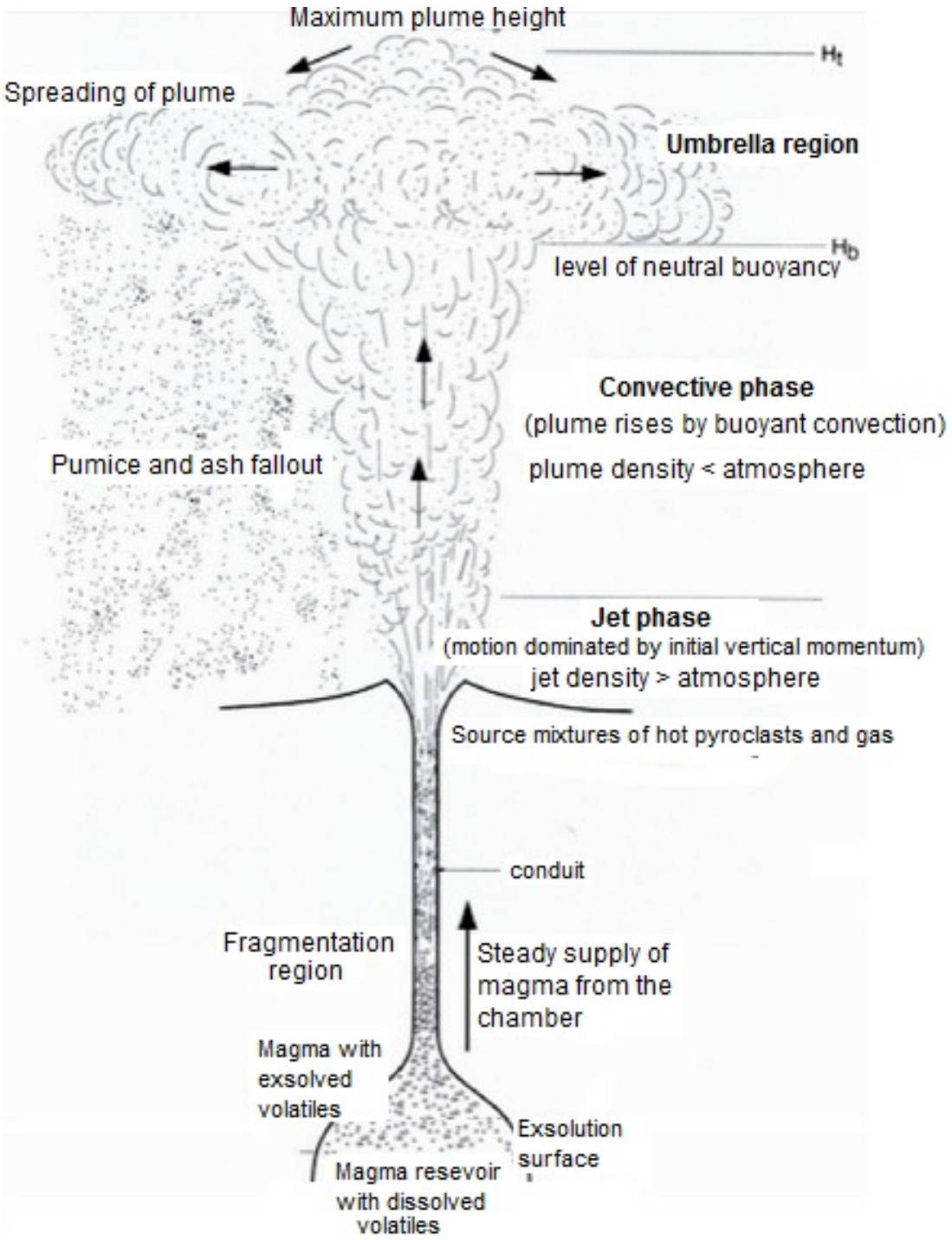

Figure 1.5: Cross-sectional model of an eruption - Regions in the magma and eruption column. Diagram taken from the website *http* : *//www.geo.mtu.edu/ raman/Ashfall/Syllabus/Entries/*2009/6/21$_C$*olumns.html*

2. The fragmentation surface occurs at the top of the magma column. It separates the zone of magma containing exsolved gas from the overlying eruption column. Fragmentation of the magma is generated by rapid gas expansion and bubble explosion.

Magmas, a mixture of molten or semi-molten rock and volatiles rise due to their low density in comparison to the surrounding rock. While rising, a depth or pressure is encountered whereby due to this decompression of magmas, the dissolved gases can no longer be held in solution. At this stage the gas begins to form a separate phase (it makes gas bubbles or vesicles), just as when one removes the cork of a champagne bottle. This process of exsolution of gas from magma is called vesiculation. Once gas bubbles are formed, due to the reduced pressure they begin to expand while continuously more gases are exsolved from the magmas. Fragmentation of the bubbles' walls then begin at the fragmentation surface. Here, the gas bubbles grow during ascent and due to the build-up of gas pressure within the gas bubbles they become unstable and explode releasing the gas pressure. The gas content controls the velocity of the eruption and its release is confined to the diameter of the magma column. Low viscosity of liquid magma aids the expansion of gases, and upon reaching the Earth's surface, gases released from bursting bubbles easily expand to atmospheric pressure. This leads to a non-explosive eruption usually as a lava flow. However, a relatively higher viscosity (of liquid magma) makes it harder for the gases to expand leading to a pressure build up inside the gas bubbles. In contrast to the non-explosive eruption, the pressure build up within these bubbles causes them to burst explosively on reaching atmospheric pressure, hence causing an explosive volcanic eruption.

Volatiles which are present within magmas are the driving force of eruptions as briefly explained in the earlier section. Dissolved water (H_2O, a main volatile in magmas) affects the ascent dynamics by increasing the eruption mass flow-rate (Papale *et al.*, 1998, Wilson *et al.*, 1980) due to reduced magma viscoscity (Textor *et al.*, 2005). On the other hand increasing amounts of carbon dioxide (CO_2) (the second main volatile component), reduces mass flow-rate (Papale & Polacci, 1999, Textor *et al.*, 2005). This reduction is found to be due to the large increase in the gas saturation pressure (due to the presence of increased CO_2), which results in earlier H_2O exsolution and an increase of the mixture viscosity (Holloway, 1976). Such effects on lava flow rates

are affiliated to the differing solubilities of the two volatiles. Gas exsolution occurs at higher pressures when CO_2 is present than if H_2O was the only volatile species present. This is because CO_2 is poorly soluble (Holloway & J.G, 1994, Papale & Polacci, 1999). The developed gas phase carries a fraction of all the volatile components. In doing so, it reduces the amount of H_2O dissolved in the magma. Hence, greater CO_2 can result in more gas available for expansion and acceleration (favouring magma flow), as well as hindering magma flow in more viscous magma. Numerical simulations suggest that the latter effect is the dominant one (Textor *et al.*, 2005). Greater comprehensive knowledge in conduit flow processes can be found in Textor *et al.* (2005).

On the whole, non explosive eruptions are generally favoured by low gas content and low viscosity magmas (basaltic to andesitic magmas). Such eruptions usually begin with fire fountains due to release of dissolved gases (Walker, 1981). Explosive eruptions in contrast are generally favoured by high gas content and high viscosity (andesitic to rhyolitic, silica rich magmas). Furthermore, explosive bursting of bubbles fragments the magma into clots of liquid that cool during their fall through the air. These solid particles are known as pyroclasts (hot fragments) and tephra or volcanic ash.

Although the dynamics related to the magma column have been discussed, however such processes are not treated in this study.

1.3.2 Eruption column

The fragmentation surface is the point source of the eruption. Above this fragmentation surface lies the eruption column, a region of hot gas and broken pyroclastic particles (transported from the ground into the atmosphere).

The eruption column rising from the fragmentation surface into the troposphere/stratosphere undergoes some progressive behavioural changes (both physical and mechanical), allowing the column to be sub-divided into three regions (Sparks (1986), see Fig.(1.5):

1. the gas thrust/jet phase region in the lower column (driven by gas expansion),

2. the convective region in the upper column (driven by the constant release of thermal energy from internal ash (where applicable), entrainment of environmental air and microphysical changes in the column) and

3. the umbrella region (also known as the "downwind plume") at the top of the eruption column.

Internally powered by gas expansion (decompression) at the base of the eruptive column, the gas thrust region is where gas and plastic magma particles are in vertical movement. Initially, the gas thrust is denser (it's overall density depends on the particle-to-gas ratio) than its surrounding air because of its incorporation of pyroclastic particles. It is driven up by its own kinetic energy (Woods, 1988). The jet on exit experiences a drag by the atmosphere and a downward acceleration from gravity. And as the pyroclastic particles fall out (as ballistics), the turbulent margins of this region entrain the surrounding air, which continues to travel towards the interior of the column. Before the jets own kinetic energy is spent, this entrained air expands due to the hot fragments of magma and other materials within the jet and as a result the density of the plume (mixture of particles, volcanic gases and air) is reduced. The hot gases in the column are now less dense than that of the atmosphere. At this point, the gas thrust gives way to convective uprise (the column is said to become buoyant) and hence, development of the convective thrust region comprising majority of the eruptive column (Woods, 1988).

In humid coastal and tropical to subtropical environments, moisture from the surrounding air is also entrained into the plume. The convective plume is driven by the constant release of thermal energy from internal ash (where applicable) and the resulting latent heat release from the condensed water vapour in the column further adds to it's buoyancy. The different entrainment ratios of the colder surrounding air into the column during the ascent steadily decreases the temperature of the column and it eventually reaches a certain height whereby the bulk density of the column becomes equal to that of the atmosphere (atmospheric air becomes less dense with height) (Herzog *et al.*, 1998, Valentine, 1997). The plume is now said to have reached a neutral buoyancy state and is known as an 'umbrella cloud'.

Where amounts of entrainment are not sufficient to make the eruptive plume lighter than surrounding air, the plume decelerates until its velocity reaches zero (not having had enough time to mix with the atmosphere). The density of the plume at this altitude is greater than that of its surrounding atmosphere and the column starts to fall towards the surface of the Earth. This generally happens at much lower heights

(at a few kilometers, Woods (1988)) and such an eruption is known as a 'collapsing' column whereby, the particle-gas mixture may further flow outward as a pyroclastic flow.

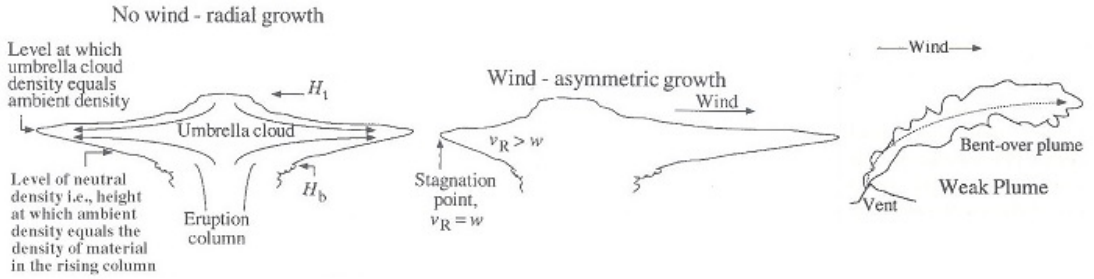

Figure 1.6: Volcanic plume dispersion - From left: a volcanic plume dispersion in a no wind/stable winds environment, dispersion of the eruption cloud to the right affected by wind (middle figure), a bent over plume deflected comparatively strong winds. From Sparks *et al.* (1997)

In a calm atmosphere (very weak winds) the axis of the column is vertical and the umbrella cloud is centered directly over the vent and it disperses symmetrically in both directions as shown in Fig.(1.6, left). The bottom of umbrella region (H_b) is where densities of the plume and the surrounding air are equal. Continued upward mobility towards the top of the umbrella region (H_t) is controlled by momentum and is commonly known as an "overshooting". In case of an overshooting the column slumps back gravitationally towards the height where its density equals that of the air. The interaction between the downward and upward flow result in a wedge like form (Sparks *et al.*, 1997). Most eruption columns penetrate the atmosphere with a cross wind which can alter the entrainment process along with distorting the shape of the plume. The atmospheric structure varies with altitude, latitude and seasons (Sparks *et al.*, 1997). The spreading and dispersal of volcanic plumes within the atmosphere result from interaction with atmospheric motions and stratification. All columns experience wind throughout their height and can affect plumes in different ways depending on their strength and size. However, the umbrella region is often asymmetric due to the effect of high atmospheric winds. In a cross wind, larger plumes rise almost undistorted by the wind (whereby the column axis will be slightly deflected) and as the lateral velocity begins to decrease, the plume interacts with the wind as shown in Fig.(1.6, middle). Here the stagnation point occurs on the left hand side where the wind velocity (v_R)

equals the velocity of the plume (w). Weaker plumes as is the case for majority of the PdF eruptions, interact much faster with the cross winds and can appear as a "bent-over" plume as depicted in Fig.(1.6, right).

1.4 Man and volcanism

Briefly, some major past eruptions are outlined especially in terms of their significant (direct or indirect) affects on society and environment.

1.4.1 Vesuvius eruption and Pompeii

The eruption of Vesuvius of 79 AD caused extensive destructions all over the Campanian area, engulfing the cities of Pompei, Herculaneum, Oplonti and Stabiae (Giacomelli *et al.*, 2003). The eruption followed a long quiescence period and the inhabitants of the area were surprised by the volcanic events. The first part of the eruption was characterized by a widespread dispersal of pumices from a high eruptive column. Carey & Sigurdsson (1987) estimated the height of the eruption column during the development of the Plinian phase of as 14 km reaching up to 26 km during the emission of white pumice and then to 32 km during the emission of grey pumice immediately before the deposition of pyroclastic flows. The second part of the eruption, characterized by pyroclastic flows emplacement, caused major damages with extensive life losses in most of the towns surrounding the volcano. In Pompeii, the major casualties during the first phase resulted from roof collapses (Carey & Sigurdsson, 1987). During the second phase, people were killed either by physical trauma due to the kinetic energy of the pyroclastic density currents (PDCs) flow or by suffocation because of the ash-rich atmosphere. Overall 394 corpses were excavated in the pumice fall deposit while 650 in PDCs deposit. A total of 1044 victims were recovered and another 100 victims are estimated on the basis of many groups of scattered bones and finally, Carey & Sigurdsson (1987) estimate another 464 still buried in regions partially excavated.

1.4.2 Laki eruption, Iceland

Thordarson & Self (2003) show that during the Laki eruption in $1783 - 1784$ in Iceland approximately 122 megatons (Mt) of sulphur dioxide (SO_2) was emitted into the

atmosphere and maintained a sulphuric aerosol veil that hung over the Northern Hemisphere for more than 5 months. Approximately 95 Mt of the total SO_2 was transported into the upper troposphere/lower stratosphere and the eruption column extended up to 13 km (Thordarson & Self, 2003). The eruption had a devastating impact upon the ecology of Iceland and the death of approximately 25 % of the island's population. The aftermath resulted in induced illness, subsequent environmental stress and famine (Steingrímsson & Kunz, 1998, Thorarinsson, 1979, 1981). The environmental impacts such as dry sulphurous fogs (due to 175 Mt of sulphate (H_2SO_4) aerosols) were removed as acid precipitation as shown by Thordarson & Self (2003) and extreme heat, chemical pollution, along with tremendous storms of thunder, lightning and hail were reported from northern Scotland to Sicily (Brayshay, 1999, Stothers, 1996). Grattan *et al.* (2003) report how significant increases in the national death rate in England coincided with the early phases of the eruption. They further link the dry fog of 1783 to the symptoms observed in certain populations (difficulty in breathing, eye and skin irritation, headaches, loss of appetite and tiredness) due to severe exposure to air pollution. Apart from the impacts on climate and population in the northern hemisphere (NH), Oman *et al.* (2006) have shown from both observations and climate model simulations that NH high-latitude eruptions produce changes in atmospheric circulation in the NH summer, weakening the African summer monsoon, reducing precipitation and consequently reducing the flow in the Nile and Niger rivers.

1.4.3 Eruption of Mount Tambora

The island of Sumbawa, home to Mount Tambora, is located in present day Indonesia. During the eruption of Mt. Tambora on 5th April 1815, thundering detonations were heard as far as 1400 km away in the Molucca Islands (Stothers, 1984). Light ash fall began on eastern Java and continued till the 10^{th} of April when the eruption intensified and the sound from the explosions were heard possibly up to 2600 km in Trumon on the island of Sumatra (Stothers, 1984). A loss of about 92,000 lives have been estimated on Sunbawa and Lombok, furthermore, avolume of 150 km^3 of tephra has been estimated (up to 1300 km away from the source) (Self *et al.*, 1984, Stothers, 1984). A region extending to about 600 km west of the volcano was plunged into darkness for three days (Oppenheimer, 2003a, Sigurdsson & Houghton, 2000). The eruption had a dramatic impact on the earth's climate as approximately 60 Mt of sulphur was ejected

into the stratosphere (up to 43 km in altitude) forming a global sulphate aerosol veil (Oppenheimer, 2003a). The dimming of stars including brilliant sunsets and twilights were observed in Europe as an immediate atmospheric result (Stothers, 1984). The following year there were noticeable disruption to weather patterns e.g. anomalously cold weather experienced in the north-eastern USA, maritime provinces of Canada, and Europe, giving way to it being called "the year without a summer" (Oppenheimer, 2003a, Self *et al.*, 1984, Sigurdsson & Houghton, 2000, Stommel & Stommel, 1983). The global human impact was such that massive crop failures and damage lead to famine, disease and social unrest in many parts of the world (Oppenheimer, 2003a, Self *et al.*, 1984).

1.4.4 Pinatubo eruption

The Pintubo eruption in the Philipines in 1991 created a giant umbrella cloud of minimum 35 km in altitude (Koyaguchi & Tokuno, 1993) and ejected 17 - 20 Mt of SO_2 in the middle to lower stratosphere (Bluth *et al.*, 1992, Robock *et al.*, 2007, Self *et al.*, 1998). The SO_2 formed sulphate aerosol cloud attained global coverage about 1 year after the eruption (persisting for up to 3 years) (Self *et al.*, 1998), decreasing the amount of Earth's net radiation and in effect producing a climate forcing. In response to this sulphuric cloud a temperature decrease in excess of 0.5° was observed in the northern hemisphere - NH (Dutton & Christy, 1992, Hansen *et al.*, 1993). Several studies (Farman *et al.* (1985), Hofmann & Solomon (1989), Prather (1992), Wolff & Mulvaney (1991), amongst others) have shown that sulphate aerosols in the stratosphere can catalyse 'heterogeneous reactions' (Eatough *et al.*, 1994) that affect global ozone abundance. Ozone depletion was indeed observed (partly due to another eruption; Mt. Hudson, Chile) over Antartica (Barton *et al.*, 1992, Doiron *et al.*, 1991), at altitudes of 9 - 11 km (Deshler *et al.*, 1992), along with an unprecedented increase in the "Ozone hole" of the southern hemisphere (SH) (Brasseur, 1992, Hofmann *et al.*, 1992, 1994a). In contrast to the rather global cooling, the observed winter warming (two winters following the eruption) in the NH is known to be a dynamic response to volcanically produced temperature gradients in the lower stratosphere (from aerosol heating and ozone depletion, and to reduced tropospheric storminess (Stenchikov *et al.*, 2002)). In response to a global cooling there is a decrease in the atmospheric water vapour (Soden *et al.*, 2002, Trenberth & Dai, 2007). Dai *et al.* (2004) link the eruption to the drought

conditions experienced by a significant percentage of the world, a year following the eruption. Overall, Trenberth & Dai (2007) indicate a relationship between the increase of sulphate aerosols in the atmosphere and the hydrological cycle. Since the eruption of Pinatubo, great interest amongst atmospheric scientists were sparked and a tremendous amount of research studies has since been conducted especially in the area of aerosol clouds and their global climatic effects enhancing our understanding and better climate model predictions.

1.4.5 Soufriere Hills, Montserrat

An example of an evacuation of a populated area due to the danger posed by a volcanic eruption in recent times is that of Soufriere Hills volcano located at Montserrat. Dormant for years, the Soufriere Hills erupted in July 1995. About two-thirds of the population (about 7000 people) was evacuated. Sparks & Young (2002) outline how between 1995 to 1997 Soufriere Hills had displayed a wide range of volcanic phenomena;

- generation of pyroclastic flows (through lave dome and fountain collapse),
- vulcanian and sub-plinian explosivity (accompanying tephra fall),
- entrance of pyroclastic flows into the sea,
- sector collapse with formation of a debris avalanche,
- a high-velocity pyroclastic density current and
- generation of lahars (a volcanic mud-flow, mixtures of water and tephra).

Pyroclastic surges had caused significant damage to large areas of vegetation and buildings in most part of the island (Baxter *et al.*, 2005, Cole & Stinton, 2010).

1.4.6 Eyjafjallajokull, Iceland

The eruptions of Eyjafjallajokull (located in Iceland, eruptions of 2010) 6-9 months after the event caused various physical symptoms (tightness in the chest, cough, phlegm, eye irritation, psychological morbidity symptoms and dyspnoea) in residents living in the exposed areas (Carlsen *et al.*, 2012). However, they are mostly remembered for disruptions they created to air travel across western and northern Europe. Although the

volcanic plume rarely rose above 7 km in altitude (Petersen *et al.*, 2012), it was unusual in two ways. One is the duration of the eruption (8 days) which contrasts with Plinian eruptions that lasts some hours rather than days (Mastin *et al.*, 2009, Sparks *et al.*, 1997). Second is the amount of ash dispersed to the south and south-east direction, over a large part of Europe (Gudmundsson *et al.*, 2012), even if the concentrations were quite low (Ansmann *et al.*, 2010, Pietruczuk *et al.*, 2010, Schumann *et al.*, 2011, Stohl *et al.*, 2011). This dispersion of ash resulted from a sustained eruption of fine ash and an increased frequency of the north-westerly winds, 71% in comparison to 49% on average during this season (Petersen *et al.*, 2012). The disruption to air traffic from the 15 to 23 April for Northern Europe followed by more airport closures and cancelled flights in the following weeks, affected millions of passengers and generated huge economic costs and losses (Harris *et al.*, 2012). Even such modest (Wilson *et al.*, 1978) eruptions have stressed the importance of hazard assessment and risk management (Gudmundsson *et al.*, 2012).

1.5 Outline

This chapter may be seen as a prelude to the thesis as it has simply introduced various eruption styles of volcanoes, magma compositions and viscosity and most importantly the basic eruption dynamics. Some basic information relating to conduit dynamics (where the processes leading to surface eruption of the volcano takes place) have been addressed followed by the surface volcanic explosion dynamics. This rather brief chapter also introduces to the reader various eruptions that have taken place in relative recent times, concentrating of their impacts on climate, air pollution, health issues amongst societies along with relative economic costs incurred.

The objective of this chapter was to introduce various vocabulary used by the scientists in the field, and to introduce the general ideas behind the dynamics of an eruption. For this reason, the objective of the thesis is presented in the following chapter proceeding the more interesting literature review on the relevant topics.

2

Volcanic eruption impacts and consequences to models

Contents

It is well known that eruptions can cause climatic variations and air pollution degradation as seen earlier in chapter 1 through various eruptions of recent times. Due to their direct and indirect impacts on our society, such natural events are frequently monitored and reported (Forsyth, 1988, Franklin, 1784, Wegmann, 2012). We have briefly seen in chapter 1 how depending on the location and size of the eruption, atmospheric conditions and volcanic gases released can create,

- physical effects on climate,
- health concerns amongst population,
- social effects through population migrations and displacements, and
- economic effects.

Although all these implications are of serious concern in our society, for the purpose of this thesis, we focus to develop the climate and air pollution impacts caused by volcanic gases due to injections into the stratosphere and troposphere respectively. Hence, we first develop a review of volcanic volatiles (section 2.1) including the role of these emissions in the stratosphere and troposphere. Section 2.2 discusses some models used by the scientific community for either research purposes or as an alert system. This section further guides the reader to the particular case of Piton de la Fournaise (volcano of study) and outlines the challenges faced by the scientific community (section 2.3). Finally, section 2.4 outlines the thesis objectives.

2.1 Volcanism and atmospheric chemistry

Emissions from volcanic eruptions are a significant source of atmospheric gases (and particles) which, influence the tropospheric and stratospheric trace-gas budgets. The quantity and nature of gases emitted from volcanoes depend on the amount and composition of magma (see section 1.2). The quantities of various gaseous species released during an eruption vary from one eruption to another.

Volcanoes contribute to the aerosol burden by two ways, emissions of SO_2 and the subsequent formation of sulphuric acid (H_2SO_4; which nucleate to form new aerosols or condense on pre-existing aerosols) and direct emissions of sulphate aerosols (discussed further in the next section). Volcanic ash particles have limited climatic impact due to their short lifetimes in the troposphere relative to the efficient dry deposition. Only sub-micron volcanic ash can participate to the climate forcing due to their relative smaller size and longer lifetimes (Langmann, 2014).

The most common and abundant volcanic gases released from eruptions are water vapour (H_2O), carbon dioxide (CO_2), sulphur dioxide (SO_2) and hydrogen sulphide (H_2S). H_2O represents 50 - 90 % by volume of gas phase and the contribution of CO_2

is estimated between 1 - 40 % by volume of gas (Textor *et al.* (2004) and references therein). Despite the relatively high abundances of H_2O and CO_2, the contribution of volcanic emissions to the global atmosphere for these two gases is limited due to their high background concentrations (Cadle, 1980, Schmincke, 1993, Textor *et al.*, 2004).

Textor *et al.* (2004) report that sulphur species contribute between 2 - 35 % by volume of gas phase, SO_2 and H_2S being the most abundant (much lower quantities of carbon disulphide (CS_2) and carbonyl sulphide (COS)). However, it might be worth noting that although COS are emitted in much lower quantities compared to SO_2 and H_2S, the residence time of COS in the atmosphere is of several years (Kjellstrom (1998), Steele *et al.* (2009), Textor *et al.* (2004), amongst others). COS is able to diffuse into the stratosphere due to it's relative inertness and form sulphate particles upon oxidisation (contributing to reactions which involve stratospheric ozone chemistry and implications for the atmospheric radiation balance) (Andreae & Crutzen, 1997, Schlesinger & Bernhardt, 2013, Steele *et al.*, 2009, Sturges *et al.*, 2001, Textor *et al.*, 2004).

This being said, SO_2 is one species emitted from volcanoes which has clearly been shown to have the potential to affect the climate system through it's reaction with OH (hydroxyl) radical in the gas phase or through oxidation in clouds (Robock, 2000). These reactions form a sulphate (H_2SO_4) aerosol cloud. Gaseous SO_2 is converted into H_2SO_4 aerosols within about 30 days (Coffey, 1996). SO_2 species are also an important oxidant in volcanic plumes (Robock, 2000). von Glasow (2010) show how the lifetimes of OH radicals are drastically reduced (to the point of being virtually absent) in a volcanic plume which contain high concentrations of SO_2. Sulphate aerosols have a lifetime of a few days in the troposphere (Mather *et al.*, 2003), whereas in the stratosphere these volcanic aerosols can persist for years (Robock, 2000) as there is no wet deposition.

The detection of bromine monoxide (BrO) by Bobrowski *et al.* (2003) from a non-explosive volcanic plume at Soufriere hills volcano, Montserrat, has directed great attention of the scientific community to the possible contributions of bromine oxides in the troposphere (Theys *et al.*, 2009). Furthermore, halogens are considered to play an important role in volcanic plume chemistry (von Glasow, 2010). BrO since it's detection by Bobrowski *et al.* (2003) has been measured in several other volcanic plumes (quiescent degassing) (Bobrowski *et al.* (2007), Kern *et al.* (2009), Oppenheimer (2006), Theys *et al.* (2009), amongst others). The inorganic halogen compounds are mainly

emitted as hydrogen chloride (HCl; reported by Textor *et al.* (2004) to contribute 1 - 10 % by volume of gas phase), hydrogen bromide (HBr; contributes 10^{-3} % by volume of gas phase) and hydrogen fluoride (HF, although HF is not always present; Delmelle & Stix (2000)) (Gerlach, 2004). A study by von Glasow (2010) show how high levels of reactive bromine in the plume (leading to extensive ozone (O_3) destruction) can be maintained for several days (Boichu *et al.*, 2011, Kelly *et al.*, 2013).

In comparatively lesser amounts, eruptions also emit mercury (Hg) vapour, nitrogen oxides (NOx) (von Glasow *et al.*, 2009) and even gold (Meeker *et al.*, 1991). Only a few measurements are available for emissions of Hg and NOx. The volcanic plume chemistry of these volatiles is also an active area of research (von Glasow *et al.*, 2009), along with their atmospheric impacts.

2.1.1 Volcanic eruptions as a climate forcing agent

Franklin (1784) and Mitchell (1961) were amongst the first to discuss the impact of volcanic eruptions on our climate (Robock, 2000). Since, countless research studies have been conducted and a brief summary of the known effects are outlined here.

Studies by Symons (1888) on the 1883 Krakatau eruption and Robock & Mass (1982) on the 1980 Mt. St. Helens eruption have shown how small amounts of tephra can remain in the stratosphere for up to a few weeks. However, very small climatic impacts are associated to this release (Wegmann, 2012).

On the other hand, the volatiles ejected during an eruption, especially SO_2 derivatives have been shown to considerably impact the climate and remain in the stratosphere for years (compared to a residence time of a few days in the troposphere) (Robock, 2000). The impact on climate is achieved through the reaction of SO_2 with H_2O and the OH (hydroxyl) radical, forming a sulphate (H_2SO_4) aerosol cloud. Due to the characteristic of the stratosphere and the associated winds, the aerosol cloud is advected around the globe in a few weeks (Robock, 2000, Wegmann, 2012). This process depends on the timing and geographical position of the eruption (Bluth *et al.*, 1992, Robock & Matson, 1983, Wegmann, 2012). The perturbation caused by the H_2SO_4 cloud through radiative effects is the main reason for climatic variations. The incoming short-wave solar radiation is scattered by this H_2SO_4 cloud, while a significant proportion is backscattered to space (Robock, 2000, Wegmann, 2012), thus increasing the Earth's albedo. The amount of scattering that takes place is dependent on two

factors, the wavelength of the incoming radiation and the size of the scattering particle (in this case the H_2SO_4 aerosol). Some solar radiation does get forward scattered by the aerosol clouds and deflected by the aerosols, it continues toward the Earth's surface at a different angle. Overall, there is a local solar heating through absorption as solar radiation is retained by a substance and converted into heat. Heat resulting from the absorption of incoming shortwave radiation is emitted as longwave radiation by the Earth and the atmosphere. Most of this outgoing radiation is absorbed by the aerosol cloud. On the whole, these processes have a net cooling effect on the lower atmosphere, while a local net heating is observed in the altitude of the aerosol cloud (Robock, 2000, Wegmann, 2012). The classic idea described here is depicted in Fig.(2.1).

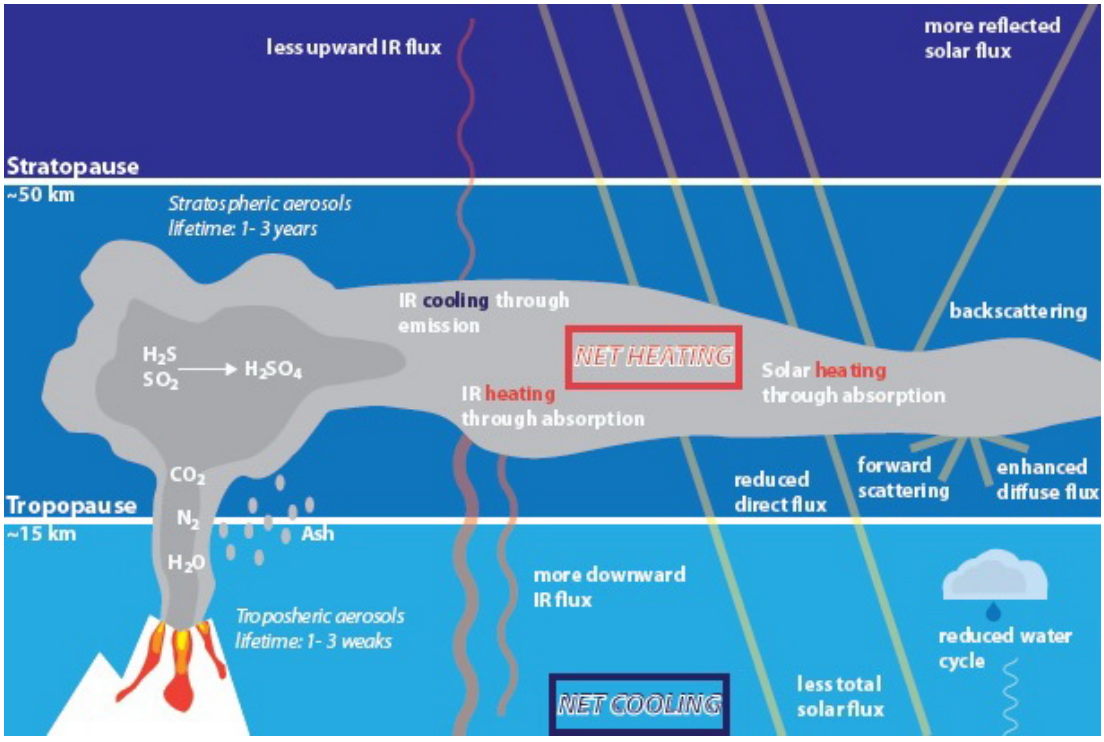

Figure 2.1: Climatic impacts - Schematic picture of climatic impacts after explosive volcanic eruptions on temperature and water cycle. Diagram taken from Wegmann (2012)

Apart from the effects on the Earth's albedo, volcanic aerosols in the stratosphere, can also influence the O_3 chemistry (Wegmann, 2012). O_3 is created through the process of photolysis, whereby, the solar radiation strikes oxygen (O_2) molecules causing the two O_2 atoms to split apart. When this free atom interacts with another O_2 molecule,

they join and form O_3 (also known as the Chapman's cycle). Furthermore, O_3 is also naturally broken down in the stratosphere by sunlight and through chemical reaction with various reaction surfaces such as compounds containing nitrogen, hydrogen and chlorine (Robock, 2000). However, all these factors are altered by volcanic aerosols (Wegmann, 2012). In general it is found that volcanic aerosol concentrations decrease O_3 concentrations. For example, H_2SO_4 aerosols act as a surface for chlorine activation and O_3 depletion. On the other hand, volcanic H_2SO_4 aerosols lead to an increase in surface UV (ultra violet) radiation. The net effect is considered such that, O_3 depletion lets more UV through the atmosphere than is backscattered by volcanic aerosols (Robock, 2000, Wegmann, 2012).

In the following sub-sections the most important effects of this perturbed radiation regime on temperature and precipitation are briefly discussed.

2.1.1.1 Influence on temperature

We have just seen how outgoing long-wave and incoming short-wave radiations are absorbed and deflected by the aerosol cloud. On the whole this leads to changes in the earth's temperature on shorter times scales, reducing Earth's surface temperature (Wegmann, 2012). Robock (2000) based on observational data states that this effect is limited to one to four days after the eruption.

On longer time scales, the reduced solar short-wave radiation reaching the Earth's surface leads to a global summer cooling (Robock, 2000). However, surface warming in the northern hemisphere (NH) during the winter season is also a feature of eruptions taken place in tropical regions as observed after the Pinatubo eruption of 1991 (Dutton & Christy, 1992, Hansen *et al.*, 1993, Robock, 2000, Wegmann, 2012). Although there are numerous theories on how winter warming is triggered (Robock, 2000, Wegmann, 2012), most common one links the stratosphere with observed surface temperature anomaly. Briefly, this theory suggests an intensification of the North Atlantic Oscillation (NAO)-like circulation (linked to the aerosol heating of the stratosphere) transporting more humid, warm oceanic air masses to the northern parts of Eurasia (Robock, 2000, Shindell *et al.*, 2004, Wegmann, 2012). A more greater but simplified explanation of this chain reaction between various atmospheric circulations can be found in Wegmann (2012).

2.1.1.2 Influence on water cycle

Volcanic eruption have significant impact on temperatures at regional and global scales. The links between the impacts of explosive eruptions on the global water cycle are far less developed (Li & Sharma, 2013, Trenberth & Dai, 2007, Wegmann, 2012). Especially, when comparing our current knowledge on the temperature anomalies produced as a result of volcanic aerosol loading.

Greater aerosol loading in the atmosphere results in greater number of cloud condensation nuclei (CCNs) and can prolong the life times of clouds, resulting in reduced precipitation. Furthermore, reduced incoming solar radiation by the aerosol cloud, results in less energy available for evaporation and hence, reduced water vapour in the atmosphere (Robock, 2000, Soden *et al.*, 2002, Trenberth & Dai, 2007, Wegmann, 2012). This further leads to a decrease in cloud cover, associating it to further reduced precipitation. However, this being said, it is known that during the "Year without summer" (see sect. 1.4.3), Europe had experienced more hail, rain and cloud cover (Auchmann *et al.*, 2012, Pfister, 1992, Trigo *et al.*, 2009, Wegmann, 2012).

Earlier studies such as those conducted by Ramanathan *et al.* (2001) and Yuan *et al.* (2011) connect greater aerosol loading of tropospheric plumes to a weaker hydrological cycle. Recently, Schmidt *et al.* (2012) through modelling studies investigated the cloud albedo radiative forcing under the impact of volcanic degassing for two cases. One for pre industrial era (hence lower tropospheric aerosol loading from anthropogenic sources) and 'present day' case. They found that the number of mean cloud droplets (annual average) over the global surface was higher for the pre-industrial era than the present day case (i.e 40% greater compared to 10% respectively). In turn, impacts on the global cloud albedo were also observed. Apart from the discussion on climatic impact through radiative forcing by tropospheric aerosol loading, Langmann (2014), also detail how climate can be affected through the modification of the global carbon cycle. The basic idea is, volcanic ash rich in trace metals and especially iron sink into the oceans providing marine plankton with nutrients. This further increases the oceanic 'bio-geochemical' (Langmann (2014)) processes, resulting in a plankton boom. This increase in surface organic-oceanic carbon, increases the downward carbon flux in oceans, and after a series of events within the oceans eventually increases the outgassing of carbon dioxide to the atmosphere. This process of phytoplankton growth has

been observed after the 2008 eruption of Kasatochi, Alaska (Langmann, 2014). There is still a huge gap in scientific research between the tropospheric volcanic ejecta and the hydrological cycle, along with the feedback between oceans and atmosphere after such eruptive events.

2.1.2 A focus on the tropospheric sulphur cycle

Numerous sources (biomass burnings, marine phytoplankton, fossil fuel burnings and of course volcanic activity) emit sulphur species in either gaseous or in the form of aerosols into the atmosphere (Schmidt, 2013)

SO_2 emitted into the atmosphere is lost through either dry deposition or oxidation. SO_2 is oxidised by the OH radicals in a series of reactions (R(2.1)-(2.5)) and in the presence water, sulphur trioxide (SO_3) is rapidly converted (R(2.6)) to H_2SO_4 (Harris *et al.*, 2012, Pham *et al.*, 1995).

$$SO_2 + OH + M \longrightarrow HSO_3 + M \tag{2.1}$$

$$SO_2 + OH + M \longrightarrow HOSO_2 + M \tag{2.2}$$

$$HSO_3 + OH \longrightarrow SO_3 + H_2O \tag{2.3}$$

$$HOSO_2 + OH \longrightarrow SO_3 + HO_2 \tag{2.4}$$

$$HSO_3 + O_2 \longrightarrow SO_3 + HO_2 \tag{2.5}$$

$$SO_3 + H_2O \longrightarrow H_2SO_4 \tag{2.6}$$

The characteristic rate of gas-phase reaction is a few % per hour during the day (Stockwell *et al.*, 1990). H_2SO_4 rapidly nucleates to either form new aerosols or sticks onto existing aerosols (Harris *et al.*, 2012, Schmidt, 2013). Dissolved hydrogen peroxide (H_2O_2) and ozone (O_3) further react with SO_2 in cloud droplets or pre-existing aerosols. Major multiphase processes occurring in aerosols or cloud water are:

$$SO_2(g) + H_2O_2 \longleftrightarrow SO_2 \cdot H_2O(aq) \tag{2.7}$$

$$SO_2 \cdot H_2O(aq) \longleftrightarrow H^+ + HSO_3^- \tag{2.8}$$

$$HSO_3^- \longleftrightarrow H^+ + SO_3^{2-}, \tag{2.9}$$

followed by the irreversible reaction

$$H_2O_2 + HSO_3^- + H^+ \longrightarrow SO_4^{2-} + 2H^+ + H_2O. \tag{2.10}$$

$$O_3(aq) + SO_2 \cdot H_2O(aq) \longrightarrow H^+ + HSO_4^- + O_2 \tag{2.11}$$

$$O_3(aq) + HSO_3^- \longrightarrow HSO_4^- + O_2 \tag{2.12}$$

$$O_3(aq) + SO_3^{2-} \longrightarrow SO_4^{2-} + O_2 \tag{2.13}$$

The main sink for nss-SO_4^- is through wet deposition, also known as acid rain when the concentrations of nss-SO_4^{2-} (non-sea salt sulphate, i.e. sulphate which is not directly emitted by sea bubles but created by reactions in the atmosphere) are high (Schmidt, 2013). There are also further 'heterogeneous reaction' (Eatough *et al.*, 1994) rarely treated in global models that simulate volcanic eruptions (Schmidt, 2013). Aqueous phase oxidation in clouds can contribute up to 80−90% of sulphate formations.

2.1.3 Volcanic eruptions and air pollution

Atmospheric pollution may be of both anthropogenic and natural origin (FinlaysonPitts & Pitts Jr., 1999, IPCC, 2000), however, one of the most important natural causes of air pollution are caused by volcanoes (both during and between eruptions in forms of fumeroles) (Mather *et al.*, 2003, Oppenheimer *et al.*, 2003b).

Natural sources (i.e. absence of explosive volcanic events) represents about $\frac{1}{4}$ of the total atmospheric sulphur budget (approximately $20 - 25$ TgS/year) (Graf *et al.*, 1997, Lucas & Akimoto, 2007). The sources of dimethyl-sulphide (DMS) oxidation over the oceans and SO_2 emitted directly by volcanoes (mildly-erupting/outgassing)

are reported by Lucas & Akimoto (2007) to be of about 15 TgS and $5 - 10$ TgS per year respectively. In general these two natural sources are of comparable magnitude (Graf *et al.*, 1997). However, the annual sulphur flux from volcanoes has been estimated by numerous studies (table 2 from Textor *et al.* (2004)) to be as little as 0.75 TgS (Kellogg *et al.*, 1972) up to 25 TgS (Lambert *et al.*, 1988). Two distinct types of volcanic activity contribute to the total volcanic SO_2 flux, namely, sporadic eruptions (Mt. Pinatubo, Philippines) and continuous degassing (e.g. Mt. Etna, Italy). Sporadic activity is estimated to contribute only 1% (averaged over long time-scales, e.g. 1 year) to the total tropospheric sulphur flux (Andres & Kasgnoc, 1998), hence, it is the continuous degassing of volcanoes that contributes the most to the global SO_2 budget. On the whole, Textor *et al.* (2004) outline how the uncertainty in volcanic sulphur emission flux is mainly due to the different extrapolation techniques employed and the inclusion of non-monitored volcanoes. Nonetheless, as stated by Schmidt *et al.* (2012) "distinguishing between the natural and anthropogenic sources are most definitely aided by such time-averaged logs of volcanic sulphur emissions".

We have already seen (section 2.1.1) how explosive eruptions, which are relatively well studied, have an impact on climate through the stratospheric loading of volcanic materials and volatiles. The stratospheric aerosol clouds discussed in the previous sections have been widely studied, however, in contrast, the impacts of such volatiles in the troposphere (from both an atmospheric and an environmental aspects) are poorly understood. The role of small eruptions and continuous degassing on the atmospheric composition has been largely recognised (Graf *et al.*, 1997, Mather *et al.*, 2003). Especially emissions from effusive volcanoes with sustained magmatic and hydrothermal degassing. Such eruptions are more frequent (along with their frequent emissions) compared to the rare, larger events. Mather *et al.* (2003) report volcanic SO_2 release from continuous eruptions comparable or even larger than the release by sporadic eruptions. The problematic concerning such eruptions is of a relatively different nature than the sporadic types. Primarily, in terms of their atmospheric and environmental impacts in the troposphere.

Amongst other gases, SO_2 emitted during volcanic activity (Bhugwant *et al.*, 2009) is of most concern, due it reacting chemically with sunlight, oxygen, dust particles, and water in the air to form a mixture of sulphate aerosols, and other oxidized species. The

interaction of these species in the atmosphere is through nucleation and / or condensation. Furthermore, secondary gas emissions such as those by HCl gas are created (mixture of hydrochloric acid and concentrated seawater) when lava flows encounter oceans, known as lava haze or laze. As for the emissions into the stratosphere, tropospheric aerosol loading also play an important role in the atmospheric radiation, directly by absorption and scattering of radiation of shorter wavelength, and indirectly by changing cloud cover and cloud properties (Albrecht, 1989, Hobbs *et al.*, 1982, Kaufman *et al.*, 2002, Lesouëf, 2010, Mather *et al.*, 2003). Anthropogenic sulphur emissions are extremely studied and are known to have a large effect on the Earth's radiative budget, however, Graf *et al.* (1998) concluded that volcanic sulphur emissions may too have similar degree of effect (despite the lower source strength in comparison) due to differences in their source altitudes. This is because anthropogenic emissions are generally entrained in the planetary boundary layer (the part of the atmosphere that interacts directly with the Earth's surface, stretching for up to approximately 2 km) where lifetimes of species tend to be low. However, volatiles from eruption types in discussion are emitted into the lower to upper free troposphere (Graf *et al.*, 1998, Mather *et al.*, 2003, Stevenson *et al.*, 2003) where lifetimes are relatively higher.

Aiuppa *et al.* (2007) discuss the chemical processing of SO_2 and H_2S in volcanic gas plumes. From direct sampling of plumes up to 10 km away from the source, Aiuppa *et al.* (2007) found that the plume was diluted as the distance from the vent increased. The gas concentrations measured at various distance from the vent decreased exponentially with increased distance. However, the SO_2 ratios to halogens such as HCl, HF and $H2S$ were found to be relatively constant throughout the plume ageing. Through 2 sets modelling experiments (cloud and cloud-free conditions), Aiuppa *et al.* (2007) showed that during cloud free regime, the HCl and HF concentrations are constant as the plume ages, as is also the case for SO_2. In the two types of cases, the HCl concentration was found to be constant. Aiuppa *et al.* (2007) suggests that despite the fact that under the cloudy case, one would expect the uptake of HCl in the cloud droplets, the measured concentration do not agree with their hypothesis. Even the $\frac{SO_2}{H_2S}$ for several km away from the source remained constant. Aiuppa *et al.* (2007) suggest that this is found to be true in modelling studies only when H_2S chemistry is not accounted for. Overall, it is not clear what reactions preserve this volatile during the plume advection.

Volcanic aerosols and gaseous compounds, in particular SO_2, can also be sources of risk to ecosystems and population's healths on a local to regional scales (Allen *et al.*, 2000, Baxter *et al.*, 1982, Delmelle *et al.*, 2001, Grattan *et al.*, 2003, Mannino *et al.*, 1996). Further discussion of these impacts are stated in the following sub-sections. Although brief descriptions of SO_2 derived pollutants and laze will be given, however, for the purpose of this PhD thesis, the main interest will remain that of SO_2 gases and their atmospheric impacts, while further directing this section towards PdF specific eruptions.

2.1.3.1 SO_2 fluxes and measuring tools

In the case of volcanic eruptions SO_2 fluxes provide scientists with useful indications regarding the activity itself. For example, one can obtain information regarding the dynamics of magma degassing (Theys *et al.* (2013) and references therein) i.e.

- precursor: changes in SO_2 flux are used as a precursor for eruptions,
- marker: gradual increase in SO_2 indicates replenishment of the magmatic system,
- marker: gradual decrease in SO_2 indicates the depletion of volatiles from magma
- marker: gradual decrease in SO_2 indicates end of an eruptive period

Furthermore, SO_2 flux evolution can help in (Theys *et al.*, 2013);

- quantification of the Earth's sulphur budget,
- quantification of other volatiles calculated by scaling their concentration ratio to SO_2, and
- establishing a 'total' gas emissions inventory of volcanoes.

For these reasons amongst others (e.g. modelling data input), the quantification of SO_2 fluxes is pertinent. As SO_2 has low background concentrations in the atmosphere, it is easy to identify from remote sensing techniques. There exist numerous observational tools that are deployed which aid in quantifying such a flux e.g. ground based stations, satellites, and aircraft measurements. Table 2.1 contains a list of some selected tools.

Table 2.1: Selected tools that aid in quantifying SO_2 fluxes

Instrument	Spatial resolution	Spectral range	Literature example
ASTER - Satellite	15 m / 30 m/ 90 m	0.5 - 11.6 μm	Urai (2004)
MODIS - Satellite	250 m / 500 m / 1 km	645 nm - 14.2 μm	Novak *et al.* (2008)
SEVERI - Satellite	1 km / 3 km	0.4 - 13.4 μm	Corradini *et al.* (2009)
IASI - Satellite	12 km	3.7 - 15.5 μm	Clarisse *et al.* (2008)
GOME2 - Satellite	80 $\times$ 40 km	240 - 793 nm	Rix *et al.* (2012)
OMI - Satellite	13 $\times$ 24 km	250 - 500 nm	Yang *et al.* (2007)
DOAS - Ground based	high	416 - 460 nm	Bobrowski *et al.* (2010)

Satellite provide SO_2 in a form of a vertical column (VC, expressed in Dobson unit, DU), representing the amount of SO_2 molecules in a column overhead per unit surface area. 1 DU represents 2.69 $\times$ 10^{16} molecules per cm^2 (Theys *et al.*, 2013). As the satellite pixel size is known the total mass of SO_2 is calculated from the retrieved VC. Furthermore, by applying certain scaling laws/algorithms to this calculated mass, one is able to estimate SO_2 flux. Height reached by volcanic plumes influences the types of techniques deployed for collecting useful SO_2 flux data.

Satellites operate at various resolutions, have different spatial coverage and orbits. Satellites are not only able to provide a global coverage, but are also able to provide data for non-monitored volcanoes. However, there are notably various difficulties that arise when estimating SO_2 mass flux (after Theys *et al.* (2013) and Boichu *et al.* (2013)). One of the largest uncertainties clearly lies in the pre-assumed constant plume height. As the SO_2 mass profile is highly variable throughout its height and over time, this results in a dispersion of SO_2 along different paths. Another important characteristic of this dispersion is that the concentrations of SO_2 depend on its chemical evolution. Hence, information on the transport and loss of SO_2 is compulsory from the release at the source point to the point of observation. Furthermore, this plume ageing largely depends on the various altitudes layers. Satellites may just partly cover the extend of the SO_2 dispersion and they are not able to detect weak and low-lying plumes. Furthermore, the limitations of the retreived VCs are highly limited in accuracy due to the possible aerosols and clouds present.

2.1.3.2 Volcanic smog, Laze and Acid rain

Hawaii's Kilauea Volcano has been in semi-continuous eruption since January 1983 providing large source of SO_2 (Porter *et al.*, 2002). It has since become a major health hazard for the inhabitants of the island. SO_2 is oxidised and converted to sulphate through reaction with OH and H_2O in clear sky or efficient reaction within clouds (FinlaysonPitts & Pitts Jr (1986), see section 2.1.2). The mixture of acidic aerosols and gases produce a hazy atmospheric conditions known as a volcanic smog, termed 'VOG' (Sutton *et al.*, 2000). This VOG then carried by trade winds and sea breeze is advected into a populated city such as Hilo (one of the cities located on the biggest of the Hawaiian Islands). Long terms effects of VOG are unknown, however, short term exposure to heavy VOG can affect pre-existing respiratory ailments. The two main components that trigger health effects are SO_2 and fine particles. Some physical complaints as experienced by some Hawaiian populations were headaches, sore throat, chest tightness, flu-like symptoms amongst others (Sutton *et al.*, 2000). Pattantyus & Businger (2014) demonstrate that the continuous emissions and subsequent formation of aerosols can have an impact on the micro-physics and storm development.

Another atmospheric hazard due to SO_2 through aqueous processes can lead to acid rain (Hofmann *et al.*, 1985, Stevenson *et al.*, 2003a). Simply, if the acid chemicals in the air are advected into areas where the weather is wet, the acids can fall to the ground in the form of rain, snow, fog, or mist (wet deposition). As this acidic water flows over and through the ground, it affects a variety of vegetation (through direct exposure and through changes in soil nutrients (Krug *et al.*, 1983, Likens *et al.*, 1972) and ecosystem (Gorham *et al.*, 1984). In areas where the weather is dry, the acid chemicals may become incorporated into dust or smoke and fall to the ground through dry deposition, sticking to the ground, buildings, homes, cars, and trees (Dolske, 1995). Dry deposited gases and particles can be washed from these surfaces by rainstorms, leading to increased run-off.

The third category is that of volcanic haze, called 'laze'. Extreme heat from lava entering the sea/ocean rapidly boils and vaporizes seawater, leading to a series of chemical reactions (Resing & Sansone, 1999). The boiling and reactions produce a large white plume, as shown in Fig.(2.2) for the eruption of PdF in April 2007. It contains a mixture of HCl acids (dominant) and HF acids (Kullman *et al.*, 1994). As

Figure 2.2: 6 April 2007 - Piton de la Fournaise - Left - three different plumes over the PdF during the collapse of the Dolomieu crater; SO_2 plume (orange), H_2O plume (white), ash plume (dark grey - due to crater collapse). Right - H_2O plume (laze) due to lava entering the ocean. Pictures taken from Tulet & Villeneuve (2011), and pictures taken by R.Delmas

laze is a local phenomena (near the sea/ocean) vegetation under the direct plume is affected (Kullman *et al.*, 1994). The HCl acid comes from the breakdown of seawater-derived chlorides during sudden boiling. Because the lava is largely degassed by the time it reaches the sea, any HCl coming from it is insignificant by comparison (Resing *et al.*, 2002).

High emissions of gases such as sulphur, chlorine and fluorine advected in the troposphere have huge damages in populations' health, vegetation, livestock and ecology in general (Delmelle *et al.*, 2002) as was the case with the Lakagigar eruption in Iceland.

2.1.3.3 The particular case of Piton de la Fournaise

Studies on volcanoes comparable to that of the PdF have highlighted an important degassing during eruptions. However, almost no study on the atmospheric transport of the plume had been conducted around the PdF volcano.

Volcanic Observatory of Piton de la Fournaise (OVPF) has been monitoring PdF for more than 20 years. Data collected from a large network of seismic sensors are primarily used to study the behaviour of the volcano along with forecasting and eruption analysis. However, only a limited attention had been paid to the potential dangers of gas and dust plumes exhaled during eruptions. However, the eruption of April 2007, showed that plumes heavily laden with SO_2, acid as well as fine particles of lava (Pele's hair)

and volcanic ash were likely to reach inhabited areas of the island, causing health and environmental problems.

The eruption of 2007 has been described by scientists as "the eruption of the century" for PdF for the following reasons (Lesouëf, 2010):

- The outflow of lava rarely observed above 8 - 10 $\times$ 10^6 m^3 reached an exceptional level, the total volume as estimated by OVPF as more than 180 $\times$ 10^6 m^3.
- The lava projections exceeded 100 m in altitude.
- At an average speed of 60 km/h the lava reached the ocean causing a plume of laze with an estimated height of more than 5 km on the 5th and 6th April (Tulet & Villeneuve, 2011).
- Fine particles of lava and Pele's hair were swept by the plume and dispersed throughout the island.
- Under the effect of solar radiation VOG was formed and acid rain was also observed which was associated with numerous environmental and health problems during the period of this atmospheric pollution.
- Ash plumes were also observed on the 6th April directly related to the collapse of the Dolomieu crater caused by the eruption.
- Consequently, the impact on Reunion island's population and the environment have also been considerable. The unhabited village of Tremblet was affected by ash fallout and lapilli (pyroclasts of size ranging from 2 to 64 mm) along with sulphur gases and acid rain. In some areas respiratory problems were experienced by the habitants related to high levels of sulphuric gas. Acid rain had damaging effects on crops along with groundwater pollution and also the distribution system of drinking water was impacted.

SO_2 concentration levels emitted in ambient air cause considerable environmental and sanitary impacts (EPA, 2012, MEDDTL, 2011) as seen from the April 2007 eruption of PdF. Since a decade the World Health Organization (WHO), the European Community and the French Ministry of Environment (MEDDTL: Ministere de l'Écologie, du Developpement Durable, du Transport et du Logement) have established

SO_2 guideline levels, following the severity of the impact of this pollutant on human health and on the environment. For the protection of human health, the hourly limit values of 350 $\mu g/m^3$ are not to be exceeded more than 24 times a year, and daily limit value of 125 $\mu g/m^3$ are not be exceeded more than 3 times a calender year (MEDDTL, 2011). MEDDTL also set the yearly "limit value for the protection of ecosystem" (LV) at 20 g/m3. Furthermore, the quality objective (QO) threshold is set to 50 $\mu g/m^3$ (annual average), the "recommendation and information threshold" (SRI) is set to 300 $\mu g/m^3$ (hourly average) and finally the "alert threshold" (SA) is set to 500 $\mu g/m^3$ (hourly average during 3 consecutive hours). The ORA (Observatoire Reunionnais de l'Air) and MEDDTL however, do recognise that Reunion Island is under the influence of volcanic emissions and this threshold may be exceeded, when PdF is in eruption. It is thus important to conduct the monitoring of this pollutant, in order to take the adequate measures of air pollution and also to study its long-term trends and effects.

In a rather comprehensive study by Bhugwant *et al.* (2009, 2011), continuous SO_2 concentrations were used measured by ORA (Observatoire Reunionnais de l'Air) between 2 eruptions of PdF, namely, December 2005 and April 2007 (for greater detail see Bhugwant *et al.* (2011)). They analysed the spatial distribution of SO_2 concentration and its temporal evolution during several eruptions of PdF, in conjunction with other parameters, such as seismic and meteorological data. Bhugwant *et al.* (2009) established a correlation between the seismic variability and the SO_2 concentration variation in the vicinity of the volcano. Furthermore, they showed that the rainfall influences the SO_2 spatial variability in particular, over the eastern to northern regions of the island, via scavenging processes. Lesouëf (2010) and Bhugwant *et al.* (2009) have both demonstrated how the spatial distribution of SO_2 particularly arises due to the island's topography coupled with trade winds and land/sea breezes. Using MODIS (Moderate Resolution Imaging Spectroradiometer) satellite imagery and superimposed horizontal winds extracted from the atmospheric model ALADIN-Réunion of Météo-France, Lesouëf (2010) show how the volcanic plume of April 2007 prevailed in the boundary layer. The volcanic plume contoured the island from the south and was transported to the west coast by lower altitude winds of the south-east and south-west region. This corresponds well to the synoptic flow of terrain perturbed trade winds (Lesouëf, 2010). This transport was also captured by the simulations conducted by Lesouëf (2010) and further showed how the tracer plume is trapped in the wake of the island (in the west

region) due to the presence of wake vortices that tend to fold the plume to the land. Importantly, Bhugwant *et al.* (2009) showed that although the QO and LV, based on an annual average were not exceeded over the island during 2005-2010, however, SRI as well as the SA were both exceeded in some inhabited regions close to the volcano during the April-May 2007 eruption.

On the whole, Lesouëf (2010) demonstrated how Meso-NH (non-hydrostatic meso-scale atmospheric model, Lafore *et al.* (1998)) model was capable of reproducing, at least in a qualitative way the SO_2 concentrations at different regions of the island (despite the non-activation of chemistry, i.e. absence of numerical reaction schemes related to various transformation of SO_2 in the model). Importantly, Lesouëf (2010) simulations highlight how the transport phenomenon is the main cause of contamination of half of the island placed downwind. It is hence clear that the implications for human health and environmental changes, on local-to-regional scale are considerable, even during the eruptions of PdF.

2.2 Volcanic columns and ash cloud: models and challenges

Volcanic eruptions are unsteady multiphase phenomena. They encircle processes across a great number of scales, from molecular and microscopic to macroscopic, synoptic and global (Textor *et al.*, 2005). A wide variety of processes in volcanic eruptions as outlined below are inter-related (Textor *et al.*, 2005):

- Ascent dynamics and processes such as fragmentation, chemical reactions and mass transfer below the surface of the earth are studied by conduit flow models.
- The atmospheric dispersal of the erupted volatiles during rapid processes as such that occur in the jet region of the eruption column are examined by high energy plume models.
- In the vicinity of the eruption, buoyant column models examine the sedimentation and ash dispersal from the eruption column, along with the dynamics of the column itself.

- Ash tracking in dispersal models is linked to the atmospheric dispersion of volcanic clouds. Such model largely focus on long-range prediction of ash location for aviation safety.

- The climate impact is investigated using global models.

Due to the wide variety of processes associated to volcanic eruptions in both space and time, a single model cannot encompass all relevant processes (Textor *et al.*, 2005). Therefore, various models exist that study the impacts of eruptions on the atmosphere and of course examine the eruption dynamics itself. Typically, as seen above one temporal and spatial scale is used to study an aspect related to volcanic eruptions.

For the purpose of this PhD, in this section after Textor *et al.* (2005), we will discover processes related to volcanic columns, but most importantly, we will discover why these processes are a great challenge in terms of modelling. Along the way a few examples of various model that exist are outlined with some examples on the kind of processes they treat. However, this is by far not a complete list of models that exist.

2.2.1 Atmospheric dispersal processes: high energy plume models

Transient multi-phase flow models (magnitude and direction of a flow changes with time, as opposed to steady-state flow) are dedicated to rapid and non-equilibrium processes induced by ejection of gas-particle mixture at high speed, high pressure, high temperature and a wide range of particle grain sizes. In a multiphase flow-approach the eruptive mixtures are treated as non-homogeneous flows, i.e. the volume occupied by a generic gaseous, solid, or liquid phase cannot be occupied at the same position in time and space by the remaining phases (Neri & Macedonio, 1996, Neri *et al.*, 2003, Textor *et al.*, 2005, Valentine & Wohletz, 1989, Wohletz *et al.*, 1984). Such models have only been used to study the rapid and local processes due them being computationally very demanding.

The initial velocity of materials supplied to the volcanic eruption column is constrained by the decompression process of a volcanic jet (Gilbert & Sparks, 1998). During the initial stages of an eruption, following the initial explosion, a shock wave propagates ahead of the eruptive mixture into the atmosphere. Over the first 10 - 30 seconds during the abrupt changes in pressure, a sequence of non-linear waves develop as illustrated by Dobran *et al.* (1993), namely, rarefaction waves (accompanied by an expansion of

the medium) and compression waves (accompanied by compression of the medium). Models such as the numerical 2D/3D PDAC (Pyroclastic Dispersal Analysis Code) are able to illustrate the complex patterns of volcanic jets, which are characterised by an interplay between rarefaction and compression waves (Esposti Ongaro *et al.*, 2007, Neri *et al.*, 2003). It has also been used to simulate the formation of pyroclastic density currents by the collapse of the volcanic column and their propagation over the actual volcano topography by Neri *et al.* (2007).

Another example of a multi-phase flow model is the 2D/3D Lagrangian particle model (LPAC), which has been used for the dynamics of clasts ejected during explosive eruptions (de' Michieli Vitturi *et al.*, 2010). Such a study has highlighted the key role played by the background flow field, pressure and drag forces on the large particle dynamics during explosive eruptions. Another regime studied using such models is the unstable behaviour between fully convective and fully collapsing regimes (Di Muro *et al.*, 2004, Neri *et al.*, 2002). The output variables of such models include; gas pressure, gas velocity, gas temperature, particle volume fraction as a function of particle size and particle velocities (de' Michieli Vitturi *et al.*, 2010). High energy plumes create deposits and such plumes are multi-scale processes in terms of formation, dispersion and collapses.

More information and references for various studies of such regimes can be found in Textor *et al.* (2005).

2.2.2 Buoyant volcanic column and proximal dynamics: buoyant column and dispersal models

Numerical simulations of the buoyant volcanic column and its dispersal require description on the conditions both within the eruption column and in its local environment. Equations needed to describe the eruption dynamics are complicated due to the plume characteristics e.g. high velocities, temperatures and particle concentrations in an eruption column (Textor *et al.*, 2005). Such complex dynamics are not included in models discussed in previous sections, due to the need for much greater computational time which limit the application of multiphase models to large domain and long time scales needed for dispersal.

There has been a great evolution in numerical models of volcanic columns and ash clouds over the last few decades. The first models introduced to the scientific

community were widely, 1D steady-state model (Wilson *et al.* (1978), Woods (1988), amongst others), built on the seminal 'top hat' formalism published by Morton *et al.* (1956). Useful for first estimations of plume dynamics, like vertical density and velocity profiles, later models such as those by Glaze & Baloga (1996), Glaze *et al.* (1997), Tabazadeh & Turco (1993) were applied to study influence of atmospheric conditions, estimations of water vapour and volcanic gases injections to high altitudes.

In recent times both the rise of the eruption column from the lithosphere to the stratosphere, and the dispersal of the plume of volcanic particles and gases have been simulated with the same model, ATHAM (Active Tracer High resolution Atmospheric Model (Herzog *et al.*, 1998, Oberhuber *et al.*, 1998). ATHAM is a 3D non-hydrostatic plume model which resolves prognostic equations for meteorological, micro-physical and chemical variables (including aerosols). It is used at high horizontal resolution (100 - 500 m) and over large domains. Hot mixtures of gas and aerosols is prescribed at the surface of the model to mimic volcanic forcing. A turbulence closure scheme describes sub-scale processes in the eruption column (Herzog & Oberhuber, 2003). In order to perform numerical simulations, the equation system describing the eruption are approximated, by discretisation in time and space, and by applying advanced numerical techniques to integrate the system (Textor *et al.*, 2005).

Far majority of these models are used for explosive eruptions. Effusive eruptions have not been modelled to a great extent. Such models can provide greater understanding into the in plume chemistry and the ageing of tropospheric volcanic emissions (an area of research not well characterised).

2.2.3 Ash dispersal at regional, continental and global scale

Two types of models exist at regional to global scales. There are operational models used by the Volcanic Ash Advisory Centres (VAACs) and research models (e.g. WRF-CHEM coupled with volcano database by Grell *et al.* (2005), Meso-NH model (Lafore *et al.*, 1998) coupled with ORILAM chemistry module by Tulet *et al.* (2003, 2005, 2006), global circulation model (GCM) with coupled chemistry as used by Graf *et al.* (1997)). A common feature of such models is that they do not resolve the eruption column dynamics.

There are numerous ash tracking models used for predicting the long-range dispersion of volcanic ash clouds to primarily prevent ash-aircraft interactions. Most of

these models are built by two scientific communities, volcanological or meteorological. Far-field dispersal of ash and volcanic volatiles are determined by atmospheric motions described by the advection-diffusion equation (Textor *et al.*, 2005). There also exist Hybrid models which use both Lagrangian and Eulerian formulation such as HYSPLIT (Draxler & Hess, 1997) and is in use by one of the VAACs located in Washington D.C, U.S.A. In order to mitigate volcanic ash hazards, ash tracking models are used by VAAC and serve as an interface between volcano observatories, meteorological agencies and air traffic control centres. Such models simulate the movement of airborne ash using meteorological field data sets from observations or from other model simulations (Textor *et al.*, 2005). This is to say that the input sources of such models are mostly either from direct observations, field works, sample distributions, satellite observations and/or simulation outputs amongst other techniques.

The input parameters of dispersal model are, height of the eruption column, the mass eruption rate (MER), erupted mass, and-or particle characterisation (size, density, shapes etc.). A database containing volcanic eruption characteristics developed by Mastin *et al.* (2009) is used as an input data for VAAC or regional models such as WRF-CHEM. However, Mastin *et al.* (2009) outline how there are significant uncertainties on ash prediction by VAACs within a factor of 10 due to the relation between mass flow rate estimates from plume heights. A Eulerian model MOCAGE (VAAC model used in Toulouse, France; Josse *et al.* (1994)) was tested by Kaminski *et al.* (2011) for 2 different ash injection rates (the only input parameter that was different by a factor of 10). They found that although the shape of ash dispersal by the two cases were comparable, the ash concentration (in the zone of highest density) was different by a factor of 10. Mastin *et al.* (2009) used the Eulerian ASH3D ash dispersal model (an advection-diffusion model) to examine the discrepancy between observed and modelled ash cloud size. For this particular study only the wind advection was activated (with numerical diffusion). In one case a constant plume height was maintained throughout the simulation (i.e. a constant MER), in contrast, the other used a time-varying plume height following radar measurements (hence, the MER was too adjusted using Mastin *et al.* (2009)). A greatly reduced eruption intensity resulted in a reduced ash cloud size by about 20%. Further more a reduced model resolution of about a third (affecting inturn the numerical diffusion of the model), further reduced the ash cloud size by another 50%. However, reducing the MER by a factor of 10 did not appear to have

any significant influence on the modelled as cloud area. Hence Mastin *et al.* (2009) infer that ash cloud concentrations are highly sensitive to Eulerian model resolution (and hence numerical diffusion), and input parameter of eruption cloud height and MER history. On the whole, the tested scenarios by Kaminski *et al.* (2011), Mastin *et al.* (2009) demonstrate how variations in the input source parameters have a direct impact on modelled ash dispersion estimates. As suggested by both Mastin *et al.* (2009) and Kaminski *et al.* (2011), the differences between VAAC model predictions and observations during the Eyjafjallajokull eruption of 2010 may have resulted due to errors in the source input data used by VAAC forecasting.

HAZMAP (Macedonio *et al.*, 2005) and tephra2 (Bonadonna *et al.*, 2005) developed by the volcanological community are analytical advection-diffusion models for tephra deposition. Such models sufficiently simplify the wind fields so that the tephra thickness is described by an explicit mathematical expression and since no numerical integration is required, these models execute faster than Lagrangian or Eulerian advection-diffusion models (Schwaiger *et al.*, 2012). Finally, in a different class we have models developed by the meteorological community such as REMOTE (Langmann *et al.*, 2009) and the Weather Research and Forecasting model (WRF-CHEM) models that are used for volcanic ash tracking, included in the numerical weather prediction models. These models can simulate the full dynamics of the atmosphere coupled with effects such as ash loading and SO_2 conentrations. However, such models require a huge computational resource (Schwaiger *et al.*, 2012).

2.2.4 Overview

There has been an overall progression in models and numerical simulations in terms of advection and dispersion of plumes characterized by their numerical framework (Eulerian versus Lagrangian) (Schwaiger *et al.*, 2012). Lagrangian models (used by most VAACs) have two important advantage over Eulerian models, firstly, computationally less expensive and secondly, they display less numerical diffusion (Schwaiger *et al.*, 2012). However, since Lagrangian models use number density of the particles (i.e. the number of specified objects per unit volume) to calculate the total mass loading and concentrations of aerosols, some inaccuracy in calculations may be observed (Schwaiger *et al.*, 2012). Especially, if the region in investigation has low particles. In contrast, Eulerian models calculate the evolution of the concentration of ash at every point in the

model domain, resulting in a more direct calculation. Hence, such model framework do not suffer from losses in accuracy (Schwaiger *et al.*, 2012).

Overall in terms of tractable operational calulations and research investigations on global grids, Eulerian models are best suited for 3D set-up (Schwaiger *et al.*, 2012). Especially, with the increasing computer resources, the plume dynamics and global coverage could be represented with such Eulerian models.

Our modelling capabilities have been largely applied to stratospheric injection of atmospheric loading. There is a clear evidence that such transports affect the Earth's radiation budget and hence the the climate (Robock, 2000). The stratospheric chemical cycle in terms of ozone depletion is also well documented. Although there is some inference that volcanic emissions could also have an impact on the hydrological cycle (Langmann, 2014, Ramanathan *et al.*, 2001, Schmidt *et al.*, 2012, Yuan *et al.*, 2011), there is still a clear gap in our understanding linking the two. In contrast, the tropospheric emissions and their impacts have relatively recently come into discussion. There is a great lack in understanding the fate of tropospheric plumes (Delmelle *et al.*, 2002, Mather *et al.*, 2003). The areas of active research include, tropospheric plume chemistry and plume ageing. A main reason is due to the lack of data from sporadic and quiet degassing volcanoes along with the complex chemical reactions within high temperature plumes (Aiuppa *et al.*, 2007). Another constraint is the lack of monitoring data for majority of the world's volcanoes in general. However, it is recognised that tropospheric aerosol loading too have an impact on the earth's radiative budget (Langmann, 2014).

Prescription of initial spatial distribution of the ash cloud is also vital, in particular the cloud height and its variation with different atmospheric conditions, as it is a crucial parameter for accurately forecasting ash dispersion (Textor *et al.*, 2005, Tupper *et al.*, 2003). Furthermore, the ash dispersal models often have coarse resolutions and small scale dynamics e.g: thunderstorms are not captured by the model. Such models also do not include particle removal by precipitation, or ash aggregation (Textor *et al.*, 2005, Tupper *et al.*, 2003). Due to such restrictions of the model, forecasts by such models are not accurate and can lead to substantial over or under warning, enhancing risks and economic costs (Lacasse *et al.*, 2004, Rose *et al.*, 2013).

One option illustrated by Patra *et al.* (2012) is the use of Lagrangian models to determine the plume height. Lagrangian model is initialising with magmatic tempera-

ture, vent diameter, eruptive velocity, material density along with atmospheric profiles of water vapour, temperature, density etc. Through several iterations of the model, with various possible eruptive inputs, Patra *et al.* (2012) determine from the model the likely range of eruption rates that would have caused the plume to reach a certain observed height, during an event. This height is then used an input to VATD. However, a more efficient method would be to represent the injection height in the models rather than having them prescribed.

2.3 On the importance of plume heights

In 2011, the International Volcanic Ash Task Force (IVATF) emphasized that: "The most important areas of future work comprises such challenging issues as increased monitoring of active or potentially active volcanoes, enhanced volcanic ash cloud detection and prediction capabilities and better knowledge of the hazardous health effects to aircraft occupants of volcanic gases, including SO_2". Currently, none of the Volcanic Ash Advisory Centers (VAAC) are required to forecast volcanic SO_2 dispersion operationally (VANHEIM, 2013).

While eruptive stratospheric plumes and their atmospheric impacts have been extensively studied in the past (Robock & Oppenheimer, 2003, Robock, 2000), the impacts of tropospheric emissions from volcanoes are far less well-characterised.

On the whole, in terms of aviation safety, as well as for air quality and climate studies, the correct determination of the volcanic plume height (vertical zone in which a buoyant plume begins to transport horizontally away from its source) is of a central issue. The height reached by volcanic material upon ejection determine the ageing, dispersal and impact of the volcanic plume.

Direct measurements of the eruption intensity or mass flow rates (MER) are challenging. A common approach is to use observed column heights to derive MER (Pyle, 1989) based on a simple empirical relationship where, for a given temperature, the column height is proportional to the fourth root of the MER (Morton *et al.*, 1956). Degruyter & Bonadonna (2012) pointed the large uncertainties on the prediction of ash dispersal due to this hypothesis. This approach has serious limitations which can lead to large uncertainties. Ripepe *et al.* (2013) show that this relationship is not pertinent anymore for bent-over plumes. Tupper *et al.* (2009) report on the sensitivity of

the plume height to the environment. Simulation with ATHAM model produced very different plume heights with the same eruption intensity; a deep convective volcanic plume in the moist tropics (plume altitude of 15 - 20 km), in contrast to the lower eruption height in dry sub-polar environment.

We have also seen how volcanic ash transport and dispersion models (VATDs) are used to forecast the location and movement of ash clouds over hours to days in order to define hazards to aircraft and to communities downwind. Height reached by eruption columns is an important input parameter (Mastin *et al.*, 2009). Hence, accurately characterizing these plumes and their vertical structures is necessary to produce useful local-, regional-, and national-scale forecasts.

2.4 Thesis objectives

From the above review it is clear that majority, if not all of these models are primarily used for explosive volcanic eruptions. There appears to be a clear lack of a forecasting models and numerical simulations in terms of air quality on local to regional scales. In case of an eruption, the lack of such a forecasting model clearly means lack of 'alertness' to populations in the vicinity and regional area of the volcano.

The study by Lesouëf (2010) is very encouraging, as it shows the ability of Meso-NH model to reproduce the observed atmospheric phenomena during the April 2007 eruption of PdF. Hence, the results from Lesouëf (2010) has paved the way for a project that aims to develop a forecasting system of volcanic plumes at a regional scale. Therefore, the overall challenge of this thesis is to take a step forward in building a forecasting system for atmospheric dispersion at local scale that is activated in case of an eruption and most importantly, it is quickly executable.

For this purpose there is a need for a deep injection model suited to be implemented in a $\sim$ 1 km resolution model, with the capability to forecast the plume in the current atmospheric environment. The principle aim of this study is to model the deep injections of volcanic emissions in form of a passive tracer into the low to mid troposphere developed as consequence of intense but very localized input of sensible heat near eruptive vents. For this purpose the study relies on a multi-scale approach with a 3D meso-scale model Meso-NH (described in chapter 3). The model allows simulations of the atmosphere dynamics and chemistry over a large range of scales, from

Large Eddy Simulations of buoyant plumes, to simulation of pollution dispersion over the whole island. The grid-nesting capability allows for running simultaneously several models at different scales and resolutions.

The strategy for this study is such, a case study of Piton de la Fournaise eruption of 2010 is used, whereby a parameterised column model based on a modified updraft model for shallow convection is proposed. This parameterisation is used in an idealised case and validated against a Large Eddy Simulation (LES). Such strategy whereby validation of a convective parameterisation is performed using LES has been used in the meteorological community during the last 20 years. Hourdin *et al.* (2002) state how LES are particularly well adapted to the study of the convective boundary layer for which resolved large-scale motions are believed to play a dominant role. There are two important advantages as stated by Hourdin *et al.* (2002) in validating a parameterization against LES rather than observations. The first one is that the experimental conditions are precisely known and can easily be modified. The second one is easier access to specific diagnosis.

As a secondary aim, this parameterisation is further tested in a real-case 3D set-up, and first results of the SO_2 passive tracer injected in the modelled volcanic updraft is compared against SO_2 data collected from ground stations around the Island.

3

1D idealised simulation and parameterisation of January 2010 PdF eruption

Contents

In this chapter, we firstly introduce the model used in this study. In section 1 the parameterisation of shallow convection scheme implemented in Meso-NH is detailed. Furthermore the importance of entrainment through turbulent mixing, a key parameter in convective plumes is addressed. Sections 2 and 3 of this chapter is an article accepted by the 'Geoscientific Model Development'−GMD journal and details the modifications of the shallow convection scheme. The chapter continues with results and analysis section ending with conclusions.

3.1 The atmospheric model

The model used to undertake this study is the research Meso-NH (Mesoscale Non-Hydrostatic) model, (Lafore *et al.*, 1998), enables to simulate convective motion and flow over sharp topography. Meso-NH jointly developed by the Laboratoire dAerologie (LA) and the Centre National de Recherches Meteorologiques (CNRM), is an anelastic eulerian model.

The non-hydrostatic approximation of Meso-NH allows simulating atmospheric motion from the large meso-scale down to the micro-scale, known as Large eddies. The governing equations follow a Eulerian system of partial differential equations, through different mechanisms (e.g. advection, Coriolis force, pressure force, turbulence and diabatic sources). The following variables are prognosed: the three components of the velocity u, v and w, the dry potential temperature (θ), the various mixing ratios of the different water species, r_*, and the turbulent kinetic energy (TKE), e, along with, an arbitrary number of scalars variables, s_*. Meso-NH model version MNH-4-9-3 is used in this study.

A number of parameterisations are used in the model such that processes that occur at sub-grid scales can be well represented. A Rapid Radiative Transfer Model (Mlawer *et al.*, 1997) is used to calculate the radiation. The energy exchanges between the surface and the lower atmospheric levels are parameterised according to the SURFEX scheme described in Masson *et al.* (2013). There are four possible surface types allowed within the model (i.e. natural surfaces, urban areas, oceans and lakes) and the natural land surfaces are represented by the ISBA (Interactions Soil-Biosphere-Atmosphere)

scheme (Noilhan & Mahfouf, 1996) The shallow convective processes are parameterised according to the formulation of Pergaud *et al.* (2009), discussed in greater detail below. For the purpose of this study the deep convective parameterisation is de-activated. The turbulence scheme is a 1.5 order prognostic turbulence scheme (Cuxart *et al.*, 2000), based on a prognostic equation for sub-grid kinetic energy. The LES version of the model uses the 3-D turbulence scheme while 1D simulations uses a purely vertical scheme. Finally, the micro-physics follows the work of Pinty & Jabouille (1998).

Meso-NH can be used in either real case simulations or an ideal case set up. Furthermore, one can either introduce topographical files within the model or simply use it in a flat terrain configuration. In the case when topographic files are introduced, a geometric height is computed based on a terrain-following coordinate transformation. The initial and lateral conditions in the model can be constrained by the user by providing radio-soundings or operational re-analyses fields. The model further has 'grid-nesting' capabilities enabling simultaneous two-way simulations for models of various resolutions. A chemical module is also available for on-line coupling. Further information and model related documents can be found on the model's website: http://mesonh.aero.obs-mip.fr/mesonh/.

Meso-NH has already been used as research tool for simulating forest fires. Simulations of atmospheric plumes from intense heat source points have been performed using Meso-NH to represent the impact of forest fires on the dynamic and chemistry of the atmosphere. A study by Strada *et al.* (2012a) simulated forest fire plumes at 1 km resolution which showed good agreement with observations where high sensitivity to the atmospheric stability was observed. Simulations of the eruption column dynamics, chemistry dispersal in the proximal environment and the volcanic cloud tracking at regional scale rely on similar numerical and conceptual approaches as the ones used for the study of the forest fire plumes.

3.1.1 Parametrisations for shallow convection

For the purpose of this thesis two fundamental parameterisations in Meso-NH are presented in further detail, namely, the turbulence scheme known as Eddy Diffusivity (ED) scheme and the Mass-Flux (MF) scheme used in shallow convection. The combined EDMF (Eddy-Diffusivity / Mass Flux) scheme (Hourdin *et al.*, 2002, Pergaud *et al.*, 2009, Siebesma *et al.*, 2007, Soares *et al.*, 2004) accounts for both the local and

the non-local turbulent transport for cloudy shallow convection and dry convection. The vertical turbulent fluxes in the model are dealt with by ED scheme, while the bulk MF approach is commonly used to parametrise shallow and deep convection. The EDMF combined approach is particularly adapted for simulations at resolution coarser than 1 km (Honnert *et al.*, 2011).

In general the prognostic equation for a scalar variable ϕ can be written as following,

$$\frac{\partial \bar{\phi}}{\partial t} = -\frac{\partial \overline{w'\phi'}}{\partial z} + F_\phi \tag{3.1}$$

where w is the vertical velocity and F_Φ is a source term. In the EDMF framework, the vertical turbulent flux of a conservative variable ϕ is defined as

$$\overline{w'\phi'} = -K_\phi \frac{\partial \bar{\phi}}{\partial z} + \frac{M_u}{\rho}(\phi_u - \bar{\phi}) \tag{3.2}$$

where ρ is the air density, K_ϕ is the turbulent diffusivity coefficient for the variable ϕ, M_u is the convective mass flux in the updraft, defined as $M_u = \rho a_u w_u$, (where a_u is the updraft fractional area, w_u is the vertical velocity in the updraft). Finally, $\bar{\phi}$ is the mean value at he grid scale and ϕ_u is the updraft value of the variable ϕ. In such a formulation, the updraft size is assumed to be very small compared to the grid size, such that the environmental values are considered equal to the mean values (Pergaud *et al.*, 2009). For high resolutions (sub-kilometric) the mass flux is removed from the above term (Eq.(3.2)) as the convective boundary layer is fully resolved by the LES equations.

3.1.1.1 Parameterised turbulent ED terms

The prognostic equation in 3.2 is solved by introducing additional parameterisations for the ED coefficient K_ϕ. After Cuxart *et al.* (2000), K_ϕ is proportional to a mixing length (L, a key parameter) and a velocity scale (which is the square root of the Turbulent Kinetic Energy (TKE, e)). Hence, it is described as,

$$K_\phi = C_\phi L \sqrt{e}, \tag{3.3}$$

and here, C_ϕ is a constant coefficient.

A progonostic equation for TKE is used in the model and it is assumed that there is a local balance between the advection, shear, buoyancy, diffusion and dissipation terms.

There are two choices of mixing length formulations and it is the only parameter that varies between the LES and the meso-scale configuration. In a standard 3D LES framework, the closure of the system relies on the expression as defined in Eq.(3.4)

$$L = (\Delta x \Delta y \Delta z)^{1/3}, \tag{3.4}$$

This expression defines the size L at which energy is supplied to the turbulence, within the so-called inertial range, the largest energetic eddies L feed energy of the turbulence down to scales where the dissipation mechanism starts to dominate. Hence, the largest unresolved eddies are by definition, the size of the grid cell.

The vertical turbulent mixing in meso-scale application is assumed to be the dominating flux compared to the horizontal mixing (i.e. turbulent fluxes are assumed purely vertical down to a resolution of 1 km). For this case, the Bougeault & Lacarrere (1989) formulation is used. It computes L at every vertical level, since the vertical resolution is higher than the horizontal counterpart. For a given level, L is defined as a function of the distance that a parcel of air, having the kinetic energy of the initial level, can travel upwards l_{up} or downwards l_{down}, before being stopped by buoyancy effects (i.e. the parcel will stop when the cumulated buoyancy accelerations equal the initial kinetic energy). Hence, the length-scale for meso-scale 'mode' is defined as

$$L = \sqrt{l_{up} l_{down}}. \tag{3.5}$$

This method allows the length-scale at any level to be affected not only by the stability at this level, but also by non-local effect of remote stable zones or the presence of ground.

3.1.1.2 The Mass-Flux (MF) scheme

In a grid box multiple convective updrafts can exist, the basic idea of a bulk mass flux approach is to divide grid cells into an updraft zone and an environmental zone. Hence, a single updraft carrying the properties of the ensemble of the updrafts is modelled.

The underlying assumption of such an approach is that the individual updrafts do not interact with one another but solely with their environment.

The mass flux in Eq.(3.2) is defined by both ϕ_u and M_u. The sub-script u is used to denote variables in the updraft.

The basic idea of EDMF (Pergaud *et al.*, 2009) involves depicting dry thermals as buoyant air rising from the surface and developing in the Convective Boundary Layer (CBL). These vertical developing columns interact with their surrounding air through turbulent mixing and hence, air masses are entrained and detrained to and from the column respectively. Hence, the mass flux and its evolution is determined by the diagnostic equation ensuring the mass balance, whereby, E represents the inward mass flux from the environment to the updraft and detrainment D represents the outward mass flux from the updraft to the environment (Eq.(3.6))

$$\frac{\partial M_u}{\partial z} = E - D, \tag{3.6}$$

or

$$\frac{1}{M_u}\frac{\partial M_u}{\partial z} = \varepsilon - \delta, \tag{3.7}$$

where ε and δ are the fractional mass entrainment rates (m^{-1}) and E and D are the entrainment and detrainment rates (s^{-1}). Hence the M_u evolves along the vertical depending on both entrainment and detrainment rates as shown in Fig.(3.1).

.

As per Siebesma (1998) and Pergaud *et al.* (2009), the evolution of a conserved parcel charateristic ϕ_u during the ascent is defined as

$$\frac{\partial M_u \phi_u}{\partial z} = E\bar{\phi} - D\phi_u \tag{3.8}$$

which using Eq.(3.6) is simplified to

$$\frac{\partial \phi_u}{\partial z} = -\varepsilon(\phi_u - \bar{\phi}), \tag{3.9}$$

where ϕ_u is the updraft conserved variable and $\bar{\phi}$ is its mean value on the grid. The evolution of the updraft conservative variables such as θ_{lu} (liquid potential temperature) and r_{tu} (total mixing ratio) are determined using Eq.(3.9).

The updraft vertical velocity equation is given by Eq.(3.10),

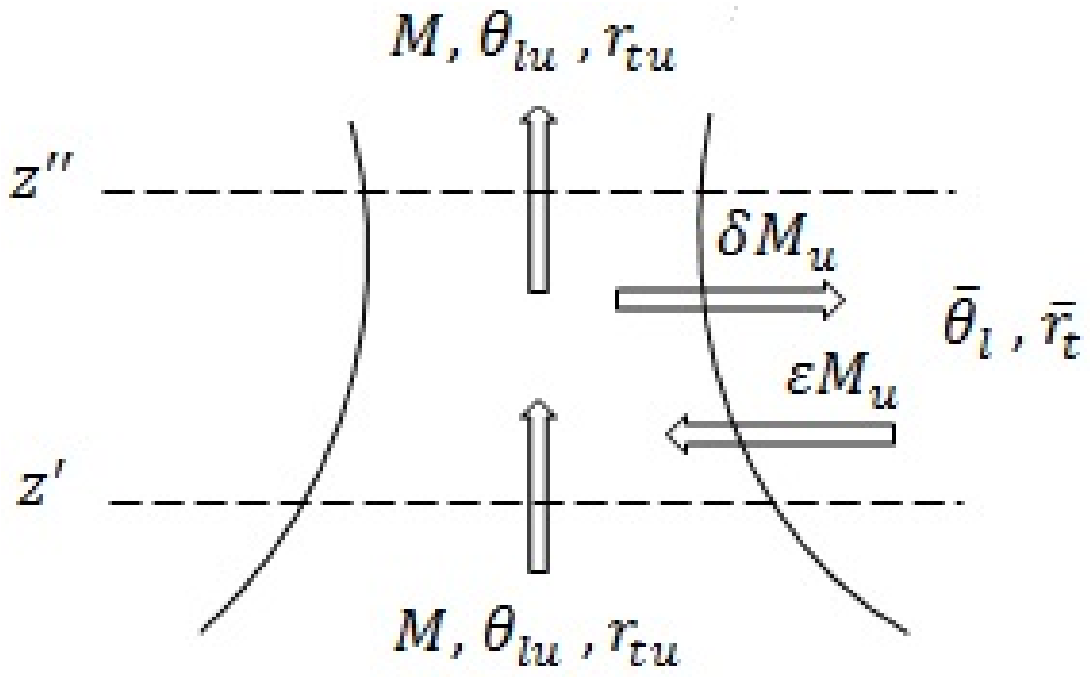

Figure 3.1: Variations of the updraft characteristics - Updraft mass flux M_u, θ_{lu} (updraft liquid potential temperature), r_{tu} (updraft total mixing ratios) dependent on the mixing with the environment through $E = \varepsilon M_u$ and $D = \delta Mu$. Figure from Pergaud *et al.* (2009)

$$w_u \frac{\partial w_u}{\partial z} = aB_u - b\varepsilon w_u. \tag{3.10}$$

Hence, the mass flux profile depends on the vertical velocity, which is further affected by the updraft buoyancy (B_u) and entrainment of the environmental air (a drag term). The B_u acceleration is evaluated related to the difference of virtual potential temperature (θ_v) between the updraft and its environment, in the absence of phase change in water: $B_u = g(\theta_{u,v} - \bar{\theta_v})/\bar{\theta_v}$; where parameters $a = b = 1$ (Simpson & Wiggert, 1969). The vertical velocity equation (Eq.(3.10)) can be solved to find the top of the updraft imposing $w_u \to 0$ as a boundary condition. Now, since eqs.(3.7) and (3.10) for M_u and w_u are independently diagnosed, the updraft fractional area (a_u) is allowed to vary vertically through the diagnostic Eq.(3.11),

$$a_u = \frac{M_u}{\rho w_u}. \tag{3.11}$$

The updraft area, a_u is used to diagnose the cloud fraction, and hence defines the sub-grid condensation scheme in the EDMF.

Pergaud *et al.* (2009) chose to draw the definition of lateral mass exchanges from the updraft buoyancy and vertical velocity. They have also chosen to differentiate the exchange for the dry portion of the updraft from the moist one. For the moist part, if the Lifting Condensation Level (LCL) is reached, lateral exchanges are computed using the entraining/detraining plume model of Kain & Fritsch (1990). The entrainment/detrainment rate for the dry portion is locally defined as an equilibrium between w_u and B_u,

$$\varepsilon_{dry}, \delta_{dry} \propto \frac{B_u}{{W_u}^2}. \tag{3.12}$$

Finally, the updraft initialization at the surface defines the mass flux as follows,

$$M_u(Z_{grd}) \propto \rho \left(\frac{g}{\theta_{v,ref}} \overline{w'\theta'_{V,s}} L_{up} \right)^{\frac{1}{3}} \tag{3.13}$$

and the vertical velocity of the updraft from the Turbulent Kinetic Energy at the ground,

$${w^2}_u(z_{grd}) = \frac{2}{3} e(z_{grd}). \tag{3.14}$$

Since the EDMF parametrisation has been developed to describe the shallow convection in the boundary layer that is produced by surface heating, such atmospheric sources of heat and water vapour are not fully applicable to volcanic clouds, especially for the first model level. Hence, it is the mass flux scheme that is modified for the use of this shallow convection scheme on the case of volcanic eruption columns (section 3.4.2).

3.1.2 Entrainment through turbulent mixing

Entrainment of ambient fluid into a volcanic plume has largely been recognised (since the first models such as the top-hat model by Morton *et al.* (1956)) as an important parameter that largely controls the dynamics of a plume. Since the initial development of the model by Morton *et al.* (1956), it has largely been adapted and used to test various aspects of plume dynamics (Carazzo *et al.*, 2008).

In terms of entrainment of an ambient fluid, the key hypothesis in Morton *et al.* (1956)'s model is that the rate of entrainment at the edge of the plume is proportional to the velocity at that height and hence the global representation of turbulence is achieved by introducing an entrainment coefficient α_E. The underlying definition of entrainment is different in Meso-NH, here it depends on the buoyancy flux and vertical velocity (Eqs. (3.8), (3.9)). Due to such differences the output variables have different mathematical representations, i.e. in top-hat model entrainment is in the form of m/s and in Meso-NH it is an output in the form of 1/m. Hence, it is difficult to directly compare outputs from this study to the numerous laboratory experiments undertaken by Carazzo *et al.* (2008), Kaminski *et al.* (2005), Matulka *et al.* (2014) (amongst others) to effectively constrain α_E. However, the main objective in the two approaches is to efficiently characterise the mixing in a plume. In general, it has been demonstrated that a constant entrainment coefficient, α_E, is not effective in representing volcanic convection and that entrainment is rather efficient in buoyant plumes (Kaminski *et al.*, 2005).

In terms of modelling a volcanic plume, the two approaches are fundamentally very different. In the top-hat approach, the height reached by the volcanic cloud is used to estimate the mass flux at the ground, where as in the approach used by Meso-NH, the plume height depends on the parameters assigned at the plume base. It will become evident in the next sections that entrainment is certainly a key parameter which needs

further investigation. The link between the two approaches in terms of the entrainment parameter and the consideration of studies by Carazzo *et al.* (2008) and Kaminski *et al.* (2005) (amongst others) are certainly in the future perspectives of the work undertaken during this study.

3.2 Abstract of the research article

In mesoscale models (resolution $\sim$ 1 km) used for regional dispersion of pollution plumes the volcanic heat sources and emissions of gases and aerosols, as well as the induced atmospheric convective motions, are all sub-grid-scale processes (mostly true for weak effusive eruptions) which need to be parameterised. We propose a modified formulation of the EDMF scheme (eddy diffusivity/mass flux) proposed by Pergaud *et al.* (2009) which is based on a single sub-grid updraft model. It is used to represent volcano induced updrafts tested for a case study of the January 2010 summit eruption of Piton de la Fournaise (PdF) volcano. The validation of this modified formulation using a reference large eddy simulation (LES) focuses on the ability of the model to transport tracer concentrations up to 1 - 2 km above the ground in the lower troposphere as is the case of majority of PdF eruptions. The modelled volcanic plume agrees reasonably with the profiles of SO_2 (sulfur dioxide) tracer concentrations and specific humidity found from the reference LES. Sensitivity tests performed for the modified formulation of the EDMF scheme emphasise the sensitivity of the parameterisation to ambient fresh air entrainment at the plume base.

3.3 Introduction

A critical factor in successfully monitoring and forecasting volcanic ash and gases dispersion is the height reached by eruption clouds, which is mainly controlled by the eruptive mass flux (e.g. Kaminski *et al.*, 2011) but is also affected by environmental factors, such as wind shear and atmospheric vertical stability (Bursik, 2001, Glaze & Baloga, 1996, Graf *et al.*, 1999, Tupper *et al.*, 2009). The term 'volcanic plume' refers to both the vertical buoyant column of gas/ash above the eruptive vent and the following horizontal transport of pollutants at the regional to hemispheric scales by the wind flow. Therefore, there is a need of numerical prediction systems coupling volcanic

plume dynamics and atmospheric circulation models. An attempt of such a system was proposed by Kaminski *et al.* (2011) for the deep tropospheric 2010 eruption of the Eyjafjallajökull volcano in Iceland.

The convective scale of a volcanic plume corresponds to the unstable region where intense but localised sensible and latent heat fluxes released by pyroclasts, gases and lava near eruptive vents generate convection which transports energy and pollutants to higher altitudes through buoyant plumes. Throughout the course of this convection, mixing of the plume with the atmosphere takes place at different levels of altitude through entrainment and detrainment. This process allows for the distribution of pollutants over a certain vertical range.

Piton de la Fournaise (PdF) is one of the world's most active volcanoes (Lenat & Bachelery, 1988) with an average of one eruption every 8 months in the last 50 years (Peltier *et al.*, 2009). Most of the studies undertaken for deep volcanic injection have been applied to stratospheric injections, which are mostly performed by large explosive volcanoes (comprehensive review by Robock, 2000). However, much less is known about the environmental and atmospheric impacts and fates of weak volcanic plumes injected into the troposphere (Delmelle *et al.*, 2002, Mather *et al.*, 2003). PdF can create a major source of tropospheric air pollution as was the case during the eruption of April 2007 (Tulet & Villeneuve, 2011). Details on the island areas affected by pollution during this eruption can be found in Viane *et al.* (2009) and Bhugwant *et al.* (2009). The air-quality standard for ecosystem and human health protection was exceeded for sulfur dioxide (SO_2) at several inhabited locations of the island (Bhugwant *et al.*, 2009).

Suzuki *et al.* (2005) developed a three-dimensional numerical fluid-dynamics model to explicitly simulate volcanic plumes and explore different dynamical regimes as function of the ejection velocity and the mass discharge rate of the volcanic material. However, the spatial resolution is very fine in their model, with a horizontal grid spacing well below the ones used in pollution dispersion models at regional scale (at best 1 km). Such a model with presumably high numerical cost is thus not applicable for air-quality prediction purposes.

Simulations of atmospheric plumes from intense heat source points have been performed using the Méso-NH (Lafore *et al.*, 1998) model to represent the impact of forest fires on the dynamics and chemistry of the atmosphere. A study by Strada *et al.*

(2012a) simulated forest fire plumes at 1 km resolution which showed good agreement with observations where high sensitivity to the atmospheric stability was observed.

Simulations of buoyant eruptive columns, chemistry dispersal in the proximal environment and the volcanic cloud tracking at regional scale can be based on similar numerical and conceptual approaches as the ones used for the study of forest fire plumes. However, volcanic eruptive vents usually cover small areas and in (at best) kilometric-resolution models used for air-quality purposes (simulation or forecasts), the localised heat source is diluted in the model grid; hence, no convection is explicitly generated.

Several types of atmospheric movements are sub-grid processes, and they are incorporated into atmospheric models through appropriate parameterisation schemes. In order to determine the evolution of volcanic plumes in the atmosphere, numerical models need to consider two different scales:

1. an implicit/convective scale corresponding to the convective plume above the erupting volcano, whose processes are sub-grid even at fine resolutions (> 500 m), and

2. an explicit/dispersion scale that corresponds to the dispersion of the volcanic plume in the atmosphere.

In mesoscale models used for regional dispersion of pollution plumes (target resolution ~ 1 km), the volcanic heat sources and emissions of gases and aerosols as well as the induced atmospheric convective motions are all sub-grid-scale processes which need to be parameterised. In this article we first briefly describe an existing sub-grid shallow convection scheme by Pergaud *et al.* (2009) used in the atmospheric model Méso-NH for conventional weather simulations. This scheme is based on a single sub-grid convective updraft approach, whereby the updraft vertical development is calculated step by step from one vertical model level to the level above. Therefore, the updraft needs to be initialised at the ground level, and this relies on local atmospheric turbulence in the scheme formulation as per Pergaud *et al.* (2009). In Sects. 3.4.2.2 and 3.4.2.3, we propose a specific adaptation of this scheme whereby the size and intensity of the volcanic heat source serve as alternative initial conditions at ground level for the modelled updraft.

Due to the computational efficiency of a one-dimensional (1-D) model and the ability to isolate a column of atmosphere for study, 1-D modelling is an ideal configuration to develop and test parameterisations (Randall *et al.*, 1996). Due to specific constraints (see Sect. 3.4.3.4), the new parameterisation is tested for an eruption observed at PdF in January 2010 not really in a 1-D model but actually in the central column of a 3×3 column model. This central column can be seen as a quasi-1-D model with open lateral boundary conditions and thereafter referred to as SCM (single column model). The choice of 1 km as horizontal resolution for SCM simulations is because it is the target resolution of future forecast models running over Réunion Island.

Simultaneously, a three-dimensional (3-D) large eddy simulation (LES) is performed (10 m resolution) using the same size and intensity of the eruption as prescribed for the SCM simulations with adapted convection scheme. Observations relating to the case study are used to evaluate the LES simulation which is further used as reference to validate the SCM results. As outlined by Pergaud *et al.* (2009), both Siebesma *et al.* (2013) and Brown *et al.* (2002) have shown that LES are robust for representing shallow cumulus convection. This methodology has been used in the past by the Global Energy and Water Cycle Experiment Cloud System Study (GCSS) (Browning, 1993) and also applied to test the scheme used to parameterise shallow convection (Pergaud *et al.*, 2009).

3.4 Volcanic plume parameterisation and model configurations

3.4.1 January 2010 summit eruption of Piton de la Fournaise

An eruption took place on 2 January 2010 around 10:20 UTC at the summit of PdF located at 2632 m a.s.l., as detected by the monitoring networks of the Piton de la Fournaise Volcanological Observatory (OVPF/IPGP) (Roult *et al.*, 2012). At 10:27 UTC a small and diluted gas plume was first visible and a vertical plume rapidly formed above the crater at 10:57 UTC. Up to seven lava fountains erupted together from the same number of vents along a fracture on the west Dolomieu crater wall (length of fracture about 60 m) and the highest lava fountain of about 30 m was emitted by the largest vent located in the middle of the fracture. Lava flows were fed by magma flowing from the vents (Fig.(3.2)) but also from hot fountain products that were remobilised

after falling to the ground. According to Roult *et al.* (2012) the eruption emitted 1.2 $\times$ 10^6 m^3 of lava in about 9.6 days; the mass flow rate decreased exponentially after the beginning of the eruption and the fountaining and gas plumes described here only occurred till 4 January 2010, whereafter mostly effusive lava flows were observed.

Figure 3.2: January 2010 summit eruption of Piton de la Fournaise - The 60 m long fissure on the inner cliff of Dolomieu summit crater emits lava flows towards the bottom of the caldera. The < 30 m high fountains (left) are the source of the ca. 1 km high vertical plume (right) of gas and vapour. Transport and sedimentation of solid particles are mostly confined to the lowest portion (< 100 m) of the plume. Pictures provided by the Piton de la Fournaise Volcanological Observatory (OVPF/IPGP).

The vertical plume above the crater (Fig.3.2; right) was relatively steady implying low winds and a level of neutral buoyancy was reached at approximately 1300 m above the fountain top (from observation). For the development of a parameterisation this case study is the least complex one compared to other eruptions of PdF since 2000. There was a well-developed vertical gas column which was weakly affected by horizontal winds and the topography of the area.

3.4.2 Description of the volcanic plume parameterisation

It is well understood that a volcanic eruption plume enters into an atmosphere that has a pre-existing stratification in terms of temperature, moisture content and wind (Bjornsson *et al.*, 2011, Petersen *et al.*, 2012). There are three dynamically distinct regions related to volcanic plumes (Sparks, 1986):

1. the gas thrust region, where the dynamics is dominated by the exit velocity at the vent and the flow near the vent is driven upward by its initial kinetic momentum;

2. buoyancy-driven convective region which covers most of the height of the plume; and

3. umbrella cloud region, where vertical motion is small and the plume disperses horizontally due to wind impacts.

For the purpose of modelling volcanic clouds using Méso-NH, we are predominately interested in the convective region of the volcanic cloud. For the kind of effusive eruption under consideration in this study, the gas thrust region extends only over few metres (see, e.g. Fig.3.3 for an eruption comparable to January 2010). For simplicity, it will be assumed that the thrust region is very short compared to the total vertical extension of the plume and that the plume is primarily driven by buoyancy. Thus, the plume will be assumed to be convective from the ground level to its top.

The current updraft model used in Méso-NH defined by Pergaud *et al.* (2009), Sect.3.4.2.1, is not adapted to volcanic plumes. We propose an adaptation of the updraft scheme (Sects.3.4.2.2 and 3.4.2.3) which is applied to volcanic plumes and consists mainly in a modification of the updraft initialisation at ground level (z_{grd}) using values inspired from terrain observations.

3.4.2.1 Sub-grid cloud parameterisation as per Pergaud et al. (2009)

The basic idea of the EDMF (eddy diffusivity/mass flux) approach is to represent vertical transport of matter and energy that occurs at the sub-grid scale in numerical simulations of the convective boundary layer (CBL) with resolutions of $\sim$ 1 km or coarser. At such resolutions vertical motions usually dominate the sub-grid transport due to

1. turbulent eddies

2. convective updrafts and compensating downdrafts.

Turbulent transport is commonly parameterised with the Eddy Diffusivity (ED) method, corresponding fluxes being written in the form of $-K_\phi \frac{\partial \bar{\phi}}{\partial z}$ where $-K_\phi$ is a

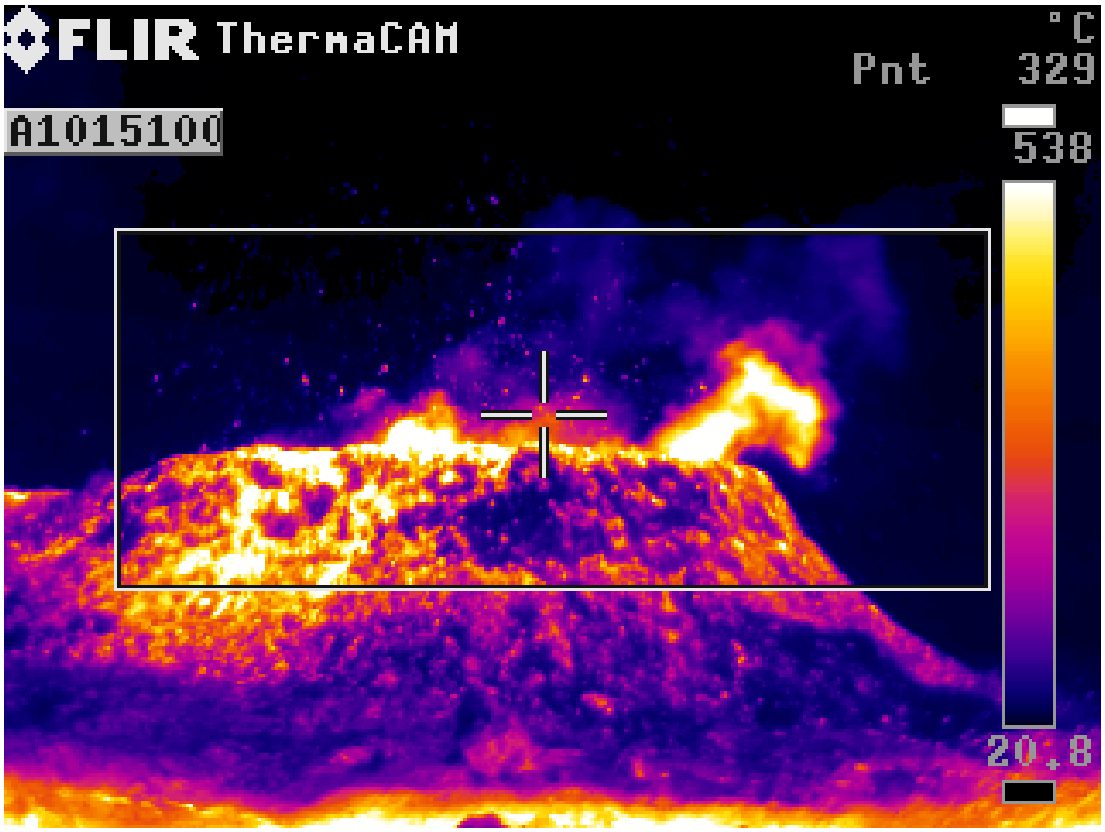

Figure 3.3: Temperature (°C) of the October 2010 eruption of PdF - Temperature (°C) of the October 2010 eruption of PdF through infrared imagery provided by OVPF. The temperature scale (right colour bar) ranges between 20.8 and 538 °C. As approximate spatial scale in this image, the crater diameter is about 25 m. (The temperature indication in the upper right corner corresponds to the central pixel marked as a cross.)

diffusion coefficient and $\bar{\phi}$ the average of any model variable ϕ (temperature, tracer mixing ratio, etc.) over the local grid cell (Holton, 2004).

A grid box can contain multiple convective updrafts. For simplicity a single updraft is considered carrying the properties of the ensemble of updrafts. This is known as the mass-flux (MF) approach. The fraction of the total area of a grid box that is covered by the updraft is known as the fractional updraft area (a_u). The corresponding net vertical flux for ϕ over the grid cell takes the form of $\frac{M_u}{\rho}(\phi_u - \overline{\phi})$, where M_u is the updraft mass flux, $\overline{\phi}$ is the mean value and ϕ_u is the updraft value of the variable ϕ.

Both ED and MF approaches have been combined in a single EDMF parameterisation such that nonlocal sub-grid transport due to strong updrafts is taken into account by MF, while the remaining transport is taken into account by ED (Hourdin *et al.*, 2002, Pergaud *et al.*, 2009, Siebesma & Teixeira, 2000, Siebesma *et al.*, 2007, Soares *et al.*, 2004, Witek *et al.*, 2011). In our approach for volcano-induced convection we only modify the MF scheme (Sect.3.4.2.2).

The two key parameters determining the mass-flux profile are entrainment (ε) and detrainment (δ), expressed as fractions of the updraft mass flux (M_u) per unit height. This simply leads to the following steady state mass-flux continuity equation:

$$\frac{\partial M_u}{\partial z} = (\varepsilon - \delta) M_u \tag{3.15}$$

The mass-flux evolves along the vertical at a rate given by the difference between the ε and δ rates. The definition of entrainment/detrainment rates is the crucial point in EDMF parameterisation as it is at this level that the physical coupling between turbulent mixing and mass flux is performed.

In Pergaud *et al.* (2009) the mass-flux profile depends on the vertical velocity of the updraft (w_u), whose vertical evolution is affected in turn by a buoyancy force (B_u), and a drag term where the entrainment of environmental air, namely lateral mixing, is accounted for:

$$w_u \frac{\partial w_u}{\partial z} = c_1 B_u - c_2 \varepsilon w_u^2 \tag{3.16}$$

The updraft buoyancy acceleration is evaluated in relation to the difference of virtual potential temperature (θ_v) between the updraft and its environment: $B_u = g(\theta_{u,v} - \overline{\theta}_v)/\overline{\theta_v}$; coefficients c_1 and c_2 are usually set to 1 (Simpson & Wiggert, 1969).

Independent solutions of Eqs.(3.15) and (3.16) permit calculating the vertical variation of the updraft fractional area,

$$a_u = \frac{M_u}{\rho w_u} \tag{3.17}$$

that is used to diagnose the cloud fraction, hence defining the sub-grid condensation scheme in the EDMF framework.

3.4.2.2 Modified EDMF - updraft initialisation

Firstly, in the current EDMF parameterisation w_u is initialised at the ground level (z_{grd}) using turbulent kinetic energy (TKE) (e) as $w_u^2(z_{grd}) = \frac{2}{3}e(z_{grd})\ w_{\mathrm{u}}^2$, which is bound to local meteorology. However, this computation is not applicable to volcanic plumes as vertical velocity in this case does not depend on the atmosphere through the TKE. During volcanic eruptions, a mixture of gases, magma fragments, crystals and eroded rocks is injected into the atmosphere at high velocity, pressure and temperature. The diverse and unpredictable variability of eruptive styles depends mostly on the complex rheology of magma and the nonlinear processes leading to the fragmentation of the viscous melt into a mixture of gases and particles (Gonnermann & Manga, 2007). Nonetheless, the explosive character of a magmatic eruption like that of January 2010 is associated with the rapid decompression and the consequent abrupt expansion of gases in the magma (**?**). In order to simplify, we consider the vertical velocity of the updraft $w_u(z_{grd})$ as the vertical velocity of the lava fountain (a variable that is mostly known from observation). The input data mentioned in this section (used for updraft initialisation) and the following sections are listed in Table 3.1.

Secondly, the updraft fraction area is simply initialised as the ratio of the fissure surface ($S_{Fis,SCM}$) by the model cell surface (S_{MNH}).

$$a_u(z_{grd}) = \frac{S_{Fis,SCM}}{S_{MNH}}. \tag{3.18}$$

Now, as $w_u(z_{grd})$ and $a_u(z_{grd})$ are both known and are independent of one another, using a similar principle as in Pergaud *et al.* (2009), the mass flux at the ground can be calculated such that

$$M_u(z_{grd}) = \rho_{mix}(z_{grd}) \times a_u(z_{grd}) \times w_u(z_{grd}). \tag{3.19}$$

The ground level density of the updraft, $\rho_{mix}(z_{grd})$, is approximated by a mixture of the two main gases at PdF (H_2O and SO_2) considered as perfect gases, such that $\rho_{mix}(z_{grd}) = \frac{P(z_{grd})}{T_u(z_{grd})R_{mix}}$, where $P(z_{grd})$ is the ambient pressure at ground level, $T_u(z_{grd})$ is the temperature of the updraft at ground level and R_{mix} represents the specific gas constant of the mixture, composed mostly of water vapour and SO_2: $R_{mix} = R(\frac{[H_2O]}{M_{H_2O}} + \frac{[SO_2]}{M_{SO_2}})$, where R is the universal gas constant; $[H_2O]$ and $[SO_2]$, and M_{H_2O} and M_{SO_2}, are the mixing mass ratios and molar mass of water vapour and SO_2, respectively.

Equation(3.19) uses ρ_{mix} rather than using density of dry ambient air (as in the standard formulation from Pergaud *et al.*, 2009, our Eq.3.17). Indeed, in magmas like those erupted in 2010 the gas melange is dominated by water vapour, i.e. about 80% of the melange mass (**?**) and the remaining 20% is that of SO_2 (i.e. $[H_2O] = 0.8$ and $[SO_2] = 0.2$ kg kg^{-1}). This gives a H_2O/SO_2 ratio of 4, which is the ratio expected by simple closed system degassing of PdF shallow magmas. This value is at the lower end of the range actually measured by the OVPF geochemical network (Allard *et al.*, 2011). Note also that $\rho_{mix}(z_{grd})$ is formulated as a perfect gas mixture, which implicitly assumes that no solid fraction is present in the atmospheric plume. This is a reasonable assumption for such an eruption, whereby volcanic ash represents a small fraction of the volcanic plume.

3.4.2.3 Modified EDMF – basal lateral mass exchange

Entrainment of ambient air through turbulent mixing plays a central role in the dynamics of eruption plumes, primarily because the plume density is controlled by the mixing ratio between ejected gas/material and ambient air (Woods, 1988). Furthermore, the amount of air entrained controls the heights of eruption columns (Suzuki & Koyaguchi, 2010). In the current EDMF (Sect.3.4.2.1); the mass-flux entrainment of the updraft ε at the ground level has a constant value of 0.02 m^{-1}, whereas δ is zero.

In this sub-section we present the modifications to the input method of ε and δ such that, for some height Δz above the ground, a desired mass of ambient air may be entrained into the updraft and conversely a desired mass of the updraft may be expelled. Above this height ε and δ are both calculated as defined by Pergaud *et al.* (2009) and the coexistence of entrainment/detrainment both continue to feed the vertical evolution of M_u.

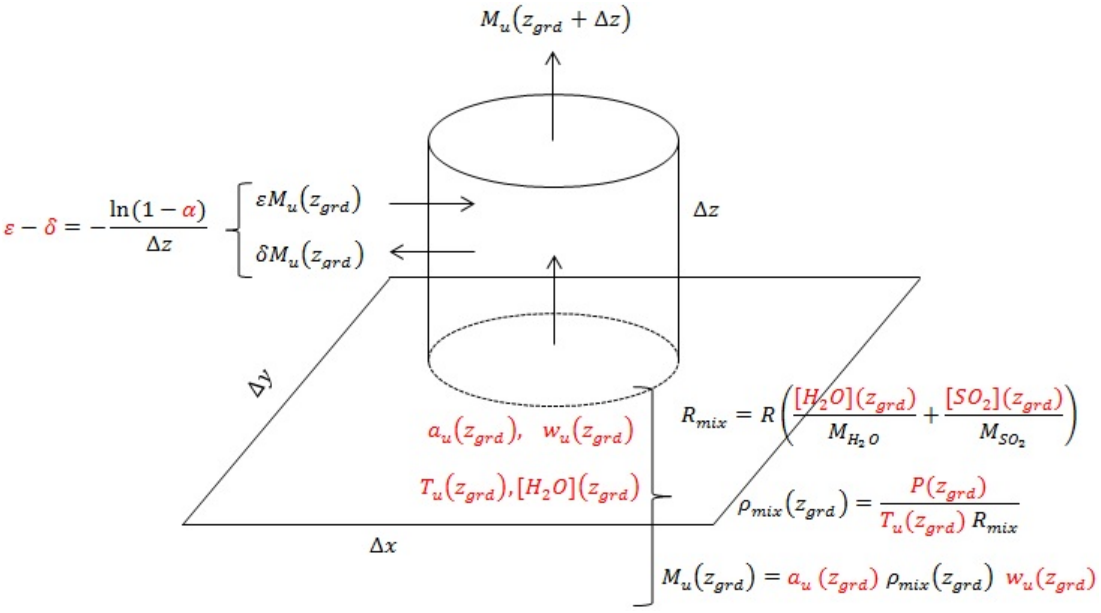

Figure 3.4: Model initialisation - Figure displaying the input data, the mass flux at ground level (z_{grd}), and the mass flux at level $z_{grd} + \Delta z$ after the incorporation of environmental air mass. The input variables of the model are highlighted in red.

The importance of adjusting the ground level ε and δ will become more apparent in Sect.3.5. However, the modifications are presented below. Figure 3.4 assembles all modifications made to the EDMF model along with the input variables (marked in red) used at ground level.

Let M_{env} represent the mass flux of environmental air that enters the updraft between levels z_{grd} and $z_{grd} + \Delta z$. Hence updraft mass flux at $(z_{grd} + \Delta z)$ is simply defined as

$$M_u(z_{grd} + \Delta z) = M_u(z_{grd}) + M_{env}. \tag{3.20}$$

Let $\alpha = \frac{M_{env}}{M_u(z_{grd}+\Delta z)}$. This value represents the fraction of environmental air in the melange at $z = z_{grd} + \Delta z$. Then, by rearranging Eq.(3.20),

$$\frac{M_u(z_{grd})}{M_u(z_{grd} + \Delta z)} = 1 - \alpha. \tag{3.21}$$

If ε and δ are constant between z_{grd} and $(z_{grd} + \Delta z)$, then, by integrating Eq.(3.15)

between z_{grd} and $(z_{grd} + \Delta z)$, Eq.(3.21) can be rewritten as

$$\frac{M_u(z_{grd})}{M_u(z_{grd} + \Delta z)} = e^{-(\varepsilon - \delta)\Delta z}. \tag{3.22}$$

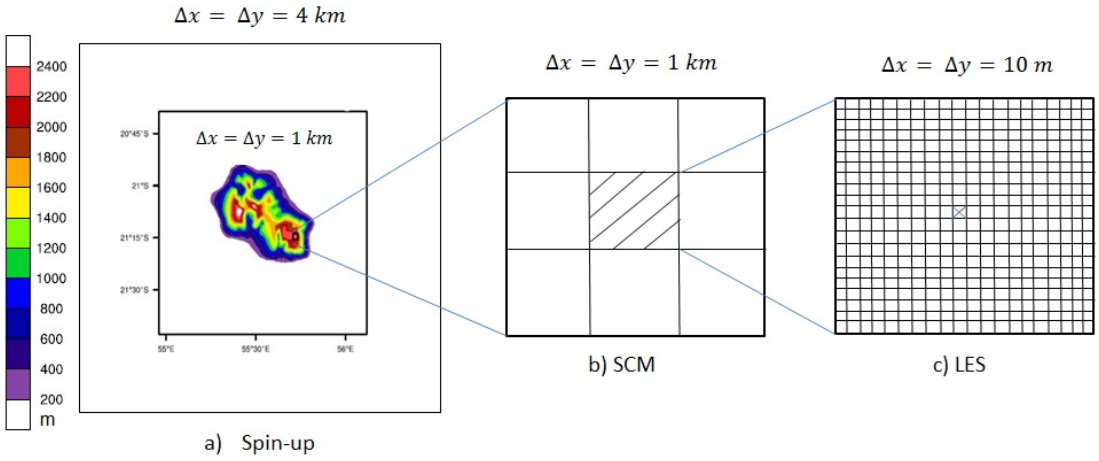

Figure 3.5: Sets of simulations performed - The interconnection in terms of the simulation domain between the three sets of simulations performed: Spin-up, SCM and LES. The single cell corresponding to the fissure is tagged for LES.

Finally, using Eqs.(3.21) and (3.22),

$$1 - \alpha = e^{-(\varepsilon - \delta)\Delta z} \Leftrightarrow \varepsilon - \delta = -\frac{\ln(1 - \alpha)}{\Delta z}. \tag{3.23}$$

For a desired fraction α of ambient air entrained in the volcanic gas column at $z_{grd} + \Delta z$, an infinity of entrainment and detrainment rate combinations can be prescribed such that Eq.(3.23) is respected.

3.4.3 Simulation set-up and configuration

For our chosen case study, three sets of simulations were run as depicted in Fig.3.5.

1. Section 3.4.3.2 describes the 3-D spin-up simulation which is used to generate background atmospheric profiles used for both the LES and SCM simulations described below.

2. Section 3.4.3.3 details the LES considered as the reference.

3. Section 3.4.3.4 outlines the (quasi) 1-D SCM simulation using the amended EDMF scheme as defined in Sect. 3.4.2.

3.4.3.1 Common features to all simulations

The Méso-NH model (version MNH-4-9-3) is used in this study; it is a mesoscale non-hydrostatic atmospheric model able to simulate convective motion and flow over sharp topography. This model has been jointly developed by Laboratoire d'Aérologie (UMR5560 UPS/CNRS) and Centre National de Recherches Météorologiques - Groupe d'études de l'Atmosphère Météorologique, CNRM-GAME (UMR3589 CNRS/Météo-France), and is designed to simulate atmospheric circulations from small-scale (type - LES) to synoptic-scale phenomena (Lafore *et al.*, 1998). All Méso-NH related documentation and articles along with various model versions are available at `http://mesonh.aero.obs-mip.fr`.

Different sets of parameterisations have been introduced for cloud microphysics (Cohard & Pinty, 2000), turbulence (Bougeault & Lacarrere, 1989) and convection (Bechtold *et al.*, 2001). The shallow convection in Méso-NH is parameterised according to Pergaud *et al.* (2009) while for the purposes of this study no deep convection parameterisation was activated. The ISBA (Interactions Soil-Biosphere-Atmosphere scheme) (Noilhan & Mahfouf, 1996) is the scheme used for land surfaces in order to parameterise exchanges between the atmosphere and the ground providing surface matter and energy fluxes to the atmosphere. The turbulent scheme implemented in Méso-NH is afull 3-D scheme that has been developed by Cuxart *et al.* (2000) with regards to both LES and mesoscale simulations. Kessler's warm microphysical scheme (Kessler, 1969) was activated during the simulation. Méso-NH can be used for idealised as well as real case studies and for the purpose of this article we focus on idealised case studies. For all simulations performed, a vertical grid composed of 72 levels in the **?** coordinates is used, with a vertical mesh stretched from 40 m at the ground to 600 m at the model top.

3.4.3.2 3-D spin-up simulation to generate background profiles

A 3-D spin-up simulation is performed to generate the background profiles which are used for SCM and LES. Two, two-way grid-nested domains with horizontal mesh sizes of 4 and 1 km are used (Fig.3.5a). Both domains have 100 points in x and y. The initial state for the simulation, as well as the boundary conditions updated every 6 h for the outermost model, is provided by analyses from the French operations forecasting

system for the Indian Ocean, ALADIN-Réunion (9.6 km resolution; Montroty *et al.*, 2008). The simulation starts 1 January 2010 at 00:00 UTC and ends 2 January 2010 at 18:00 UTC using a time step of 1 and 0.25 s for the 4 and 1 km resolution models, respectively.

Figure 3.6 shows the vertical profiles of temperature (°C), potential temperature (K) and water vapour mixing ratio (g kg^{-1}) as simulated at 10:50 UTC on 2 January 2010 by the spin-up simulation for the local area of interest (location of the PdF volcano). The ambient atmosphere is dry with water vapour concentration just under 8 g kg^{-1} at the ground and decreasing with altitude. The tropopause is found at about 16 km above ground level (a.g.l. hereafter, where the ground level corresponds to about 2.6 km above the sea) which corresponds well to tropical climates. The 0°C isotherm is located at 2.7 km, a.g.l. Those profiles are then used as initial and steady background conditions for our LES and SCM simulations.

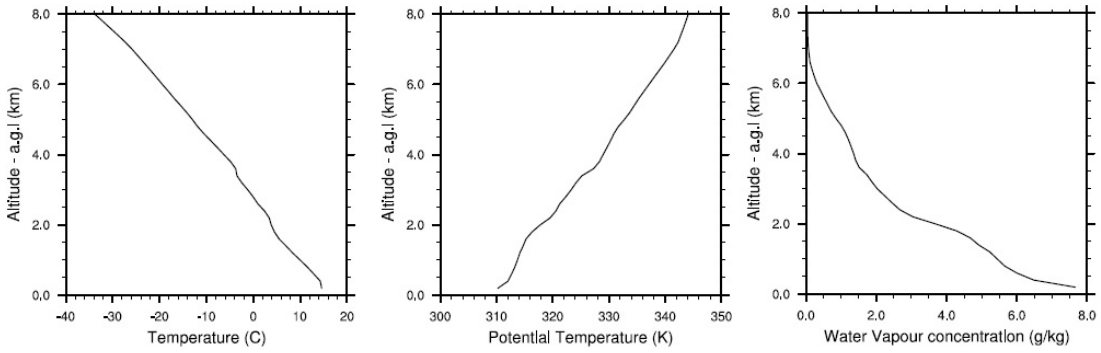

Figure 3.6: Meteorological profiles - Meteorological profiles from the 3-D spin-up model (1 km resolution) at the location of the January 2010 summit eruption on 2 January 2010 at 10:50 UTC. Vertical profiles of temperature (°C), potential temperature (K) and water vapour mixing ratio at the grid scale (g kg^{-1}). Altitude displayed is above ground level (a.g.l.), which is at 2600 m, a.s.l.

The vertical structure of trade winds over Réunion Island was investigated by Lesouëf (2010) and Lesouëf *et al.* (2011). The trade wind inversion located at about 4 km, a.s.l. (Taupin *et al.*, 1999) is described as a consequence of the descending branch of the Hadley cell circulation (Lesouëf *et al.*, 2011) where easterly winds prevail in the lower levels while westerly winds prevail in upper levels. It coincides with a temperature inversion or at least a layer of enhanced vertical static stability. This is found in Fig.3.6 (middle) at about 2 km, a.g.l. (4.6 km, a.s.l.) as an increased gradient of

potential temperature. This stable layer can behave as a barrier for development of clouds (Hastenrath, 1991) but also for plumes generated through our simulations.

It should be noted that the wind profiles as obtained from the spin-up simulation appeared to be unrealistic since the wind near the ground (7-8 m s^{-1}) was clearly overestimated; as a consequence, a strong tilt in the volcanic plume above the crater was simulated in a first tentative LES using these wind profiles (not shown) but clearly not observed in reality (Fig.3.2). In addition, no strong wind above the caldera rim of Bellecombe has been reported by Météo France for the simulation period (average 10 m wind of $2.5 \pm 0.9(1\sigma)$ m s^{-1}, with a maximum hourly mean of 4.9 m s^{-1}). For this reason, instead of using wind profiles from the spin-up simulation, we prescribed a vertically uniform and very slow wind field ($u(z) = 0.1$ m s^{-1} and $v(z) = 0$ m s^{-1}) as background wind in the LES and for consistency also in the SCM.

3.4.3.3 LES simulations

An LES model has such a high resolution that it can resolve not only convective motions but also the largest eddies (responsible for the major part of the turbulent transport). This section describes the set-up of the LES simulation considered as reference used to validate the EDMF parameterisation for volcano-induced convection.

Table 3.2 summarises the configuration of the LES model. Its horizontal physical domain is chosen to extend over 1 km × 1 km, which exactly corresponds to the size of the central column in our quasi-1-D model (see Sect.3.4.3.4). Thus, horizontal averages of the LES fields will be taken as references to validate the quasi-1-D model output profiles. The LES horizontal resolution is 10 m × 10 m, such that convection can be explicitly resolved. Due to the short simulation duration, radiative processes are neglected. As the model domain is quite small, and also to avoid complex topographic effects, the local topography of the volcano is not taken into account (except the fact that the model ground is at the correct altitude, such that the ground pressure is 78695 Pa), depicting a flat domain for simplifying the model (as also done for the SCM model detailed in Sect.3.4.3.4).

The surface mass and heat fluxes representing the volcanic mass and energy source in the LES are prescribed for one single surface cell (i.e. $S_{Fis,LES} = 100$ m^2; Fig.3.5c) with a correction factor Corr = 1.2 such that the input fluxes are consistent with that of the SCM model, where the volcanic fissure covers an area $S_{Fis,SCM} = 120$ m^2.

Let F_{H_2O} be the vapour mass flux (kg m^{-2} s^{-1}) prescribed for this particular surface cell at every model time step, then

$$F_{H_2O} = \rho_{mix} \times [H_2O] \times w_u \times Corr, \tag{3.24}$$

and similarly for the SO_2 mass flux (kg m^{-2} s^{-1}):

$$F_{SO_2} = \rho_{mix} \times [SO_2] \times w_u \times Corr. \tag{3.25}$$

The variables here (all at the ground level) have the same definitions and values as in Sect.3.4.2.2 (see also Table 3.1). Finally, let F_s represent the sensible heat flux (W m^{-2}), then

$$F_s = \rho_{mix} \times C_{p,mix} \times (T_u - T) \times w_u \times Corr, \tag{3.26}$$

where $C_{p,mix}$ is the specific heat capacity of the mixture at constant pressure such that $C_{p,mix} = 4R_{mix}$ (H_2O and SO_2 being both triatomic gases); T_u and T are the temperatures of the updraft and of ambient air outside the updraft, respectively. An appendix at the end of the text presents detailed derivations of Eqs.(3.24)-(3.26).

Steady surface fluxes are used as volcanic input in LES runs. Their values are summarised in Table 3.1.

3.4.3.4 SCM simulations

Table 3.3 shows the configuration of the SCM model. The volcanic updraft is simulated only in a single central grid column of size 1 km × 1 km; however, the total number of grid columns used is 3×3 (Fig.3.5b). This is simply to allow for the use of open lateral boundary conditions and hence avoid matter and energy to accumulate in the model.

The adapted EDMF model in Sect.3.4.2.2 is used to run SCM simulations. The variables used as volcanic input in SCM runs were presented in Sect.3.4.2.2 and are summarised in Table 3.1 along with their values. As mentioned earlier, since the gas melange in the eruption column consists of 80% of H_2O and 20% of SO_2, the SCM model is simply initialised with $[H_2O] = 0.8$ kg kg^{-1} and $[SO_2] = 0.2$ kg kg^{-1} in the updraft at ground level.

Common to both LES (Sect.3.4.3.3) and SCM runs,

- the wind profiles obtained from the spin-up simulation are not used as background conditions, instead a prescribed uniform wind field is used (u = 0.1 and v = 0 m s^{-1}; see Sect.3.4.3.2);
- radiative processes are neglected.

3.5 Results and analysis

In this section, results obtained from the 1-D SCM and 3-D LES of the case study are presented and analysed.

3.5.1 Demonstration of the need of specific heat source to generate deep plumes

A first most obvious question is whether we need to parameterise volcanic updraft. Figure 3.7 shows results from four simulations: Fig.3.7a and b shows simulation results from LES without and with volcanic heat sources, respectively, whereas Fig.3.7c and d show results from the SCM model without and with volcanic heat source, respectively. Results for Fig.3.7b follow the initialisation of the volcanic heat source as outlined in Sect.3.4.3.3 above and results from Fig.3.7d follow the initialisation of the volcanic heat source as outlined in Sect.3.4.2.2. All four simulations have been initialised with a passive SO_2 tracer as outlined in Table 3.1 and used as a tracer pollutant injected into the atmosphere.

In simulations with no volcanic heat source, SO_2 tracer is simply diffused to a few hundreds of metres above the ground and the majority of the tracer remains at low altitude (Fig.3.7a, c). Results from the reference LES simulation with volcanic source (Fig.3.7b) shows an uplift of tracer to higher altitudes, with maximum concentration around 1.0 km above the ground after 90 min, and almost no tracer above 2 km. The SCM simulation with modified EDMF (M.EDMF) results (Fig.3.7d) also show tracer lifted to much higher altitudes with the majority of the concentration levelled off at around 7.25 km. The overall tracer concentrations are vertically distributed between 4 and 11 km above the ground. It is clear that without modifications to EDMF and without initialising the LES simulation with specific volcanic heat sources, the two models are not capable to transport tracer concentrations to higher altitudes.

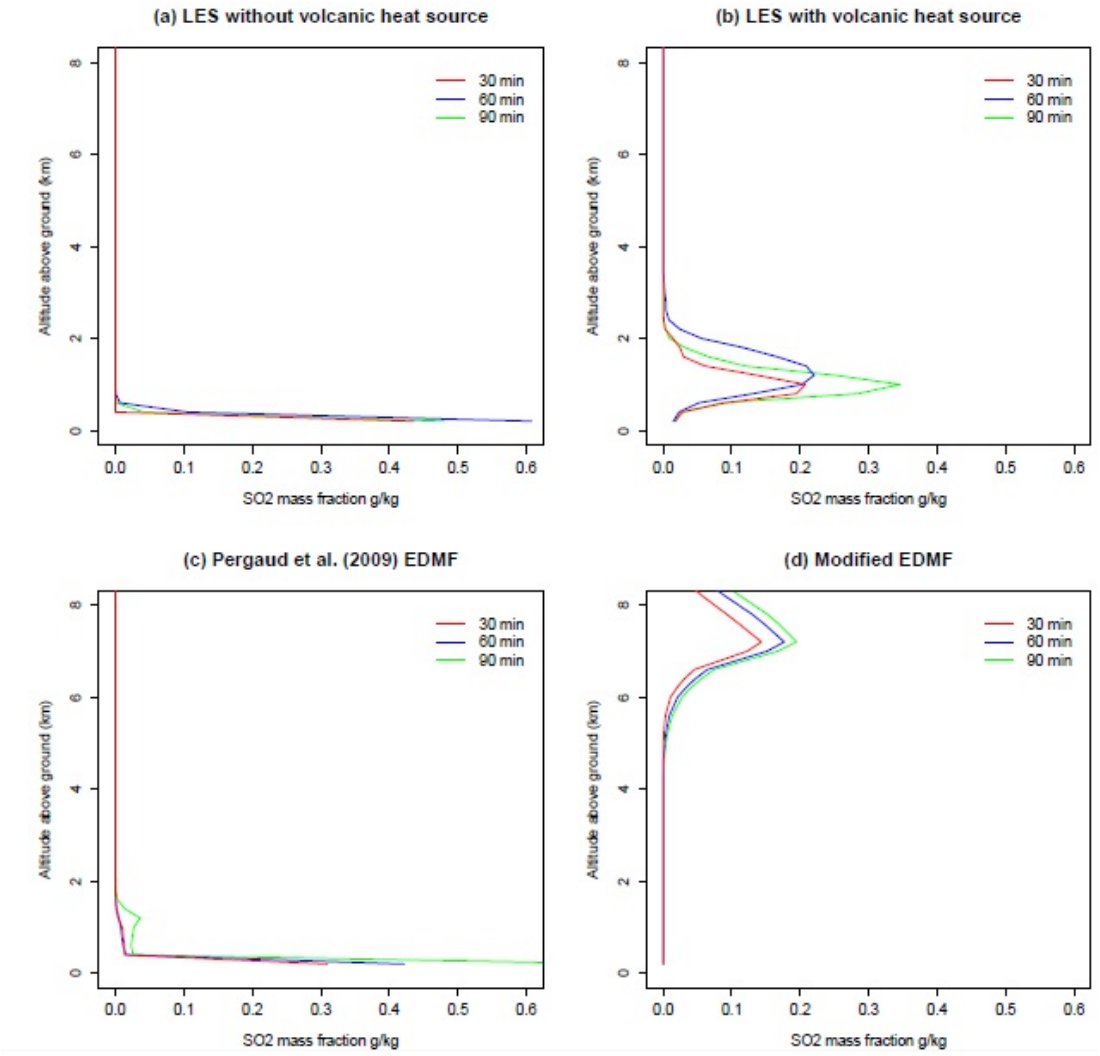

Figure 3.7: Simulation outputs for SO_2 tracer mass fractions - (a) and (b): vertical profiles of SO_2 tracer mass fractions (g kg^{-1}) horizontally averaged over the 1 km × 1 km domain of LES simulations. (c) and (d): vertical profiles of SO_2 mass fractions in the central grid cell (1 km × 1 km) of the SCM simulations. All simulations were inputted with the same SO_2 surface mass flux. Colour code for all panels: red - 30 min, blue - 60 min, and green - 90 min after model initialisation.

Although both Fig.3.7b and d show transport of tracer to higher altitudes, it is evident that, in terms of maximum detrainment height of the tracer (1.4 and 7.25 km respectively) and its vertical profile, at this stage the M.EDMF results are poorly comparable to that of the LES (the reference simulation) - the plume generated by M.EDMF being much too deep.

Hereafter, the height at which there is a maximum detrainment of the tracer will be referred to as the 'maximum injection height'. The sensitivity of the latter against entrainment and detrainment at the base of the updraft will be investigated, with the aim at obtaining better agreement between the reference LES and M.EDMF simulations.

3.5.2 Influence of entrainment/detrainment at the base of the updraft

It is well known that both entrainment and detrainment have an impact on the updraft development because they affect buoyancy at all updraft levels (Carazzo *et al.*, 2008, Glaze *et al.*, 1997, Graf *et al.*, 1999, Kaminski *et al.*, 2005, Woods, 1988).

Figure 3.8 shows the updraft temperature profile for the plume generated in Fig.3.7d. The temperature of the plume taken through infrared (IR) imagery for a similar PdF eruption in October 2010 (as no IR imagery is available for January 2010) is shown in Fig.3.3. In the buoyant region of the plume, the IR imagery shows a very rapid decrease from several hundred degrees Celcius to mostly ambient temperature within the first tens of metres above the eruptive vent. The temperature decrease in the modelled updraft (Fig.3.8) is much slower (temperatures below 200 °C only encountered well above 1 km above the ground). The comparison is very crude and qualitative but at least it shows that the updraft temperature at the base of our simulated plume is not in a correct range of temperatures and consequently the plume is too buoyant and too deep, as not enough fresh ambient air is entrained in the plume base. To correct this discrepancy there is a need to modify the entrainment and detrainment rates at the base of M.EDMF model (as described in Sect.3.4.2.3).

The question of fresh air entrainment at the base of highly buoyant plumes is actually relevant for all types of high-temperature surface sources inducing convection in the atmosphere, i.e volcanoes but also combustions and in particular biomass fires (Rio *et al.*, 2010). Volcanic or combustion hot gases are extremely buoyant and without entrainment of a large part of fresh air at the base of the buoyant updraft, the latter would accelerate dramatically and, by need of vertical mass conservation, its section

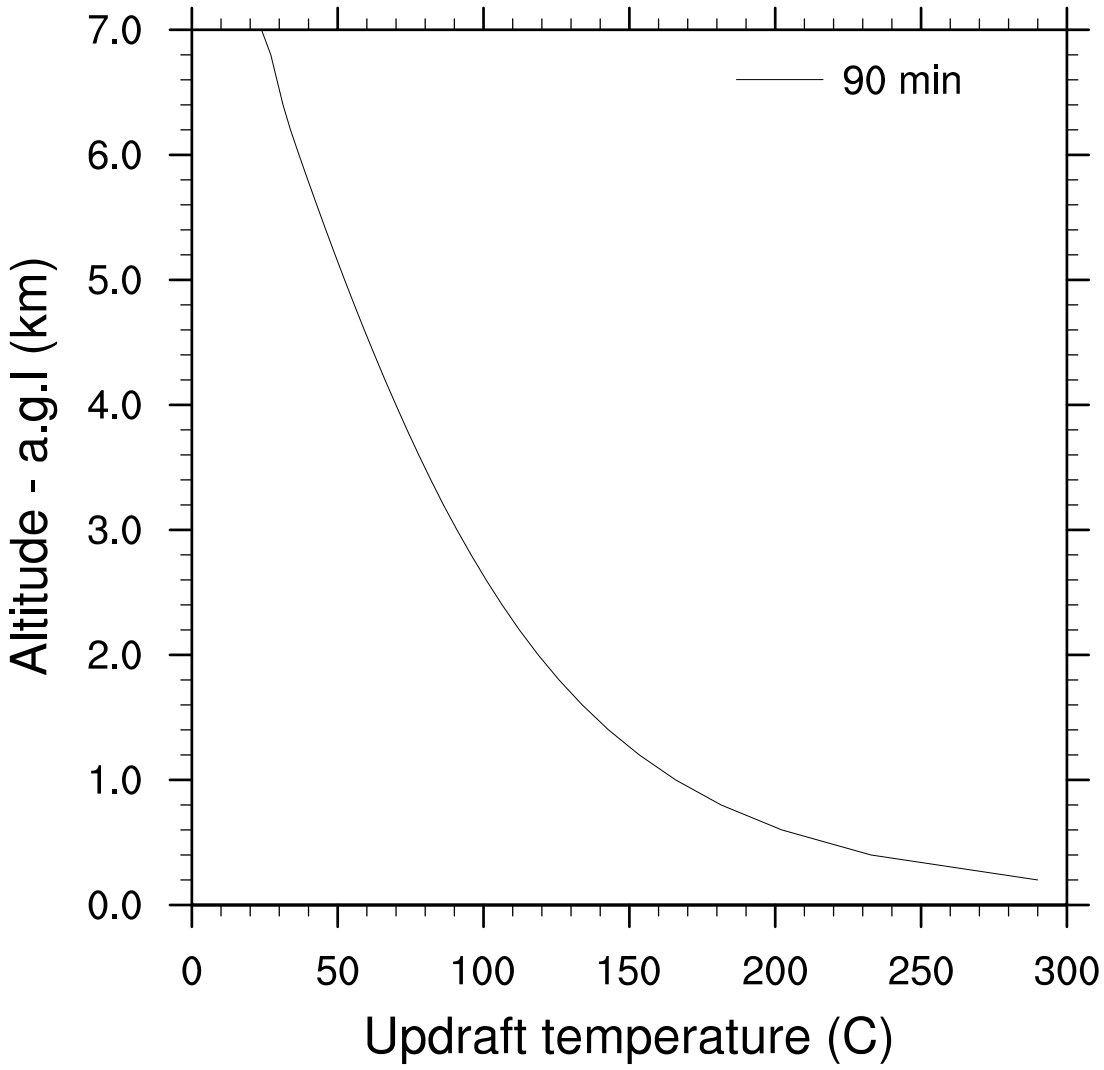

Figure 3.8: Updraft temperature profile of MEDKF simulation - Updraft temperature (°C) at 90 min in the MEDKF simulation of Fig.3.7d.

would become much thinner than the area of the ground heat source at some altitude above the ground. This is clearly not what is observed in reality, neither in volcanic nor fire plumes. To account for actual observed plumes, the concept of a basal feeding layer in which strong entrainment of fresh air occurs must be introduced. The main questions are how deep is this feeding layer, and how to model entrainment in this layer.

Rio *et al.* (2010) proposed the idea that the entrainment in the feeding layer exactly compensates the narrowing of the plume coverage due to acceleration. They apply this constraint over the full depth of the atmospheric well-mixed boundary layer.

In the present work we keep it as simple as possible. We started from the simple observation that a dominant part of fresh air has been already entrained into the plume within few tens of metres above the ground (Fig.3.8). The simplest solution was thus to prescribe a desired fraction α of fresh air at the top of the first model layer (here 40 m above the ground). The relationship between α and the entrainment/detrainment coefficients in the first model layer has been established earlier (Eq.3.23, Sect.3.4.2.3).

To compare the Rio *et al.* (2010) approach with ours, we estimated the fraction α of entrained fresh air at 40 m above the ground, using their assumption (constant updraft section between the ground and 4 ,m). Transposed to our notations, their Eq.(15) reads

$\varepsilon M_u = \frac{a_u \rho_{mix}}{2 w_u} B_u$,

and this yields

$\varepsilon = \frac{B_u}{2 {w_u}^2}$.

Assuming no detrainment in the layer, Eq.3.23 yields

$\alpha = 1 - e^{-\varepsilon \Delta z} = 1 - e^{-\frac{B_u}{2 {w_u}^2} \Delta z}$.

With our numerical values (Table 3.1) the result is $\alpha = 68\%$, which supports the idea that a dominant fraction of fresh air is entrained into the updraft within a few tens of metres.

The sensitivity of our model to a range of prescribed values of ε and δ in the first model level (i.e. within Δz above the ground) is here discussed in Fig.3.9. Firstly, assuming no detrainment ($\delta = 0$), the plume maximum injection height is found to decrease from about 10 km to almost 0 for ε in the range 0-2 Δz^{-1} (Fig.3.9a). Beyond $2\Delta z^{-1}$, the volcanic plume does not take off from the ground. A correct value with respect to the LES reference simulation (Fig.3.7b) is achieved for $\varepsilon \approx 1.8 \Delta z^{-1}$.

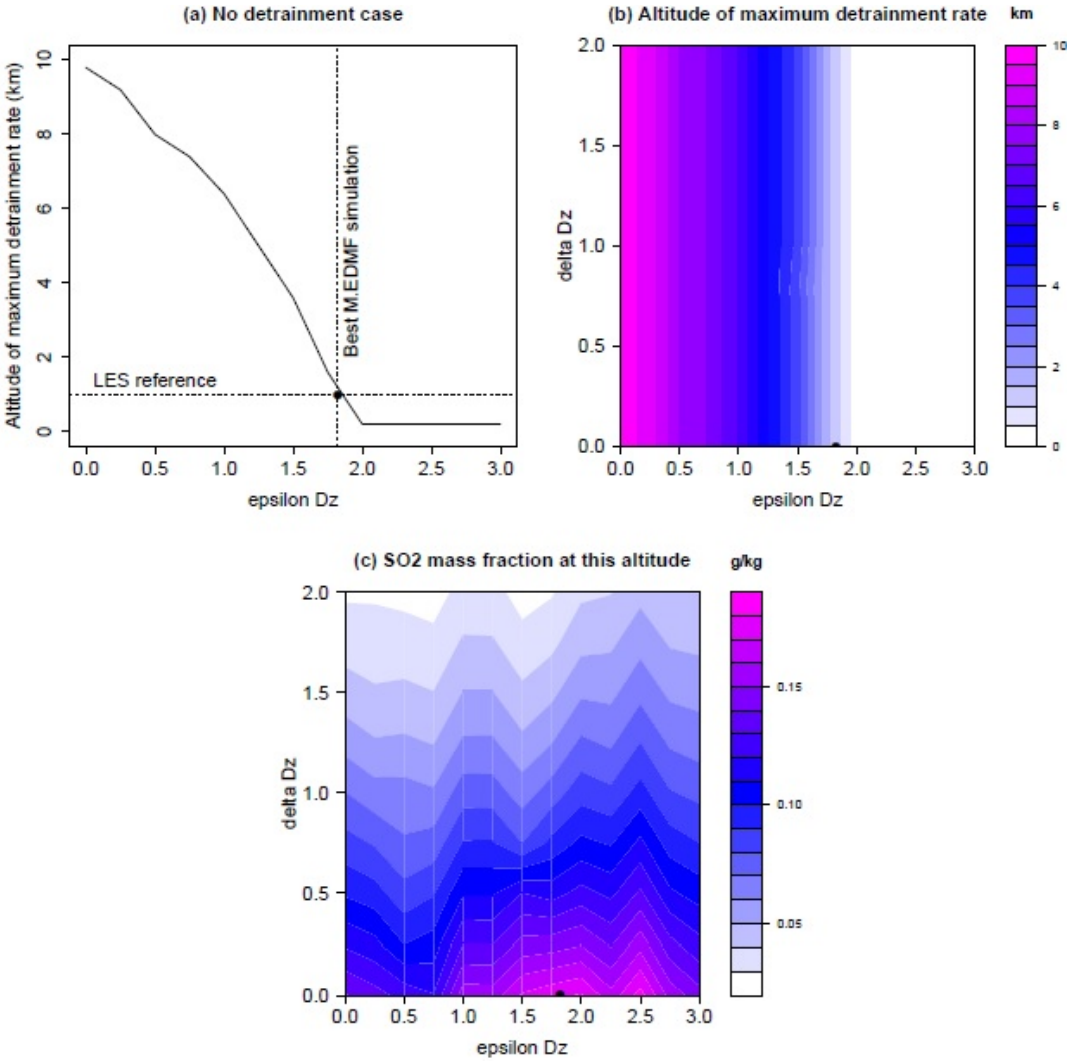

Figure 3.9: Sensitivity of plume characteristics - Sensitivity of plume characteristics to various entrainment (ε) and detrainment (δ) values prescribed for the first model level (within Δz = 40 m a.g.l.). An ensemble of 13 × 9 SCM simulations was considered to build these graphs, with dimensionless values of $\varepsilon\,\Delta z$ ranging from 0 to 3, and for $\delta\,\Delta z$ from 0 to 2 (by 0.25 steps in both cases). **(a)** $\delta = 0$ case: altitude where the maximum SO_2 mass detrainment rate is found as function of $\varepsilon\,\Delta z$. The horizontal dashed line is the maximum injection height (1.0 km) found in the reference LES. **(b)** Contour plot showing the altitude where the maximum SO_2 mass detrainment rate is found as function of both $\varepsilon\,\Delta z$ and $\delta\,\Delta z$. **(c)** Contour plot of SO_2 mass fraction in ambient air in the grid cell at this altitude. In all panels, the black dot marks the location in the ε-δ space of the best-fitted SCM simulation with respect to the reference LES simulation (see text for details).

Figure 3.9b reveals that the vertical plume development is mostly independent of detrainment. This is not unexpected, since the altitude reached by the plume is in great part driven by its initial buoyancy, the latter being affected only by entrainment but not by detrainment (which does not change the updraft intensive properties such as temperature and water vapour mass fraction). Considering the SO_2 tracer mass fraction at the altitude of maximum detrainment (Fig.3.9c), it is found to decrease with increasing detrainment in the first model layer (since less SO_2 mass is left available in the updraft).

Figure 3.10a shows the SO_2 mass fraction vertical profiles resulting from both the reference LES and the best M.EDMF simulation. The better adjustment in terms of maximum injection height is found for $\delta = 0$ and $\varepsilon = 1.82\Delta z^{-1}$, corresponding to $\alpha = 0.838$. The peak SO_2 concentration is found lower (by about 40%) and vertically more distributed than in the LES. It is clear in Fig.3.9c that adding detrainment in the first model level would not improve the result, since detrainment tends to dilute the peak concentration. Despite quantitative imperfection, the M.EDMF model is able to inject a volcanic tracer at the right altitude and at the right order of magnitude in terms of concentration, providing appropriate tuning of the basal entrainment parameter. This simulation is thereafter referred to as the best-fitted M.EDMF simulation.

Up to here, SO_2 mass fractions have served to adjust the ε and δ parameters. Figure 3.10b also shows the anomaly profiles of the water vapour mixing ratio $[H_2O]$ for the reference LES and the best-fitted M.EDMF simulation. (The anomaly is here defined with respect to the initial water vapour mixing ratio profile, i.e. as $[H_2O](z, t_{90}) - [H_2O](z, t_0)$, where t_0 and t_{90} are simulation times at 0 and 90 min, respectively.) At near ground level, the M.EDMF shows a lower water vapour mixing ratio than the LES model (this is owing to the modification in entrainment at $z = \Delta z$, which imposes a strong increase of the updraft mass flux in the first model level and, in turn, strong divergence of the water vapour mass flux which results in a negative source term for $[H_2O]$ at the grid scale). At higher altitudes (≥ 0.5 km) the M.EDMF simulation shows comparable agreement and differences with respect to the LES reference as for SO_2. Figure 3.10c and d shows the maximum detrainment observed at about 1 km, a.g.l., which coincides with the maximum of SO_2 tracer concentration (Fig. 3.10a) and water vapour anomaly (Fig. 3.10b). The entrainment and detrainment both reach nearly 0

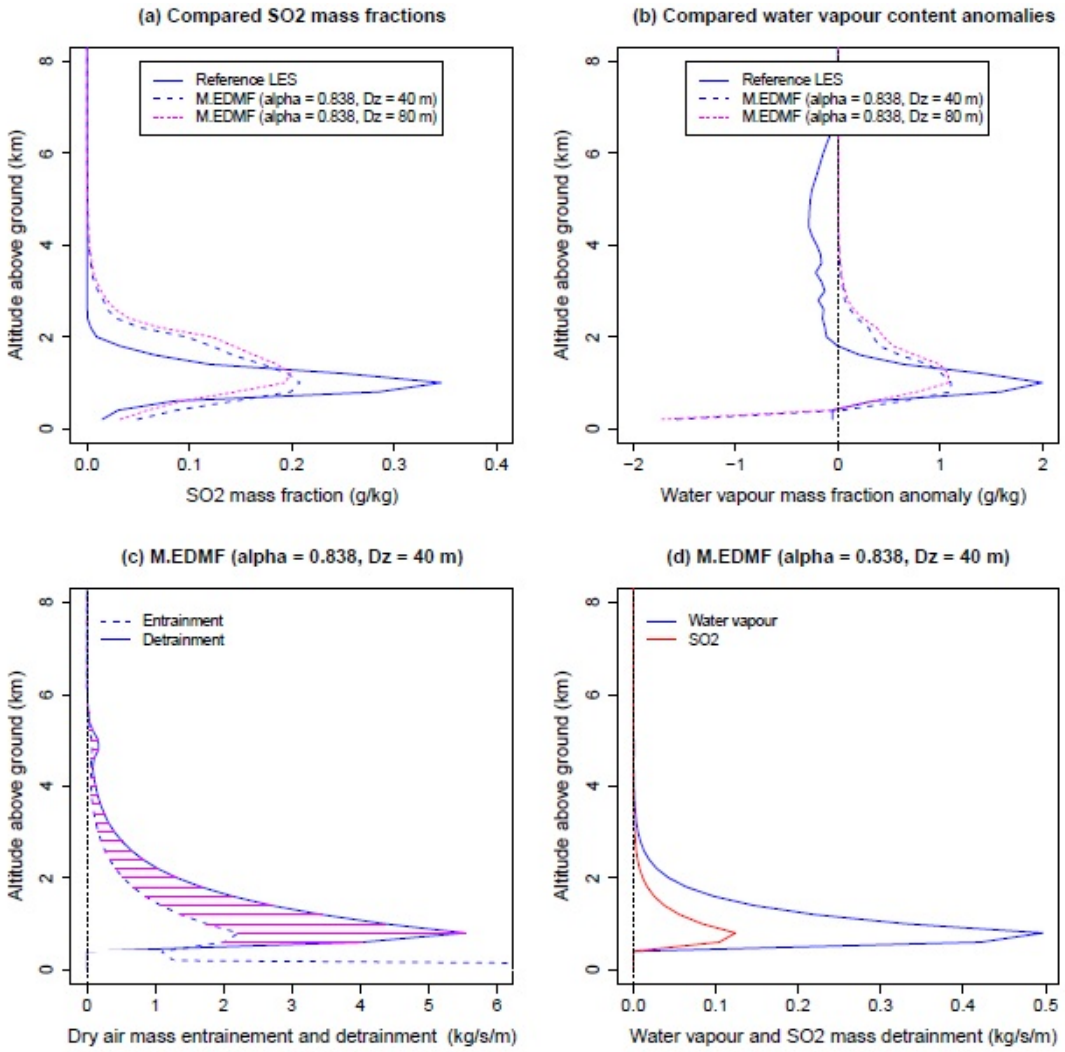

Figure 3.10: Results from the best-fitted SCM simulation with respect to the reference LES simulation (Fig.3.7b). - The best adjustment was found for $\delta = 0$ in the first model layer and a value of entrainment ε such that the fraction of fresh ambient air entrained at the top of the first model layer is $\alpha = 0.838$. **(a)** Compared SO_2 profiles in the SCM and LES. **(b)** Compared profiles of water vapour anomaly (defined as departure from the initial profile). **(c)** Profiles of dry air mass entrainment and detrainment rates ($\varepsilon\, M_u$ and $\delta\, M_u$, respectively). Where detrainment dominates, the difference is shaded in magenta. **(d)** Profiles of water vapour and SO_2 mass detrainment ($\delta[H_2O]M_u$ and $\delta[SO_2]M_u$, respectively).

at around 4 km, a.g.l. indicating the maximum height of the updraft and vanishing SO_2 mass fraction at this height (Fig. 3.10a).

In our simulation, ad hoc fresh air entrainment is prescribed only in the first model layer. The question that arises is whether the fraction α required to achieve the correct injection altitude is dependent of Δz. To address this issue, a sensitivity experiment was performed whereby a M.EMDF simulation was run with doubled vertical grid spacing ($\Delta z = 80$ m near the ground) and the same value for $\varepsilon\,\Delta z = 1.82$. This means that α is still equal to 0.838 but now this dilution factor is valid at 80 m above the ground. The resulting SO_2 and H_2O profiles are shown in Fig. 3.10a and b, respectively (magenta curves). In terms of peak altitude, intensity and vertical distribution, the profiles are very similar as in the M.EDMF simulation with $\Delta z = 40$ m. This result suggests that the required α value is not (or weakly) resolution dependent and (again) that the plume final height is primarily sensitive to its initial buoyancy at the top of the feeding layer, but much less to the depth of the latter. Clearly, further work is needed on the question of the influence of entrainment and detrainment - not only in the first model layer but also at higher levels - on the plume characteristics, but this is the subject of future improvements for our model. ————————————————-

3.6 Supporting analysis to the research article

In section 3.5.2 the article discusses the importance of entrainment into the plume generated in Fig.(3.7d). The updraft temperature (Fig.3.8) at the base of this plume is discussed and in support, here we present Fig.(3.11) which shows the vertical velocity of the updraft (left) and the updraft fractional area (right). This figure shows a updraft vertical velocity of about 70 m/s at 200 m above ground. This high velocity has a great impact on the cross sectional area of the updraft. It can be seen from Fig.(3.11, right) that the updraft fractional area decreases in size by approximately 6 times the value initialised at the ground level. This tube-like structure of the updraft cross sectional area is unrealistic. Hence, supported by the updraft temperature discussion in section 3.5.2, the question regarding if there is sufficient entrainment at the base of the plume arises.

A similar approach as the one presented in this study was undertaken by Rio *et al.* (2010). Here, a mass-flux scheme originally developed to represent the vertical transport

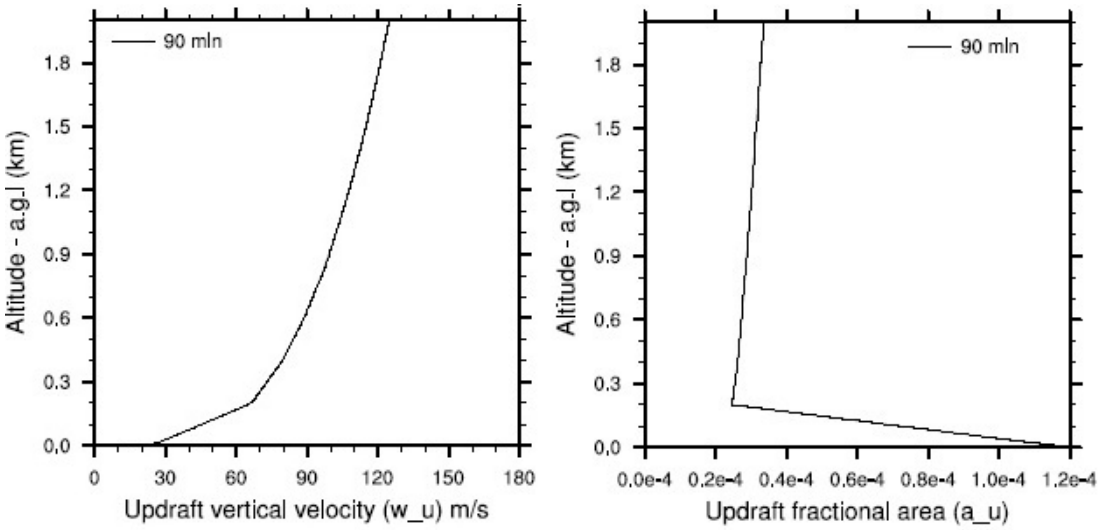

Figure 3.11: The role of high updraft vertical velocity on the updraft fractional area - The updraft vertical velocity of Fig.(3.7d) at 90 minutes (left) and the updraft fractional area of Fig.(3.7d) at 90 minutes (right)

by convective structures within the boundary layer, was adapted to represent plumes generated by fires, with the aim of estimating the height at which fire emissions are injected in the atmosphere. The parameterisation accounted for the excess of near surface temperature induced by fires and the mixing between convective plumes and environmental air. The strategy deployed by the study was to prescribe a 'feeding layer' at the base of the updraft, in which a certain amount of environmental air is introduced such that the updraft cross sectional area remains constant throughout this layer, as seen in Fig.(3.12).

Re-writing Eq(15) in Rio *et al.* (2010) by using the same notations as the ones used in this study and using eqs(3.6 and 3.7) or eq.(3.15) from this study, if $\delta = 0$ we obtain

$$\frac{\partial M_u}{\partial z} = E = \varepsilon M_u = a_u \rho_u \frac{\partial w_u}{\partial z} = \frac{a_u \rho_u}{2w_u} \frac{\partial {w_u}^2}{\partial z} = \frac{a_u \rho_u}{2w_u} g \frac{\theta_u - \theta_e}{\theta_e}, \tag{3.27}$$

where a_u and ρ_u are assumed constant and θ_e is the potential temperature of the environment (using the subscript 'e').

Now, using eq.(3.11) (or eq.(3.17)), eq.(3.27) can be re-written as

$$\varepsilon a_u \rho_u w_u = \frac{a_u \rho_u}{2w_u} g \frac{\theta_u - \theta_e}{\theta_e} \tag{3.28}$$

and is simplified to,

$$\varepsilon = \frac{g}{2w_u}\frac{\theta_u - \theta_e}{\theta_e}. \tag{3.29}$$

In other words, the entrainment in the feeding layer using eq.(3.31) after Rio *et al.* (2010) corresponds to

$$\varepsilon = \frac{B_u}{2{w_u}^2}, \tag{3.30}$$

where updraft buoyancy $B_u = g(\frac{\theta_u - \theta_e}{\theta_e})$, g is the gravitational acceleration.

By prescribing a feeding layer at the base of our updraft, such that the updraft cross sectional area remains constant throughout this layer, a certain amount of environmental air needs to be introduced in this layer. To calculate the fraction of ambient air needed, we re-arrange Eq.(3.23) using $\delta = 0$

$$\varepsilon = -\frac{ln(1-\alpha)}{\Delta z} \Longleftrightarrow 1 - \alpha = e^{-\varepsilon \Delta z}, \tag{3.31}$$

and further re-arrange eq.(3.31)

$$\alpha = 1 - e^{-\varepsilon \Delta z}. \tag{3.32}$$

Using Eq.(3.29, Eq.(3.32) can be rewritten as,

$$\alpha = 1 - e^{-\left(\frac{\Delta z g}{2{w_u}^2}\frac{\theta_u - \theta_e}{\theta_e}\right)}. \tag{3.33}$$

Applying Eq.(3.33) in this study, where $\Delta z = 40$m, $g \approx 9.8$m/s, $w_u = 24$m/s, $\theta_u \approx 1300$K and $\theta_e \approx 300$K, this equation yields,

$$\alpha \approx 0.68. \tag{3.34}$$

This means in order to keep the 'feeding layer' in this study constant, 68 % of environmental air needs to entrained into the plume base. In our study 83.4 % of ambient air was entrained into the plume base in order to validate our parameterisation with the LES simulation. Hence indicating that the feeding layer in this study is relatively constant.

3.7 Conclusions

In order to represent deep convective injections of volcanic emissions into the low to mid troposphere in case of effusive eruptions, the EDMF parameterisation by Pergaud *et al.* (2009) has been adapted. The adapted EDMF scheme takes into account the intense and localised input of sensible and latent heat near eruptive vents and induces a sub-grid convective plume.

We have shown the need to input the specific heat source in order to generate deep plumes using the Méso-NH model by adapting the EDMF scheme. LES simulations were also initialised using water vapour mass flux, sensible heat flux and SO_2 mass flux for the same area and intensities as for the M.EDMF model. In absence of appropriate terrain observations, the LES simulation (considered as a reference) was used to validate the EDMF parameterisation for volcano induced convection (i.e. M.EDMF model). The LES and M.EDMF models have both been successful in generating deep plumes and hence transporting SO_2 tracer to higher altitudes. We have further demonstrated the need to modify the existing lateral mass exchanges a few tens of metres above the localised heat source in the SCM model as without this modification the plumes generated are too deep because of overestimated temperatures a few tens of metres above the ground. The sensitivity of our model to lateral mass exchanges at 40 m above the ground (first model level above the ground) have been presented while further aiding us to tune our model such that SCM results (for SO_2 tracer concentrations) are coherent with the results obtained from LES.

Entrainment of ambient air in a volcanic plume is largely known to be one of the key parameters affecting its buoyancy. Since the first experiments by Morton *et al.* (1956), extensive research (modelling studies or laboratory experiments) has been deployed to constrain this sensitive parameter (e.g. Carazzo *et al.*, 2008, Hunt & Kaye, 2001, Kaminski *et al.*, 2005, Wright, 1984). Although great advances have been made by differentiating between the different regimes (volcanic jets, strong plumes and collapsing columns), it is clear from the comprehensive review found in Tate (2002) and Matulka *et al.* (2014) that this is still an area of open research. For our case, SO_2 concentrations have served to adjust the parameterisation parameters (prescribed ε and δ within the first model level). The best fit compared to the LES SO_2 profile was obtained with no detrainment and a large fraction of fresh air incorporated into the plume ($\delta = 0$, and

ε such that $\alpha = 83.8\%$). The resulting humidity profiles in the LES and SCM show a good agreement as well.

As this parameterisation has been used in an idealised and controlled set-up for one particular case study (January 2010 summit eruption), further work needs to be undertaken whereby the parameterisation is tested for different configurations (i.e. changes in volcanic heat sources; idealised and real case simulations). Furthermore, further investigation is needed on how entrainment and detrainment should be formulated, not only at the base but also at all levels of the updraft. Ideally, a formulation valid at all levels and for a large variety of eruption cases should be sought.

Acknowledgements

We greatly acknowledge the Piton de la Fournaise Volcanological Observatory (OVPF/IPGP) for providing pictures of the January and October 2010 summit eruptions, along with information relating to the eruptions themselves. We also thank the Méso-NH assistance team for continuous support and C.Barthe and Meteo-France for kindly providing us with ALADIN-Réunion atmospheric files as well as wind observation data. This work was performed using HPC resources from GENCI-IDRIS (grant x2014010005) and CALMIP (grant P12171). We wish to acknowledge the use of the NCAR Command Language (NCL, Boulder, Colorado) version 6.0.0 software for analysis and graphics in this paper. We thank the Observatoire des Milieux Naturels et des Changements globaux (OMNCG) and Observatoires des Sciences de l'Univers (OSU), Réunion along with the MoPAV project of the LEFE - CHAT program by INSU - CNRS (Institut National des Sciences de l'Univers - Centre National de la Recherche Scientifique) for their financial support and interest in this project. We finally thank P.Bechtold and the other anonymous referee for their careful reviews and constructive comments, as well as our colleage J.P.Pinty for helpful discussions. Edited by: R.Sander.

3.8 Appendix

3.8.1 Volcanic mass and energy sources in the LES expressed as surface fluxes

In the case of the LES, the surface fluxes corresponding to those from the volcanic updraft at surface level in the single column simulation, occur over one whole grid cell and hence the surface S, which we consider below for budget calculations, is $S = \Delta x\, \Delta y$. (Note that the ad hoc surface correction factor mentioned in the article body is here omitted.)

3.8.1.1 Mass fluxes (H_2O and SO_2)

To evaluate the mass flux of e.g. water vapour, the question to answer is what mass dm_{H_2O} is added between t and $t + dt$ into the model's lowest grid cell. Then, the mass flux F_{H_2O} reads

$$F_{H_2O} = \frac{1}{S}\frac{dm_{H_2O}}{dt}.$$

dm_{H_2O} is the H_2O mass contained in the volcanic gas injected into the atmosphere (note that it is in turn independent of the H_2O content of ambient atmospheric air). This gas is contained in a volume $Sw_u dt$ and therefore has a mass of $dm_u = \rho_{mix} S w_u dt$. Therefore, the mass of H_2O injected into the model between t and $t + dt$ reads

$$dm_{H_2O} = [H_2O] dm_u = \rho_{mix}[H_2O] S w_u dt$$

and, finally, this yields

$$F_{H_2O} = \rho_{mix}[H_2O] w_u$$

(Eq.3.24). The same rationale is also valid for SO_2, yielding Eq.(3.26).

3.8.1.2 Sensible heat flux

The surface sensible heat flux is basically the energy quantity per unit of time and surface which is efficient in causing a temperature change at constant pressure in the lowest atmospheric layer. Therefore, the enthalpy change must be considered. The enthalpy change dH_a of ambient air between t and $t + dt$ in the lowest model grid cell is related to the sensible heat flux F_s, such that

$$dH_a = F_s S dt$$

.

We want to know what enthalpy change is caused in the atmosphere by injection of a mass dm_u of volcanic gas. The total enthalpy of this volcanic gas mass (assumed to be a triatomic perfect gas of specific heat capacity at constant pressure $C_{p,mix}$) reads $dm_u C_{p,mix} T_u$. However, only a fraction of this enthalpy amount is available to heat the atmosphere. Indeed, when two bodies at different temperatures come in contact with each other, their respective final equilibrium temperatures match at an intermediate value (according to the second law of thermodynamics). Let T' be this equilibrium temperature. The enthalpy change of ambient air from temperature T to T' is

$$dH_a = dm_{air} C_{p,air} (T' - T)$$

,

($dm_{air} = \rho_{air} S \Delta z$ being the total air mass contained within the grid cell) while the enthalpy change of the volcanic gas is

$$dH_u = dm_u C_{p,mix} (T' - T_u)$$

.

The total enthalpy should be conserved during this transformation (first law of thermodynamics), such that

$$0 = dH_a + dH_u$$

.

Extracting T' from this equation yields

$$T' = \frac{T + \beta T_u}{1 + \beta}$$

,

where

$$\beta = \frac{dm_u C_{p,mix}}{dm_{air} C_{p,air}}$$

.

β can be assumed to be small, owing to the short time step used in the LES (0.01 s). Indeed, β can be rewritten as

$$\beta = \frac{\rho_{mix} S w_u dt C_{p,mix}}{\rho_{air} S \Delta z C_{p,air}}$$

.

ρ_{mix} and ρ_{air} have the same order of magnitude, and the same can be said for $C_{p,mix}$ and $C_{p,air}$. Hence, $\beta \ll 1$ since $w_u dt = 0.24$ m is small compared to $\Delta z = 40$ m. Under this assumption, $T' \approx T$ (i.e. the final temperature is close to the atmosphere's initial temperature). Therefore, the enthalpy transferred from the hot volcanic gas mass to the atmosphere is $dH_a = -dH_u \approx dm_u C_{p,mix}(T_u - T)$.

This finally yields

$$F_s = \rho_{mix} C_{p,mix}(T_u - T) w_u$$

(Eq.3.25).

Table 3.1: Variables and values used for LES and SCM models.

Variable	Notation	Model	Formula	Value	Units	Data type
Updraft H_2O mass fraction (at ground level)	$[H_2O](z_{grd})$	SCM/LES	n/a	0.8	kg kg^{-1}	Input
Updraft SO_2 mass fraction (at ground level)	$[SO_2](z_{grd})$	SCM/LES	n/a	0.2	kg kg^{-1}	Input
Updraft vertical velocity (at ground level)	$w_u(z_{grd})$	SCM/LES	n/a	24	m s^{-1}	Input
Updraft temperature (at ground level)	$T_u(z_{grd})$	SCM/LES	n/a	1323	K	Input
Pressure at ground level	$P(z_{grd})$	SCM/LES	n/a	78695	Pa	Input
Universal gas constant	R	SCM/LES	n/a	8.314	J mol^{-1} K^{-1}	Constant
Molar mass of H_2O	M_{H_2O}	SCM/LES	n/a	0.018	kg mol^{-1}	Constant
Molar mass of SO_2	M_{SO_2}	SCM/LES	n/a	0.064	kg mol^{-1}	Constant
Specific gas constant of the mixture (H_2O and SO_2) at ground level	R_{mix}	SCM/LES	$R(\frac{0.8}{M_{H_2O}} + \frac{0.2}{M_{SO_2}})$	395.49	J kg^{-1} K^{-1}	n/a
Density of the mixture (at ground level)	$\rho_{mix}(z_{grd})$	SCM / LES	$\frac{P(z_{grd})}{T_u(z_{grd}) \times r_{mix}}$	0.15	kg m^{-3}	n/a
Area of the fissure	$S_{Fis,SCM}$	SCM	n/a	120	m^2	Input
Area of Méso-NH cell	S_{MNH}	SCM	$\Delta x \times \Delta y$	1×10^6	m^2	Input
Updraft area	a_u	SCM	$\frac{S_{Fis,SCM}}{S_{MNH}}$	1.2×10^{-4}	n/a	Input
Ratio of ambient air entrained	α	SCM	n/a	0.834	n/a	Input
Area of the fissure	$S_{Fis,LES}$	LES	n/a	100	m^2	Input
Correction factor	$Corr$	LES	$\frac{S_{Fis,SCM}}{S_{Fis,LES}}$	1.2	n/a	n/a
Specific heat of the mixture	$C_{p,mix}$	LES	$4R_{mix}$	1581.96	J kg^{-1} K^{-1}	n/a
H_2O mass flux	F_{H_2O}	LES	$\rho_{mix}[H_2O]w_uCorr$	3.456	kg m^{-2} s^{-1}	Input
SO_2 mass flux	F_{SO_2}	LES	$\rho_{mix}[SO_2]w_uCorr$	0.864	kg m^{-2} s^{-1}	Input
Sensible heat flux	F_s	LES	$\rho_{mix}C_{p,mix}(T_u - T)w_uCorr$	9×10^6	W m^{-2}	Input

Table 3.2: LES model configuration.

Configuration	LES
Δ x, Δ y (m)	10
Δ t (s)	0.01
No. of points in x $\times$ y	100 $\times$ 100
Total run (min)	90
Start time (UTC)	10h50

Table 3.3: SCM model configuration.

Configuration	SCM
Δ x, Δ y (m)	1000
Δ t (s)	1
No. of points in x $\times$ y	3 $\times$ 3
Total run (min)	90
Start time (UTC)	10h50

4

First 3D application of Modified EDMF parameterisation

Contents

This final chapter reviews the first simulation of the 2010 eruption using the modified EDMF scheme in a three-dimensional configuration. Section 1 outlines the strategy of this study, while section 2 provides the configurations of the simulations performed. The results and analysis are outlined in section 3 and a conclusion for the chapter is given in section 5.

4.1 Strategy

Three ingredients with their own specific uncertainties control the atmospheric dispersion of emissions from a point source, such as volcanic plumes,

- the meteorological forcing,
- representation of the source (geometry and altitude), and
- the physico-chemical processes.

In order to test the M.EDMF parameterisation in a 3D real case set-up, a purely dynamic simulation transporting passively the plume of volcanic gas was carried out taking into account the weather conditions. Sulphur chemistry is not simulated here in this first application of the parameterisation. This test is based on a simulation of the same eruption period as for the 1D ideal case in chapter 3 of sect.**??**, i.e. January 2010 eruption which started at 10:27 (UTC), but the vertical gas plume was observed above the erupting fissure at 10:57 (UTC) (further details of the simulation is provided in the next section).

The Meso-NH version MNH-4-9-3 was used to perform the simulation. As for the simulations in the 1D set-up, two sets of simulations are performed. One, whereby the original EDMF scheme by Pergaud *et al.* (2009) is used and the other where the M.EDMF parameterisation is used.

The simulation of the volcanic gas plume proposed here (M.EDMF version) is interested in,

- the ability of the parameterisation to uplift SO_2 tracer to higher altitude and
- the transport of this passive tracer (representative of SO_2 emitted by PdF).

4.2 Configuration of the 3D simulations

The simulation starts on the 1st of January 2010 at 00:00 (UTC) and covers total period of 42 hours. The initial part of the simulation (up to 10.57 UTC, when the vertical plume developed above the fissure for the summit eruption) is the same simulation described as a 'spin-up' period in chapter 3, sect.3.4.3.2. This simulation is initialised and coupled with Aladin Reunion atmospheric files, which are updated every six hours (described in detail in chapter 3, sect.3.4.3.2). This simulation is stalled at 10.57 (UTC) and further continued as two simulations. Both simulations are restarted to cover the remaining 7 hours, whereby, one uses the 3D-EDMF shallow convection scheme of Pergaud *et al.* (2009) and the other the 3D-M.EDMF parameterisation (Fig.(4.1)).

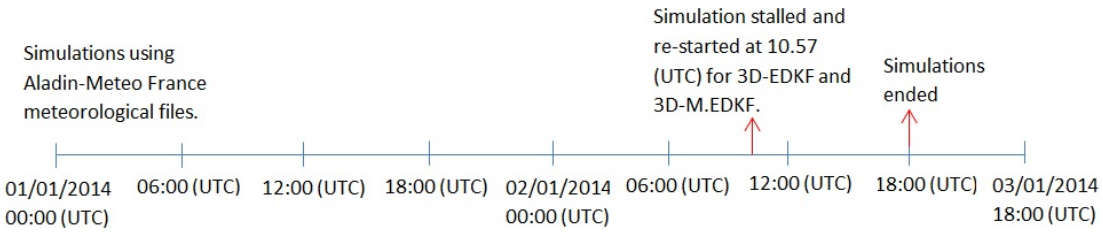

Figure 4.1: Simulation period - Schematic depicting the simulation time, coupling with Aladin-Réunion Météo-France every 6 hours. The two 3D simulations are restarted at 10.57(UTC), both initialised with a passive SO_2 tracer of 0.2 kg/kg, one using the 3D-EDMF parameterisation and the other with 3D-M.EDMF.

As described earlier in chapter 3, sect.3.4.3.2, the two simulations uses 2 grid nested domains covering both the regional and local scale, as depicted in Fig.(4.2). Two-way open boundary condition is applied to allow an exchange of information between both domains.

- The big domain has a horizontal resolution of 4 km, with a horizontal mesh of 100 × 100 points in both x and y (covering an area of 400 × 400 km^2)
- The smaller domain has a horizontal resolution of 1 km, with a horizontal mesh of 120 × 120 points in both x and y (covering an area of 120 × 120 km^2; Fig.(4.2))

Both domains are initialised with the same vertical grid of 72 levels as for the simulations in chapter 3 i.e. a vertical mesh stretched from 40 m at the ground to 600 m at the top of the model (Gal-Chen vertical system). The time-step used is 1 s and and 0.25 seconds for 4 km and 1 km resolution models respectively.

The two models are initialised with the same physical characteristics such as,

- the data for surface characteristic are obtained from ECOCLIMAT,
- a 1D turbulence scheme is used with a mixing length as described by Bougeault & Lacarrere (1989),
- the Kessler micro-physical scheme was activated (Kessler, 1969) and
- the deep convection scheme is not activated.

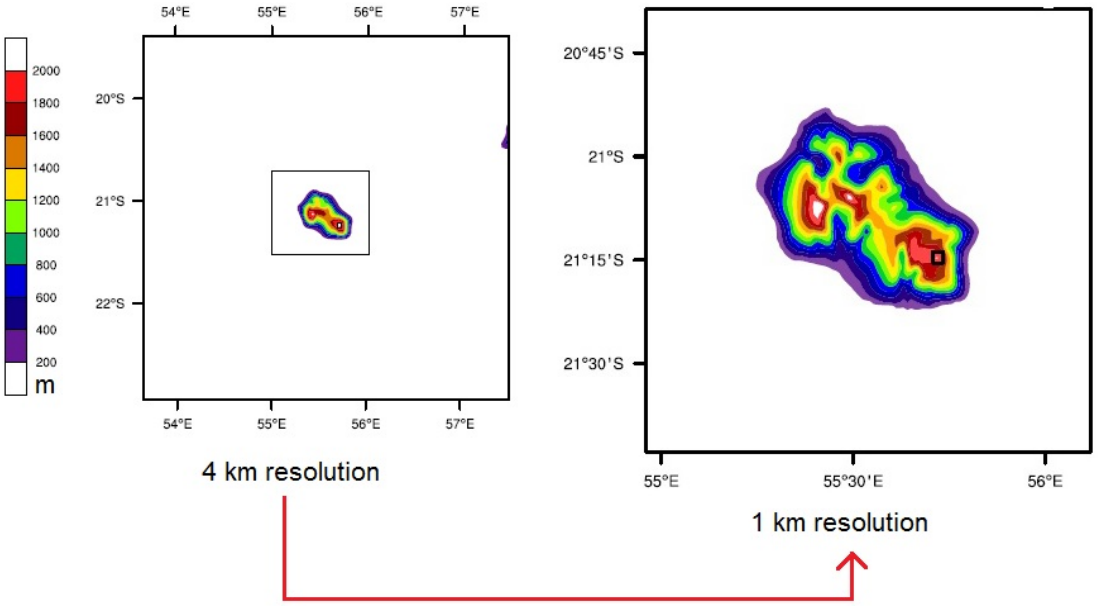

Figure 4.2: Nested grids - Two nested grids of resolution 4 km and 1 km with open boundary conditions.

A passive tracer is initialised in the 2 nested models in the same way as it was initialised in the simulation for 1D M.EDMF in chapter 3. This passive tracer is used to test the M.EDMF parameterisation, whereby SO_2 is injected into the atmosphere by the PdF volcano. The emission source is located at the summit of the volcano as in the 1D simulation and the fissure has the same size i.e. 60 m $\times$ 2 m, a total area of 120 m^2. The input concentration of 0.2 kg/kg is forced in the updraft at every time-step.

4.3 Results and analysis

4.3.1 Volcanic plume representation

To address one of the objectives of this study, we compare the results in Fig.(4.3). Results are shown for two cases, a simulation using 3D-EDMF (top four panels) and another using 3D-M.EDMF (bottom four). It shows a vertical cross section across the plume, where the top panel of every simulation 'type' is a slice in the longitudinal direction (at -21.245°S - latitude) and the bottom panel is through the latitudinal direction (at 55.711°E - longitude). To enable the comparison between the two outputs, the tracer label bar has been normalised by diving the diluted atmospheric concentration

by the maximum concentration.

Figure (4.3, for EDMF) shows that the maximum tracer concentrations remain close to the source point and the advection of the tracer by the winds also remain mostly at the altitude of the source point. In contrast, the M.EDMF outputs clearly shows that maximum tracer concentrations are found at around the 1.4 km a.g.l - above ground level (i.e. 4 km altitude a.s.l), whereby, higher concentrations of the tracer are advected to the west of the Island by the trade winds. Furthermore, due to the induced volcanic convection, we also find higher concentrations at around 2.4 km a.g.l (i.e. 5 km a.s.l) which are advected to the east of the island by the westerlies in the free troposphere above the trade wind inversion (Lesouëf, 2010). It is clear from these figures that the M.EDMF parameterisation is also effective in ejecting volcanic gaseous species to higher altitudes in a 3D configuration.

Although at this point it is evident that the vertical transport ability of the M.EDMF parameterisation is also applicable in 3D, we further compare the SO_2 profile of the 3D-M.EDMF with the results from the 1D-M.EDMF (shown earlier in chapter 3, Fig.(3.9a)) to check the coherence in terms of the maximum injection height between the two models. The results of this comparison are shown in Fig.(4.4, middle and right figures), which also shows the wind profiles extracted from the 3D-M.EDKF simulation just above the source point (left figure). The SO_2 profile from the 3D simulation was extracted from the column right above source point, where the heat and tracer fluxes were initialised.

It is encouraging to see that the maximum tracer height from the 3D-M.EDMF is the same as the 1D-M.EDMF (SCM), i.e. about 1.4 km a.g.l. As expected, note that the concentration level of the two columns are not of the same magnitude. This is largely related to the 3D set-up and the meteorological factors (Fig.4.4 displays the winds, i.e. u and v component just above the source), where as in 1D SCM, the wind profiles were stabilised. Due to this difference even the vertical distribution of the tracer in 3D set-up is slightly lower than that of the SCM model. Furthermore, in presence of horizontal wind, the horizontal divergence of the tracer mass flux, namely j_{SO_2}=[SO_2] ρ u (refer to Fig.4.5), is positive even with uniform u, since the input concentration is zero and not the output. As a result, there is a sink term in the SO_2 budget in the cell, that was not present in the 1D simulation and overall results in a reduced concentrations locally in the 3D version.

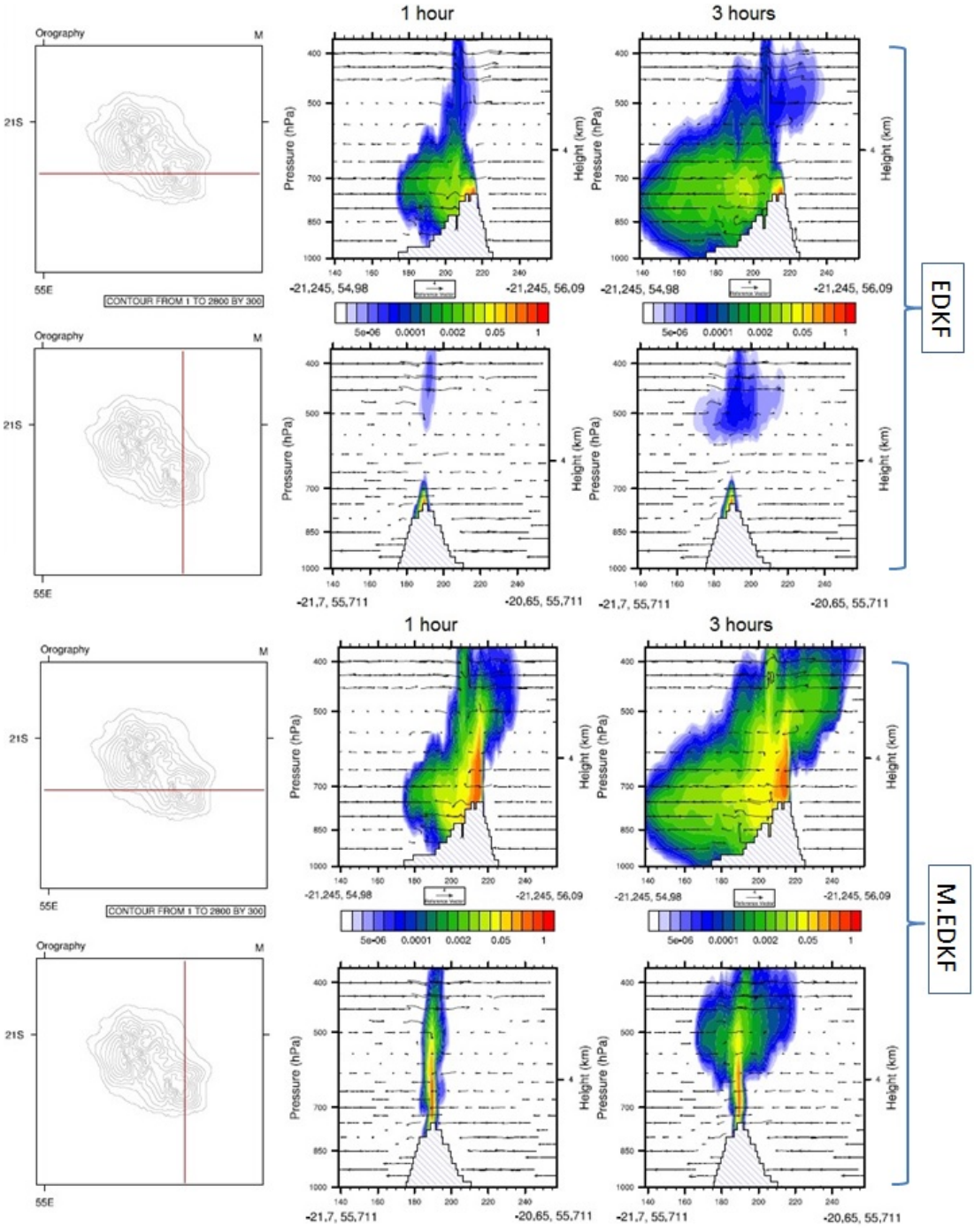

Figure 4.3: Vertical cross section - Volcanic plume representation for both EDMF (top two panels) and M.EDMF (bottom two panels) at 1 and 3 hours after the start of the eruption for 1 km resolution model. Vertical slices through the volcanic plume along the latitude (-21.245°S; top for each case) and along the longitude (55.711°E; bottom of each case). Note: (i) the SO_2 tracer concentrations have been normalised by dividing the concentrations by the maximum, (ii) a logarithmic colour scale is used for the normalised concentrations

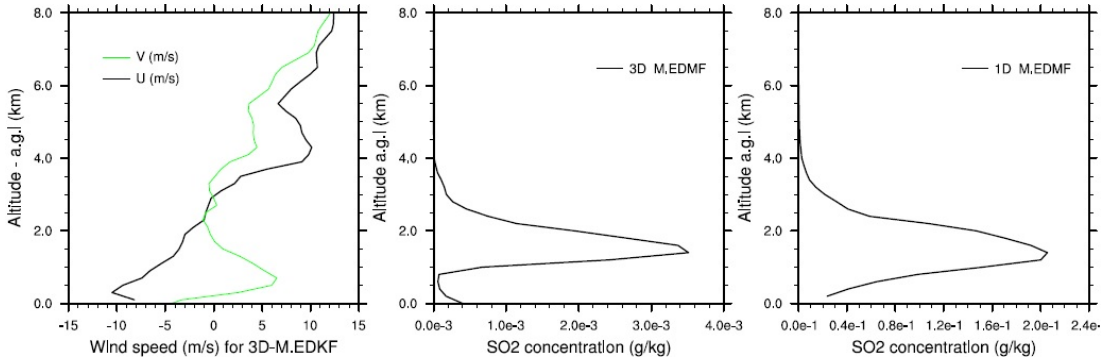

Figure 4.4: Tracer profile comparison and winds - Wind profiles for u and v component above the eruptive fissure for 3D-M.EDKF model (left). Tracer profile above the eruptive fissure extracted from 1 km resolution model of the 3D-M.EDKF simulation (middle). Tracer profile from the 1D SCM model of chapter 3, with $\alpha = 0.834$ (right). Note; the SO_2 concentration scale of the two profiles are different.

4.3.2 SO_2 measurements by ORA

Reunion Air Observatory (ORA), part of the Associations Agréées de Surveillance de la Qualité de l'air (AASQA) is responsible for monitoring air quality in La Réunion Island. During the eruption of January 2010 certain fixed stations dotted around the island collected SO_2 concentrations (locations displayed in Fig.(4.6)). The data is collected every 15 minutes with automatic SO_2 analysers SF-2000 (SERES) models through UV fluorescence spectrometry.

Due to the location of certain stations they have been grouped as displayed in Fig.(4.6). Data collected every 15 minutes from these stations (except the station of 'Bons Enfants' as data for the day of the eruption is not available) have been plotted for 3 days, i.e. 01 of January till the 03 January 2010 in Figs.(4.7) to (4.8). Except for the station of 'Bourg Murat' which is located at an altitude of 1600 m (a.s.l) and in a rural area, all stations are located at an altitude ranging from 10 - 50 m a.s.l. These stations are placed strategically around the island such that they are either under the influence of an industrial zone e.g. 'CIRFIM', 'Cambaie', 'Titan', 'La Marine' and 'Sarda Garriga' or under the influence of an urban zone e.g. 'Luther King' , 'Joinville' and 'Lislet Geoffrey'.

For stations 'Luther King' and 'Bourg Murat' majority of the collected measurements remain around 1 and 2 μg m^{-}3 for the three days. For station 'Sarda Garriga'

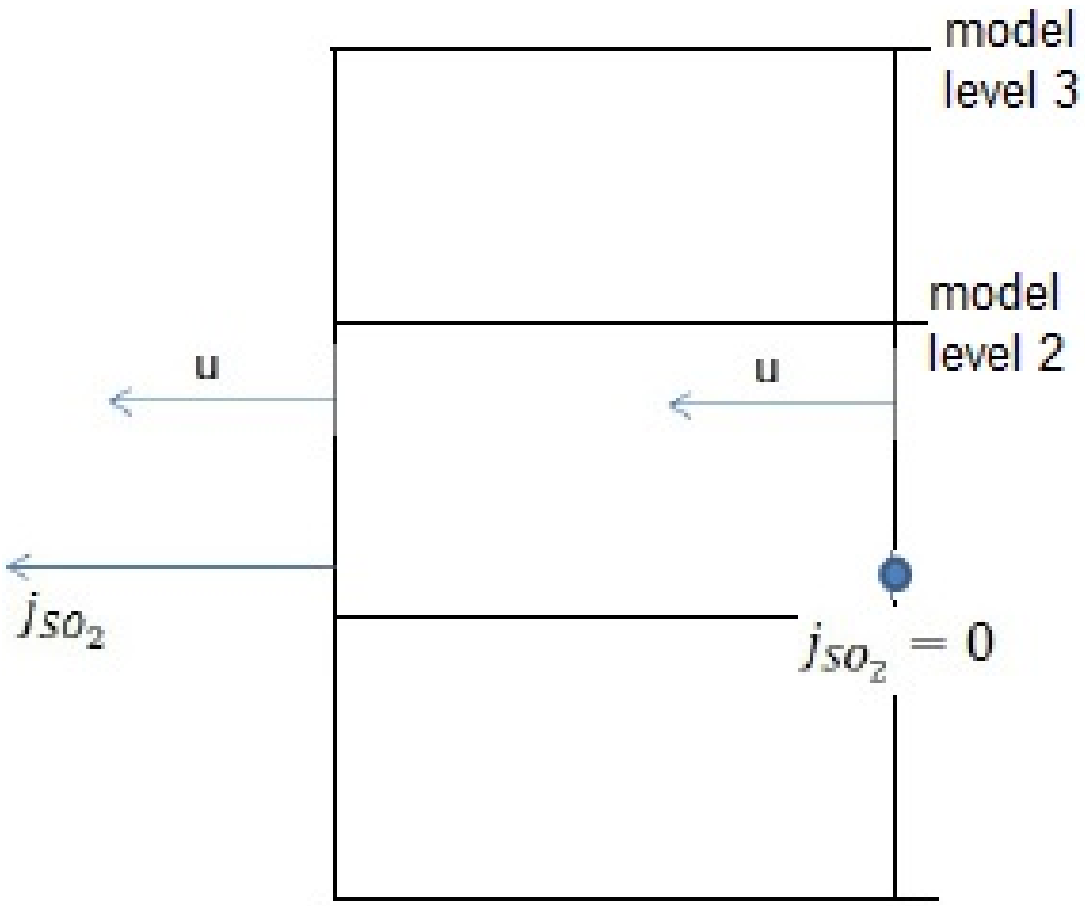

Figure 4.5: Horizontal wind in the model - Presence of horizontal wind in the model (u), input concentration is zero, i.e. j_{SO_2}

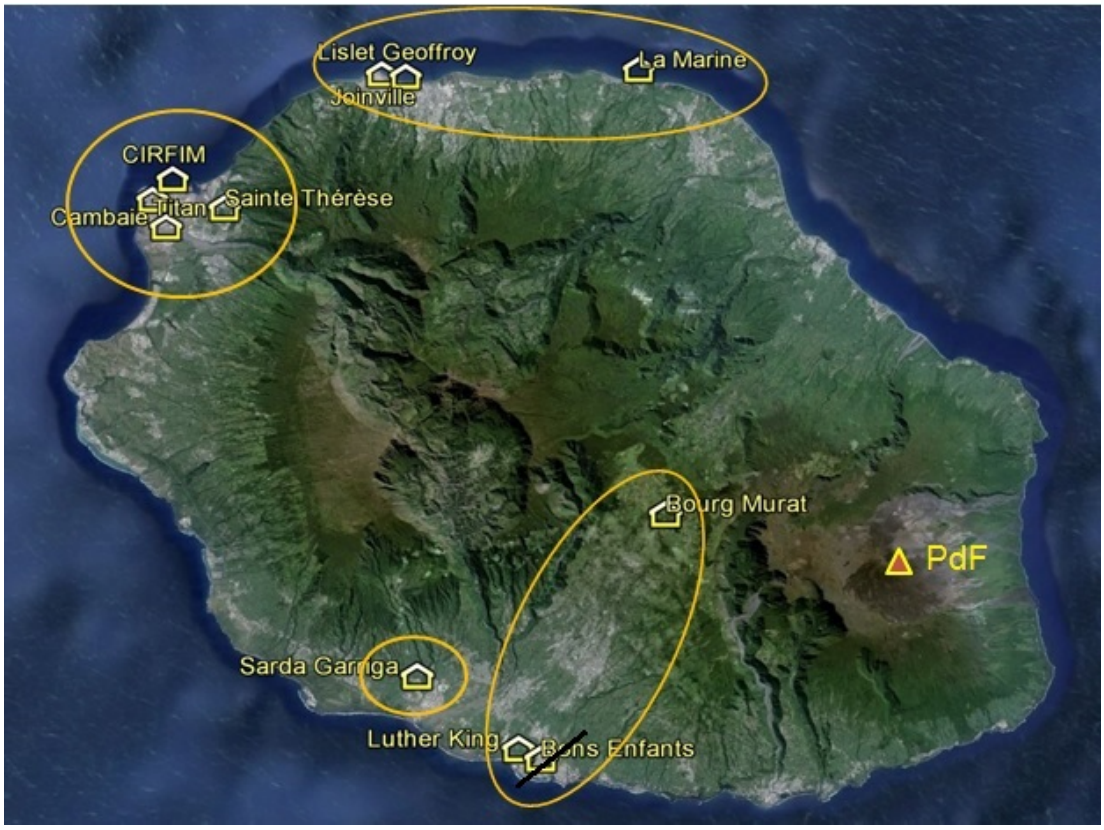

Figure 4.6: ORA pollution measuring stations - Locations of the stations around La Réunion Island that collected SO_2 data

there is one peak observed each day of around 60 - 100 μg m^{-}3 which is most likely related to the industrial zone of GOL (one of the two sugar refineries of the island) which lies in the vicinity. After the eruption started on the 02 January 14:30 (Reunion Time, RET) marked by a black vertical line, there is no observed evidence of a signal related to eruption.

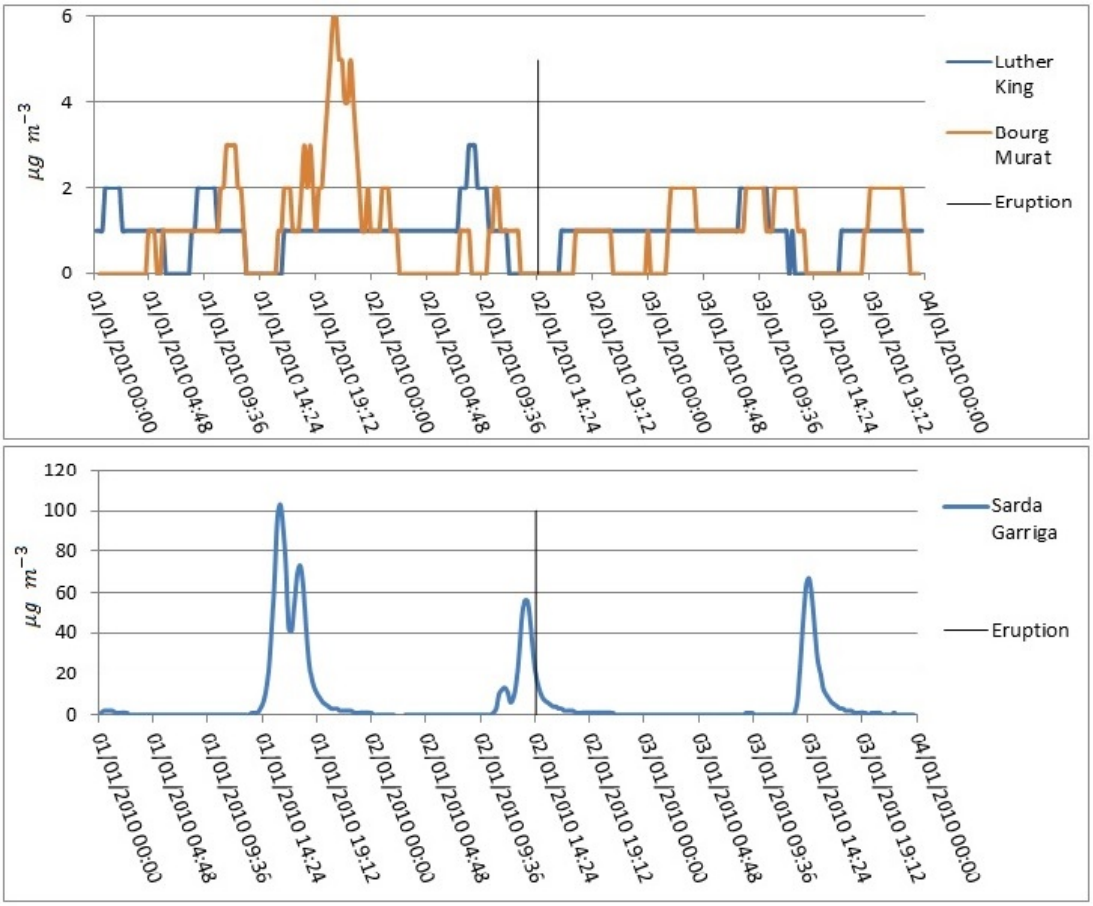

Figure 4.7: SO_2 **concentrations measured by stations in the south - south west** - SO_2 concentrations measured by three stations namely, Sarda Garriga, Luther King and Bourg Murat over three days, i.e. 01 till the 03 January 2010. The start of the eruption is marked by a black vertical line. The time of the day displayed is in RET i.e. UTC+4 hour

For the stations located in the north and north-east of the island, majority of the measurements remain below 6 μg m^{-}3 for the three days, apart from the odd peaks between 10 - 15 μg m^{-}3 for the 01 Januaray for station 'Titan' and 'La Marine'. Even for the station 'Cambaie' there is a repetitive signal every day around 14:30 with

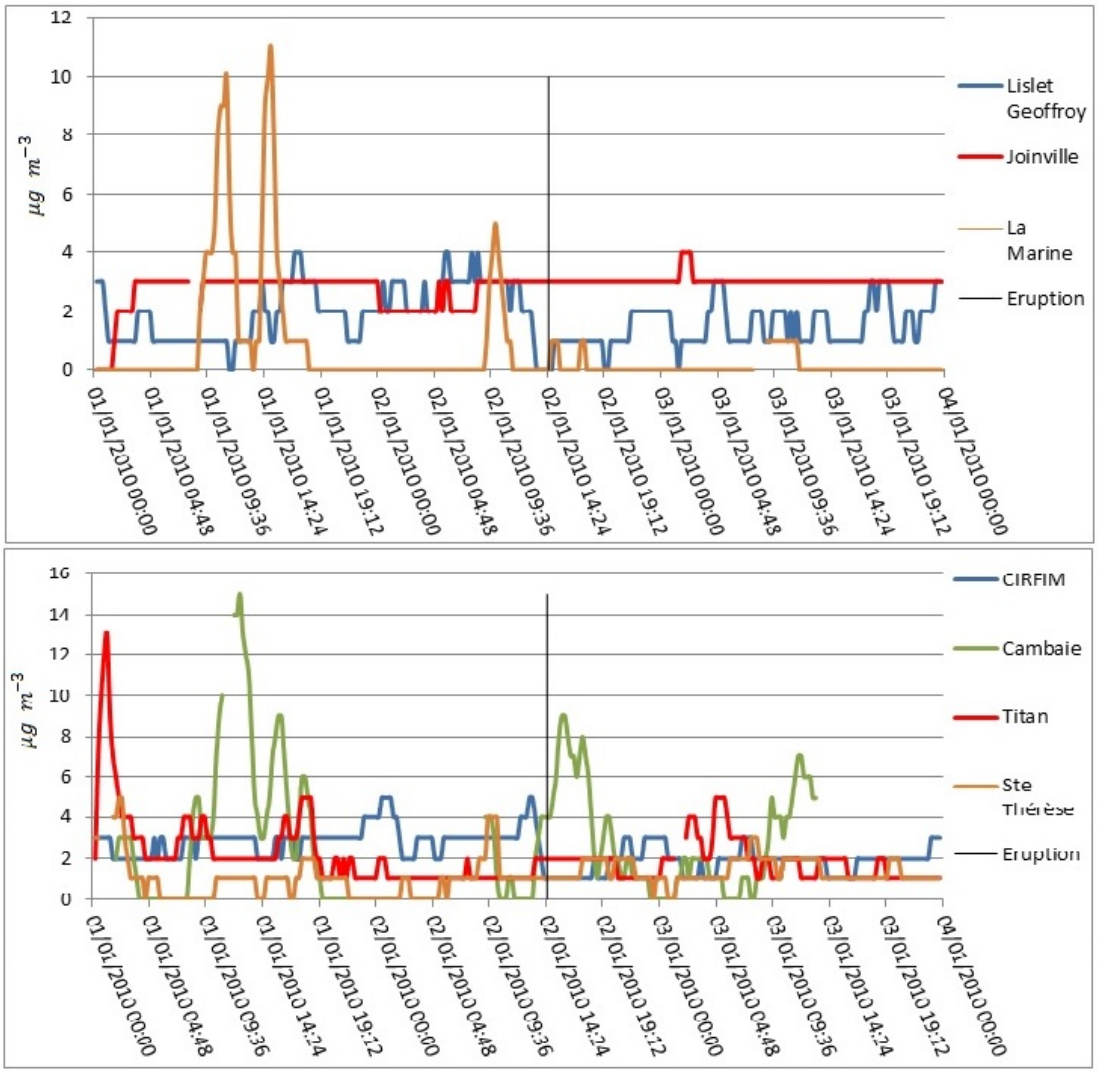

Figure 4.8: SO_2 **concentrations measured by stations in the north and north-east** - SO_2 concentrations measured by seven stations namely, Lislet Geoffroy, Joinville, La Marine, CIRFIM, Cambaie, Titan and St. Therese over three days, i.e. 01 till the 03 January 2010. The start of the eruption is marked by a black vertical line. The time of the day displayed is in RET i.e. UTC+4 hour

values ranging from 8 - 14 μg m^{-}3. On the whole there is no evidence of a signal specifically due to the eruption of 02 January. Figs.(4.7) and (4.8) both indicate the usual background anthropogenic values ranging from 1 - 20 μg m^{-}3 as indicated by previous studies such as Viane *et al.* (2009) and Bhugwant *et al.* (2009).

4.3.3 Volcanic plume transport

The 3D M.EDMF simulation was run for a total of 7 hours from the eruption start time (Fig.(4.1)). In this section we discuss the regional transport of the SO_2 tracer by the model. There already exists a considerable knowledge related to the local meteorology of islands (Lesouëf *et al.*, 2011). Lesouëf (2010) and Lesouëf *et al.* (2011) investigated the local-scale transport of pollutants over Réunion Island due to perturbations by the Island's topography and hence provides some basis for comparison with this study.

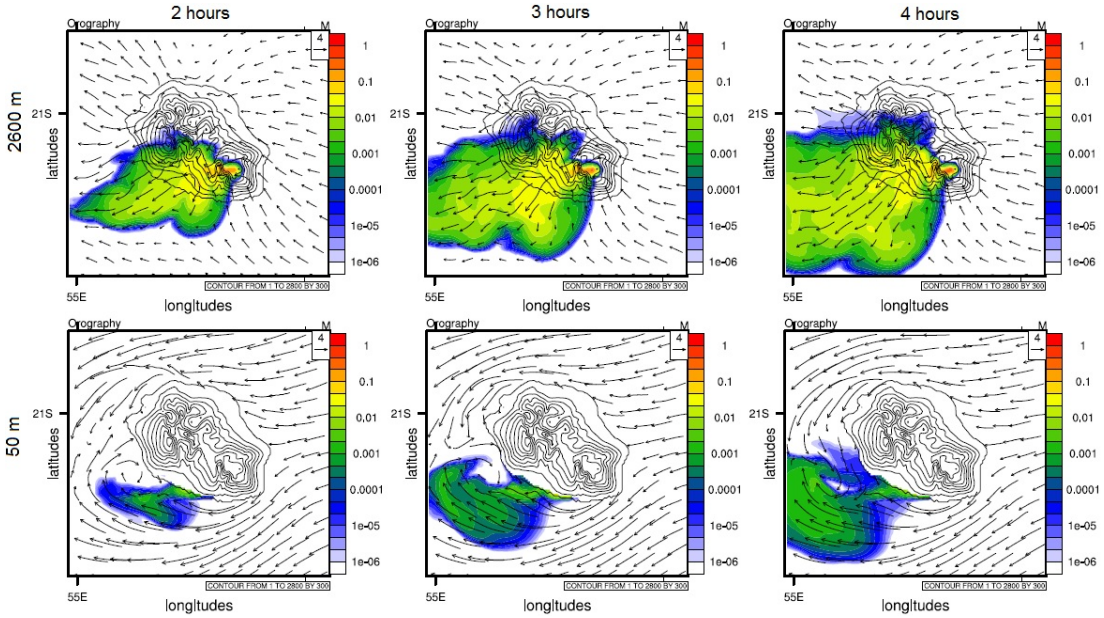

Figure 4.9: M.EDMF 3D simulation; horizontal slices - Horizontal slices of the island at 50 m a.s.l (bottom) and 2600 m a.s.l (top, PdF) at 2, 3 and 4 hours after the eruption initiation. Note, the SO_2 tracer concentrations have been normalised by dividing the concentrations by the maximum.

The simulation displays the 'usual' characteristic of the meteorological dynamics as expected when trade winds' flow is blocked by an orographic obstacle of an island. Fig.(4.9, bottom-panel) displays how the trade winds (east-north-easterly near the sur-

face (50 m), characteristic flow for the austral summer) is blocked by the orographic obstacle and splits into two flows that contour the island, also known as the 'flow around'. As explained by Lesouëf *et al.* (2011) this splitting is related to the lowest inversion layer which exists just on top of the marine boundary layer. This splitting of trade winds generates an acceleration of the winds parallel to the flow (the ones that contour the island) and a return flow on the leeward side of the island (generally opposite to the general flow) (Lesouëf, 2010). This is to say that when the general air flow bypasses an island, a wake wind grows on the leeward side of the island where the wind intensity decreases (due to the 'protective' effect played by the island's orography) and large vortices can occur. This characteristic is observed in the bottom panel of Fig.(4.9) where the tracer concentrations which have reached the sea level after 1 and 3 hours after the initialisation of the eruption are entrained in a spiral on the south-west part of the island. The tracer released at 2600 m a.s.l, is advected to the south and south east of the island by the trade winds at this altitude.

Generally the island is divided across the north-west to south-east whereby the western side of the island is most affected by the volcano emissions compared to the north-eastern side. As expected, after 1 hour of simulation time higher concentrations are observed at 2600 m in the south-west region than at 50 m altitude. However, the concentrations brought to 'Sarda Garriga' location are further transported into the valley of Gol by the uphill flow. Four hours into the simulation, it is the western region of the island that is mostly affected by the tracer. In contrast, the eastern regions of the island are substantially less impacted by the tracer, largely due to the trade wind direction.

In contrast to the ORA measurements around the island which show no signs of the volcanic plume signal, the simulation clearly show that the south, south-west sites of 'Luther King', 'Bourg Murat' and 'Sarda Garriga' are most impacted by the eruption. Furthermore, sites such as 'Titan', 'Cambaie' and 'CIRFIM' are also affected but comparatively on much lower scales than the south, south-west sites (not shown).

Figure (4.10) shows the ground SO_2 concentrations as extracted from the simulation over time for the stations just mentioned. Concentration levels for the north-east stations are not shown, as the results from the simulations were extremely low and can be considered as zero values.

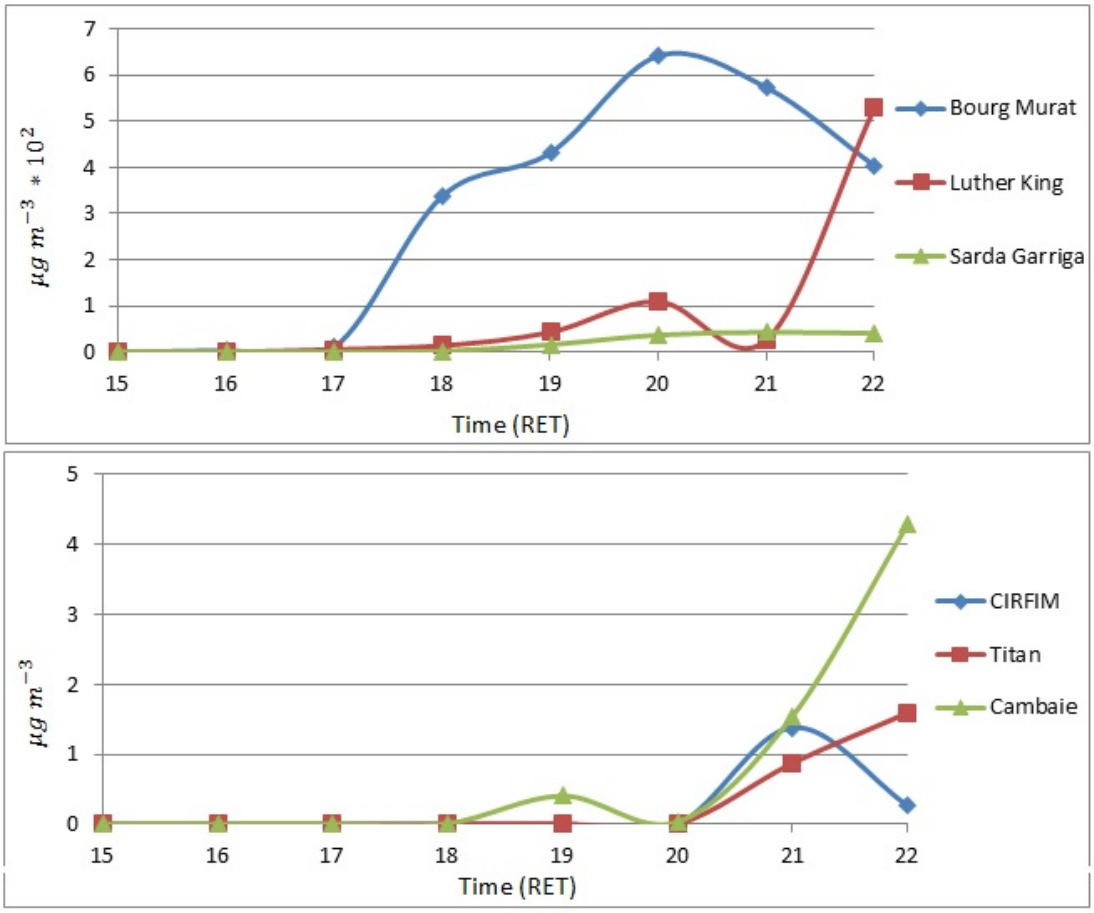

Figure 4.10: Simulated SO_2 concentrations - 2nd January 2010 - Concentrations for sites most affected by the volcanic plume during the simulation. Note, that the vertical scale for the two grouped stations are different. Simulation outputs at every hour (total of 7 hours simulation run time) since the plume initiation.

Much elevated levels of tracer concentrations are observed for the stations located in the south-west region of the island than the north-north-west regions. Most particularly for the site of 'Bourg Murat' which after 3 hours of simulation time (i.e. at 18:00 RET) show about 350 μg m^{-}3 and increase to a maximum at 620 μg m^{-}3 at 20:00 RET. This is largely due to the placement of the station at 1600 m and in the down wind of the volcanic plume. In reality, the Bourg Murat station did not sample any volcanic plume. This is an indication that the plume direction is not correct in our simulation. The concentrations for 'CIRFIM', 'Titan' and 'Cambaie' are below 5 μg m^{-}3. If SO_2 from the volcano had reached these stations, the signal might not emerge due to the 'normal' background concentrations.

Hence, a vital question arises, why isn't this signal reflected in the data collected by ORA, especially for the south-west sites?

4.4 Downwind chemistry

It is important to recognise that this simulation contains no chemical transformations of SO_2, i.e no sinks, and hence largely implicates that the values observed in the simulation are incorrect. Hence, what are the possible reasons why the south-west ORA stations did not pick up the SO_2 volcanic plume signal?

The measurements by ORA are made several km from the source and there is the potential for in-plume chemical transformation of SO_2 to sulphate aerosol, whereby the conversion rates depend on meteorological conditions. (The station at 'Bourg Murat' is located at 1600 m a.s.l and about 15 km north-west of the volcano, 'Sarda Garriga' is located at 50 m a.s.l and about 30 km west of the volcano and lastly, 'Luther King' is located at 10 m a.s.l and about 28 km south-west of the volcano). Volcanic plume ageing and removal mechanisms are not well understood, especially for tropospheric plumes e.g. the oxidation of SO_2 by OH radicals and their wet and dry deposition (McGonigle *et al.*, 2004). McGonigle *et al.* (2004) consolidates findings by previous studies stating how the uncertainty regarding the loss rates estimates vary between <1 to >99% per hour. In their study of SO_2 depletion in tropospheric volcanic plumes of Masaya volcano in Nicaragua, they found minimal variations in SO_2 fluxes for plumes travelling up to 30 minutes. Furthermore, they found that even diurnal variations in temperature and relative humidity have miminal effect on the plume ageing. In our case, the plume laden

with very high SO_2 concentrations begin to reach 'Bourg Murat' just after 2 hours of simulation time. Hence leaving sufficient time for some chemical transformations to take place. Also, Réunion Island is influenced by tropical and subtropical climates. During the austral summer (the period of study, i.e. December to February) the Intertropical Convergence Zone (ITCZ) is close to the island, resulting in high relative humidity (just above 60% for January 2010) and weak trade winds, favouring the formation of deep convective systems (Lesouëf, 2010, Lesouëf *et al.*, 2011). Such an atmosphere would favour aqueous chemistry (see sect. 2.1.2). On the whole various sinks for SO_2 are not activated in the model. Furthermore, the presence of water would further propagate reactions for H_2SO_4 formations and lastly, the aqueous phase chemistry whereby SO_2 gas molecules react with H_2O_2. Such reactions which are not considered in the simulation can be one reason as why our simulation shows much higher SO_2 concentrations then the ones measured by ORA stations. Also note that the volcanic updraft is continuously enriched with SO_2 concentrations throughout the simulation period (at every time step of the model) and in return enriching the atmosphere.

Another possible reason (not relating to the chemistry within the model) concerns the dynamics simulated by Meso-NH. Fig.(4.3) shows a strong vertical mixing (outside the eruptive column). Such a mixing might be overestimated by the model. It can not be excluded that the vertical mixing was weak in reality and the SO_2 plume remained in altitude without reaching the surface (including the Bourg Murat location, which is about 1000 m below the eruption altitude).

4.5 Conclusion

The application of the parameterisation in a 3D real case set-up has been successful in injecting tracer to higher altitudes. The results in terms of maximum height reached by the tracer representing SO_2 is in accordance with the results from the 1D SCM (chapter 3) and with the observed height of the plume on the 2nd of January 2010. The dynamics reproduced by the model in terms of trade wind direction along with the splitting effect due to the island appear to be well represented in the model. However, the vertical mixing in the simulation do appear to be over exaggerated by the model (not the case in reality). This in accuracy could be one of the reasons behind the inconsistency between the ORA SO_2 measurements and those produced by the model.

There is also the inactivation of chemistry in our simulation and hence certain sinks for SO_2 are not accounted for. One last reason but relatively small reason could be due the fact that in our simulation SO_2 concentrations are continuously emitted from the point source throughout the simulation duration. At this stage we can only speculate as to the lack of plausible chemical reactions and the inaccuracy of the model to correctly produce all the dynamics that may produce such an inconsistency. It is evident that further tests need to be carried out in a 3D configuration to further investigate the transport of the plume.

General conclusions and perspectives

Volcanic eruptions and the atmospheric dispersion of volcanic plumes burdened with volcanic gases and ash pose a great danger to populations along with a hazard for air traffic. For example, the eruption of Eyjafjallajokull in April 2010 had created a great disturbance to the air traffic. The Volcanic Ash Advisory Centers (VAAC) have the responsibility of predicting the ash dispersion in the atmosphere during major eruptions. Models used by VAAC rely on certain input parameters, such as, the eruption size and the mass eruption rates. Since such parameters are not determined by the model itself and rely on various external methods of determination (e.g. simulations, volcanic databases, etc), the uncertainties in such input parameters increase with further implications on the dispersion of these volcanic plumes and the associated risks.

The Piton de la Fournaise (PdF hereafter) volcano located on Réunion Island, as well as Kiluea in Hawaii, are mainly of type effusive. Unlike the explosive volcanoes, their volcanic plumes are limited to the lower troposphere. The ash dispersion models managed by VAAC are currently not adapted to report or alert on risks from low-lying volcanic plumes ladent with sulphur species, such as those generated by effusive volcanism. However, such plumes are known to be hazardous to populations and the environment. It has been shown during the eruption of Piton de la Fournaise in April 2007 that the alert threshold for SO_2 fixed by the MEDDTL (Ministry of Ecology, Sustainable Development, Transport and Housing) had been widely exceeded in some inhabited areas the island. However, currently no air quality model capable to alert on such volcanic hazards exist.

Operations at VAAC depend on our continuous ability to measure and model volcanic plumes of all types. In the framwork of the MoPaV-STRAP project of the LEFE

- CHAT program by INSU - CNRS is to develop softwares which are efficient and easy to integrate into operational models for crisis management. Hence, from the aspect of modelling volcanic gas plumes, this Ph.D study aims to take the first steps in parameterising effusive volcanic plumes in an atmospheric dispersal model, whereby the volcanic injection plumes can be efficiently represented. Thus, allowing a realistic dispersion of these plumes on a local to regional scale.

More precisely, the objective of the work carried out in this thesis was to study the volcanic plume convection triggered by large heat fluxes at the exit point of a volcanic vent (point source). This thesis aimed to parameterise the volcanic convection for a particular case study of January 2010 eruption of PdF using a meso-scale atmospheric research model, Meso-NH. A study (eruption case of April 2010 of PdF) conducted by Lesouëf (2010) as part of the Ph.D thesis has illustrated the capability of Meso-NH in reproducing the SO_2 concentrations at different regions of the island (despite the absence of chemical reaction schemes related to various transformation of SO_2 in the model). Hence, this model was adequately chosen in order to fulfil the objectives of this current Ph.D study.

The starting point of this thesis is to use the Meso-NH model to simulate idealised cases representing simplified but realistic vertical atmospheric dynamics. The shallow convection scheme integrated in Meso-NH, namely EDMF by Pergaud *et al.* (2009) was adapted to represent volcanic plumes. Such an adaptation was realised by initialising certain variables at the base that characterise a volcanic plume, e.g. temperature and gas composition; ejection speed; diameter of the vent/fissure. This modified scheme, appropriately named M.EDMF was implemented in a one-dimensional (1D) column model (Single Column Model, SCM hereafter) using 1 km $\times$ 1 km horizontal grid (a horizontal resolution typically used in regional atmospheric dispersion models).

Firstly an appropriate case study from one of the recent eruptions of PdF was selected on the basis of it's adequacy to this type of idealized simulation. The January 2010 summit eruption was chosen for its simple configuration; there was a well developed visible gas plume above the eruptive fissure; the plume did not appear to be affected by the winds (implying low winds). In return for this simplicity, data available for this eruption in terms of emission of sulphur, infra red images and plume height were unfortunately limited (in comparison to other more complex eruptions). Case study identified, the shallow convection scheme was modified for a correct representation of

volcanic heat fluxes and the geometry of the source point, which were sufficiently well characterised through observations.

Due to the lack of data available for the validation of this case study, a LES (Large Eddy Simulation) simulation with 10 m horizontal resolution was run for a duration of 1.5 hours. The LES simulation was initialised with the same heat flux, water vapour flux and surface geometry, as the SCM simulation. Furthermore, similar to the the SCM model a passive tracer flux representing the SO_2 emissions from the volcano were also initialised in the LES simulation.

The LES and SCM simulations are both initialised with the same meteorological profiles (of temperature, humidity and wind) which are also used as the boundary conditions. These meteorological profiles were generated by an initial Meso-NH simulation (also called spin-up) in a classic three-dimensional (3D) real case configuration. The domain of the spin-up simulation covered the entire island and it's surroundings. The boundaries of this domain were coupled with meteorological conditions provided by the operational model Aladin-Réunion by Météo France.

An initial LES simulation depicted a bent over plume at around 600 m a.g.l distorted by the atmospheric winds. The observations did not report/show such a deflection in the plume, and it was concluded that the winds were not correctly represented in the spin-up simulation. For the LES and SCM simulations conducted hereafter, it was simply chosen to force the winds at lateral limits of the models to a uniform and low value (0.1 ms^{-1}) rather than using the wind profiles extracted from the spin-up simulation (in contrast the temperature and humidity profiles were preserved). A plume of more realistic appearance was ultimately obtained by LES in these new conditions, extending up to 1.4 km in height above the ground. The observations estimated a plume height of about $1 - 1.2$ km above the ground.

The M.EDMF parameterisation was constrained such that the results from the SCM simulation were adjusted to the results obtained from the LES simulation, in terms of,

- the volcanic plume height (illustrated by the maximum detrainment height of the passive SO_2 tracer)
- the maximum SO_2 tracer concentration and
- the vertical distribution of the tracer.

During the numerous sensitivity tests for the SCM simulation, it was observed that the generated volcanic plume is very sensitive to the entrainment of fresh, ambient air at the base of the plume. The entrainment and detrainment rates at the first model level (40 m) appear to be key parameters in the M.EDMF scheme. The optimum rates of entrainment and detrainment at the plume base were identified as 83.4 % of ambient air entrained at 40 m and zero detrainment. In contrast the volcanic plume revealed to be least sensitive to temperature variations of the gas at the base of the plume, for a range of $1200 - 1400$ K.

The relevance of these results obtained in column configuration (1D) need to be confirmed by other tests in three-dimensional(3D)configuration. The results from a first test case of a 3D simulation embedded with M.EDMF scheme has proved its capacity to effectively inject volcanic gas plumes into the lower troposphere (a single source point in the classic model does not permit such an injection). The maximum injection height of the passive tracer from the 3D simulated test case matched the one from the 1D SCM model (i.e 1.4 km above the ground). However, the tracer concentrations of the 3D test simulation were lower than the 1D SCM outputs. This difference is highly contributed by the meteorological wind fields represented in the 3D model.

Although this M.EDMF scheme proved efficient in simulating the deep injections of volcanic gases into the lower troposphere (atleast for this particular case study), further tests are needed. The model shows much higher SO_2 concentrations at certain sampling stations for air quality managed by ORA (Observatoire Réunionnais de l'Air). A plausible reason as why such a discrepancy is observed is largely related to the dynamics simulated by the the model, whereby Aladin-Reunion atmospheric files were used as the large scale meteorological fields. The results from the the 3D M.EDMF simulation shows a strong vertical mixing responsible for the transport SO_2 tracer concentrations to the ground level. In reality however, the plume appears to have remained in altitude.

Consequently, further testing is essential to validate the M.EDMF scheme in terms of air quality observations. Particular points to be taken into considerations are,

- testing the parameterisation using a chemical scheme for SO_2 in order to study the in plume chemistry and most importantly the plume ageing,

- testing different eruption case studies (variations in terms of the source geometry and volcanic heat and vapour fluxes).
- the effect of model's horizontal resolution on the M.EDMF parameterisation,
- using different large scale meteorological conditions for example such as those prodiced by the ECMWF (The European Centre for Medium-Range Weather Forecast),
- further more elaborated tests on the entrainment rates at the plume base such that a universal entrainment and detrainment rate can be determined, applicable to a wide range of volcanic eruptions of effusive style.

On a different note, it is also possible to develop such a parameterisation in the deep convection scheme of the model to account for injection heights associated with large sporadic eruptions, reaching the upper troposphere.

The short-term perspectives mentioned above are directly related to the work undertaken during this study. However, in order to improve and validate further modelling studies especially in the case for better prediction of volcanic impacts the community needs to work together in two aspects,

- better characterization of volcanic volatiles and aerosols in the atmosphere and
- better characterization of the plume dynamics.

In terms of volcanic volatiles and aerosols there is a need to continuously monitor active volcanoes around the globe. Due to the risks associated with such measurements, one highly favourable technique is the use of UAVs (unmanned aerial vehicles or drones) along with the already adopted techniques involving spectrometers and satellites. Such continuous data can provide greater insight into the hot (close to the vent) and low (during transport) temperature reactions. Furthermore, greater effort from the community to invest in research such as those carried out by Carn *et al.* (2013) and McCormick *et al.* (2013) (review of OMI instrument with particular focus on its capabilities to measure quiescent volcanic plume) can help monitor low lying volcanic plumes especially in the developing countries which have largely remained unstudied. Similarly, further effort such as those carried out by the Japanese Space Agency in 2009 by launching GOSAT (greenhouse gas sensor) and NASA by launching OCO-2

can provide measurements of other volcanic species other than SO_2. Lastly in terms of modelling studies simulations of electrical fields during volcanic eruptions can provide insight into their possible effects on ash aggregation.

Conclusions générale en français

Les éruptions volcaniques et la dispersion atmosphérique de panaches chargés de gaz volcaniques et de cendres représentent un grand danger pour les populations ainsi qu'un facteur de risque pour la trafic aérien. Par exemple, l'éruption de l'Eyjafjallajokull en Avril 2010 a créé une grande pertubation du trafic aérien. Les Volcanic Ash Advisory Centres (VAAC) ont la responsabilité de prévoir la dispersion de cendres dans l'atmosphère lors d'éruptions majeures. Les modèles utilisés par les VAAC dépendent de certains paramètres d'entrée tels que la taille de l'éruption et les taux de masse éruptive. Étant donné que ces paramètres ne sont pas déterminés par le modèle lui-même et s'appuient sur différentes méthodes externes de détermination (par exemple, des simulations, des bases de données volcaniques, etc.), les incertitudes sur ces paramètres d'entrée sont importantes, et par suite, la capacité à prévoir la dispersion des panaches volcaniques et les risques associés en est fortement altérée.

Le Piton de la Fournaise, volcan situè sur l'île de la Rèunion, ainsi que le Kiluea à Hawaii, sont principalement de type effusif. Contrairement au volcans explosifs, leurs panaches volcaniques sont limitées à la basse troposphère. Les modèles de dispersion de cendres gérées par les VAAC ne sont pas actuellement adaptés à une mission d'information ou d'alerte liées à la dispersion de panaches peu profonds chargés de différentes espèces soufrées, comme ceux générés par volcanisme effusif. Or ces panaches n'en sont pas moins potentiellement dangereux pour les populations et l'environnement. Il a été démontré lors de l'éruption du Piton de la Fournaise en Avril 2007, que le seuil d'alerte en SO_2 fixé par le MEDDTL (ministère de l'Écologie, du Développement Durable, du Transport et du Logement) a été largement dépassé dans certaines zones habitées de l'île de la Réunion. Cependant, il n'existe à l'heure actuelle aucun modèle de qualité de l'air capable de donner l'alerte sur de tels risques volcaniques.

La capacité opérationelle des VAAC dépend de notre aptitude continue à mesurer et modèliser les panaches volcaniques de tous types. L'un des principaux objectifs des activités de modélisation dans le cadre du projet MoPAV-STRAP du programme LEFE-CHAT de l'INSU-CNRS, est de développer des logiciels qui soient performants et faciles à intégrer dans les modèles opérationnels de gestion de crise. Par conséquent, du point de vue de la modélisation des panaches de gaz volcaniques, cette thèse avait pour objectif de poser les premières pierres d'une paramétrisation des panaches volcaniques effusifs, utilisable dans un modèle atmosphérique de dispersion de polluants, de sorte que l'injection du panache volcanique puisse être représentée correctement sur une certaine profondeur de l'atmosphère, et permette ainsi une dispersion réaliste de ces panaches à l'echelle locale et régionale.

Plus précisément, l'objectif du travail réalisé dans cette thèse était d'étudier la convection atmosphérique du panache volcanique déclenchée par les importants flux de chaleur en surface au point d'éruption. Dans cette thèse, on a modélisé, à l'aide du modèle atmosphérique de recherche à méso-échelle Meso-NH, la convection volcanique pour un cas d'étude : l'éruption de Janvier 2010 du Piton de la Fournaise (PdF). Dans le cadre d'une précédente thése, Lesouëf (2010) avait illustré (étude de cas de l'éruption d'Avril 2010 du PdF) la capacité de Meso-NH à reproduire les concentrations de SO_2 sur différentes régions de l'île (en absence toutefois de schémas réactionnels dans le modèle liés à diverses transformations du SO_2). Par conséquent, ce modèle a de nouveau été choisi pour la rèalisation des objectifs de la présente thèse.

La stratégie de départ est l'utilisation de Meso-NH pour simuler des cas idéalisés représentant la dynamique verticale du panache atmosphérique d'une façon simplifiée, mais réaliste. On a choisi d'exploiter le schéma de convection peu profonde EDMF de Pergaud *et al.* (2009), qui est intégré dans Meso-NH, en réalisant les adaptations nécessaires à un cas de panache volcanique. Celles-ci portaient essentiellement sur l'initialisation des grandeurs caractérisant le panache convectif à sa base : température et composition du gaz ; vitesse d'éjection ; diamètre. Ce schéma modifié, dénommé M.EDMF, a ensuite été mis en œuvre au sein d'un modèle colonne unidimensionnel (Single Column Model, ci-après SCM) de 1 km $\times$ 1 km en horizontal (la résolution typiquement visée pour des modèles de dispersion atmosphérique locale).

Une des récentes éruptions du PdF a tout d'abord été sélectionnée, en premier lieu par son adéquation à ce type de simulation idéalisée. L'éruption sommitale de Janvier

2010 a été choisie par sa configuration simple : il y avait un panache de gaz visible bien développé au-dessus d'une fissure éruptive ; le panache semblait peu distordu par le vent (impliquant des vents locaux faibles). En contrepartie de cette simplicité, les données disponibles pour cette éruption en terme d'émissions de soufre, d'imagerie infrarouge du panache et de hauteur du panache étaient malheureusement limitées par rapport à d'autres éruptions (en revanche plus complexes). Le cas d'étude une fois identifié, le schéma de convection peu profonde a été modifié pour représenter correctement les flux volcaniques de chaleur et de matière, ainsi que la géométrie du point source, qui, eux, étaient suffisamment bien caractérisés par des observations.

En raison de l'absence d'observations adéquates à la validation du schéma, une simulation de type LES (Large Eddy Simulation) a été réalisée à 10 m de résolution horizontale sur une durée d'une heure trente. La LES était initialisé avec les mêmes flux de chaleur et de vapeur d'eau que la simulation SCM, ainsi que la même géométrie de la source en surface. Comme dans la simulation SCM, un flux de traceur passif représentait l'émission de SO_2 par le volcan.

Les simulations SCM et LES utilisaient en commun les mêmes profils météorologiques (température, humidité et vent) pour leur initialisation et ensuite comme conditions aux limites. Ces profils étaient issus d'une première simulation Meso-NH préparatoire (dite de spin-up) réalisée dans une configuration tri-dimensionnelle classique de cas réel. Le domaine de la simulation spin-up couvrait toute l'île et ses abords. Elle était couplée à ses bords par les champs météorologiques du modèle opérationnel Aladin-Réunion de Météo-France.

Une première simulation LES montrait un panache penché par le vent, et ne dépassant pas 600 m au-dessus du sol. Les observations ne montrant pas une telle distorsion du panache, il a été conclu que le vent n'était pas correctement représenté dans la simulation spin-up. Pour les simulations SCM et LES menées par la suite, il a été choisi de forcer le vent aux limites latérales des modèles a une valeur uniforme et faible (0.1 m/s) plutôt que d'utiliser les profils de vents issus de la simulation spin-up (les profils de température et d'humidité ont en revanche été conservés). Un panache d'apparence plus réaliste a finalement été obtenu par LES dans ces nouvelles conditions, s'étendant jusqu'à 1.4 km de hauteur au-dessus du sol. Les observations permettaient quant à elles d'estimer une hauteur de panache de 1 à 1.2 km.

Des paramètres du schéma M.EDMF ont été contraints de façon à ajuster le résultat de la simulation SCM à celui de la simulation LES, en termes de

- hauteur du panache volcanique (défini comme la hauteur de détraînement maximal du traceur passif SO_2),
- concentration maximale du traceur SO_2,
- distribution verticale du traceur.

Au cours de nombreux tests de sensibilité de la simulation SCM, il a été observé que le panache obtenu est très sensible à l'entraînement d'air frais (air ambiant) à sa base. Les taux d'entraînement et détraînement dans le premier niveau de modèle (40 m) apparaissent ainsi être des paramètres clés du schéma M.EDMF. Des taux d'entraînement et détraînement optimaux à la base du panache ont été identifiés : 83 % de l'air ambiant entraîné à 40 m, et un détrainement nul. En revanche, le panache s'est révélé peu sensible à une variation de la température du gaz volcanique à sa base, dans une fourchette de 1200 à 1400 K.

La pertinence de ces résultats obtenus en configuration colonne (1D) se devait d'être confirmée par d'autres tests en configuration tri-dimensionnelle (3D). Les résultats d'une premiére simulation 3D intégrant le schéma M.EDMF ont prouvé sa capacité à injecter les panaches de gaz volcaniques en profondeur dans la basse troposphère (ce que l'activation d'un simple point source en surface ne permet pas dans un modèle classique). La hauteur maximale d'injection du traceur passif du test 3D simulé correspond bien à celui du modèle 1D SCM (soit environ 1.4 km au-dessus du sol). En revanche, les concentrations de traceurs de la simulation 3D sont inférieures aux sorties du modèle 1D SCM. Cette différence se révèle être fortement liée aux champs de vent météorologiques représentées dans le modèle 3D.

Bien que le schéma M.EDMF se soit avéré efficace (au moins pour le cas étudié) pour simuler l'injection profonde de gaz volcanique dans la basse troposphère, de tests supplémentaires sont nécessaires. Le modèle a en effet montré des concentrations de SO_2 beaucoup plus élevées qu'observé dans certaines stations de surveillance de la qualité de l'air gérées par l'ORA (Observatoire Réunionnais de l'Air, association régionale agréée de la qualité de l'air). Une raison plausible d'une telle anomalie est en grande partie liée à l'absence d'activation des puits chimiques du SO_2 dans le modèle.

Par conséquent, d'autres tests seront essentiels pour valider le schéma M.EDMF par rapport à des observations de qualité de l'air. Des points à aborder seront en particulier

- d'utiliser dans le modèle une représentation du système chimique du SO_2 dans le but de rendre compte du vieillissement chimique de panache durant le transport,
- d'aborder différents cas d'éruption (variant en termes de géométrie de la source volcanique et des flux de chaleur et de matière),
- de caractériser l'effet de la résolution horizontale de modèle sur les résultats du schéma M.EDMF,
- d'effectuer des tests plus poussés sur les taux d'entraînement à la base du panache, de sorte qu'une valeur universelle puisse être déterminée, applicable à un large éventail d'éruptions volcaniques de type effusif.

Il est également possible de développer un telle paramétrage dans le schéma de convection profonde du modèle pour tenir compte des hauteurs d'injection associés aux grandes éruptions sporadiques (oú le panache volcanique atteint la haute troposphère).

Les perspectives à court terme mentionnées ci-dessus sont directement reliées à létude entreprise dans cette thése. Cependant, afin de pousser et de valider davantage des études par modélisation visant à une meilleure prévision des impacts volcaniques, la communauté scientifique doit avancer en parallèle sur deux aspects :

- une meilleure caractérisation des gaz et aérosols volcaniques dans latmosphère,
- une meilleure caractérisation de la dynamique des panaches.

Concernant les gaz et aérosols volcaniques, il existe un besoin de surveillance continue des volcans actifs tout autour du globe. A cause des risques associés à la mise en oeuvre de telles mesures, une technique prometteuse est lutilisation davions pilotés à distance (drones), en association à des techniques déjà éprouvées incluant les spectromètres et les mesures par satellites. De telles données continues pourraient renseigner sur les réactions chimiques se produisant à haute température (près de la bouche éruptive) et à basse température (durant le transport atmosphérique). De plus, un effort de recherche à la suite de celui entrepris par Carn *et al.* (2013) et McCormick *et al.* (2013) (revue de linstrument spatial OMI avec un intért particulier porté à sa

capacité de sonder des panaches volcaniques effusifs) pourrait aider à surveiller des panaches peu profonds, en particulier dans les pays en voie de développement, où ils ont été trs peu étudiés. Dans le même ordre didée, des projets instrumentaux tels ceux menés par la JAXA (agence spatiale japonaise) en lançant le satellite GOSAT en 2009 (observation des gaz à effet de serre), ou par la NASA avec linstrument OCO-2, pourront apporter des mesures despèces volcaniques autres que le SO_2. Enfin, la prise en compte dans les modèles numériques du champ électrique régnant dans les panaches volcaniques pourrait renseigner sur son possible effet sur lagrégation de cendres.

List of Figures

List of Tables

References

Aiuppa, A., Franco, A., von Glasow, R., Allen, A.G., D'Alessandro, W., Mather, T.A., Pyle, D.M. & Valenza, M. (2007). The tropospheric processing of acidic gases and hydrogen sulphide in volcanic gas plumes as inferred from field and model investigations. *Atmospheric Chemistry and Physics*, **7**, 1441–1450. 45, 58

Albrecht, B.A. (1989). Aerosols, cloud microphysics, and fractional cloudiness. *Science*, **245**, 1227–1230. 45

Allard, P., La Spina, A., Tamburello, G., Aiuppa, A., Burton, M., Di Muro, A. & Staudacher, T. (2011). First measurements of magmatic gas composition and fluxes during an eruption (october 2010) of piton 15 de la fournaise hot spot volcano, la reunion island. egu: Gmpv-5. oral presentation. *Geophysical Research Abstracts, EGU*, **13**, n/a–n/a. 81

Allen, A.G., Baxter, P.J. & Ottley, C.J. (2000). Gas and particle emissions from soufrire hills volcano, montserrat, west indies: characterization and health hazard assessment. *Bulletin of Volcanology*, **62**, 8–19. 46

Andreae, M.O. & Crutzen, P.J. (1997). Atmospheric aerosols: Biogeochemical sources and role in atmospheric chemistry. *Science*, **276**, 1052–1058. 37

Andres, R.J. & Kasgnoc, A.D. (1998). A time-averaged inventory of subaerial volcanic sulfur emissions. *Journal of Geophysical Research: Atmospheres*, **103**, 25251–25261. 2, 8, 44

Ansmann, A., Tesche, M., Gro, S., Freudenthaler, V., Seifert, P., Hiebsch, A., Schmidt, J., Wandinger, U., Mattis, I., Mller, D. & Wiegner, M. (2010). The 16 april 2010 major volcanic ash plume over central europe: Earlinet lidar

and aeronet photometer observations at leipzig and munich, germany. *Geophysical Research Letters*, **37**, n/a–n/a. 33

Auchmann, R., Brönnimann, S., Breda, L., Bühler, M., Spadin, R. & Stickler, A. (2012). Extreme climate, not extreme weather: the summer of 1816 in geneva, switzerland. *Climate of the Past*, **8**, 325–335. 41

Barberi, F., Bertagnini, A., Landi, P. & Principe, C. (1992). A review on phreatic eruptions and their precursors. *Journal of Volcanology and Geothermal Research*, **52**, 231 – 246. 16

Barton, I.J., Prata, A.J., Watterson, I.G. & Young, S.A. (1992). Identification of the mount hudson volcanic cloud over se australia. *Geophysical Research Letters*, **19**, 1211–1214. 31

Baxter, P., Stoiber, R.E. & Williams, S. (1982). Volcanic gases and health: Masaya volcano, nicaragua. *The Lancet*, **320**, 150 – 151, originally published as Volume 2, Issue 8290. 46

Baxter, P., Boyle, R., Cole, P., Neri, A., Spence, R. & Zuccaro, G. (2005). The impacts of pyroclastic surges on buildings at the eruption of the soufrire hills volcano, montserrat. *Bulletin of Volcanology*, **67**, 292–313. 32

Bechtold, P., Bazile, E., Guichard, F., Mascart, P. & Richard, E. (2001). A mass-flux convection scheme for regional and global models. *Quarterly Journal of the Royal Meteorological Society*, **127**, 869–886. 84

Bhugwant, C., Sija, B., Bessafi, M., Staudacher, T. & Ecormier, J. (2009). Atmospheric sulfur dioxide measurements during the 2005 and 2007 eruptions of the piton de la fournaise volcano: Implications for human health and environmental changes. *Journal of Volcanology and Geothermal Research*, **184**, 208 – 224, recent advances on the geodynamics of Piton de la Fournaise volcano. 3, 8, 44, 51, 52, 73, 118

Bhugwant, C., Bessafi, M. & Sieja, B. (2011). The surveillance of the air quality in the vicinity of an active volcano : Case of the piton de la fournaise ., air quality monitoring, assessment and management, dr. nicolas mazzeo (ed.). 51

Bjornsson, H., Magnusson, S., Arason, P. & Petersen, G.N. (2011). Assessing simple models of volcanic plumes using observations from the summit eruption of eyjafjallajokull in 2010. 76

Bluth, G.J.S., Doiron, S.D., Schnetzler, C.C., Krueger, A.J. & Walter, L.S. (1992). Global tracking of the so2 clouds from the june, 1991 mount pinatubo eruptions. *Geophysical Research Letters*, **19**, 151–154. 31, 38

Bobrowski, N., Honninger, G., Galle, B. & Platt, U. (2003). Detection of bromine monoxide in a volcanic plume. *Nature*, **423**, 273–276. 2, 8, 37

Bobrowski, N., von Glasow, R., Aiuppa, A., Inguaggiato, S., Louban, I., Ibrahim, O.W. & Platt, U. (2007). Reactive halogen chemistry in volcanic plumes. *Journal of Geophysical Research: Atmospheres*, **112**, n/a–n/a. 37

Bobrowski, N., Kern, C., Platt, U., Hörmann, C. & Wagner, T. (2010). Novel so2 spectral evaluation scheme using the 360390 nm wavelength range. *Atmospheric Measurement Techniques*, **3**, 879–891. 47

Boichu, M., Oppenheimer, C., Roberts, T.J., Tsanev, V. & Kyle, P.R. (2011). On bromine, nitrogen oxides and ozone depletion in the tropospheric plume of erebus volcano (antarctica). *Atmospheric Environment*, **45**, 3856 – 3866. 38

Boichu, M., Menut, L., Khvorostyanov, D., Clarisse, L., Clerbaux, C., Turquety, S. & Coheur, P.F. (2013). Inverting for volcanic so_2 flux at high temporal resolution using spaceborne plume imagery and chemistry-transport modelling: the 2010 eyjafjallajkull eruption case study. *Atmospheric Chemistry and Physics*, **13**, 8569–8584. 47

Bonadonna, C., Connor, C.B., Houghton, B.F., Connor, L., Byrne, M., Laing, A. & Hincks, T.K. (2005). Probabilistic modeling of tephra dispersal: Hazard assessment of a multiphase rhyolitic eruption at tarawera, new zealand. *Journal of Geophysical Research: Solid Earth*, **110**, n/a–n/a. 57

Bougeault, P. & Lacarrere, P.. (1989). Parameterization of orography-induced turbulence in a mesobeta-scale model. *Monthly Weather Review*, **117**, 18721890. 67, 84, 109

Brasseur, G. (1992). Ozone depletion: Volcanic aerosols implicated. *Nature*, **359**, 275–276. 31

Brayshay, M., M. an Grattam (1999). Environmental and social responses in europe to the 1783 eruption of the laki fissure volcano in iceland: a consideration of contemporary documentary evidence. *Geological Society, London, Special Publications*, **161**, 173–187. 30

Brophy, J. (2014). Magma composition and igneous rocks, university handout notes. 17, 18, 19, 20, 21

Brown, A.R., Cederwall, R.T., Chlond, A., Duynkerke, P.G., Golaz, J.C., Khairoutdinov, M., Lewellen, D.C., Lock, A.P., MacVean, M.K., Moeng, C.H., Neggers, R.A.J., Siebesma, A.P. & Stevens, B. (2002). Large-eddy simulation of the diurnal cycle of shallow cumulus convection over land. *Quarterly Journal of the Royal Meteorological Society*, **128**, 1075–1093. 75

Browning, K. (1993). The gewex cloud system study (gcss). *Bulletin of the American Meteorological Society*, **74**, 387–399. 75

Bursik, M. (2001). Effect of wind on the rise height of volcanic plumes. *Geophysical Research Letters*, **28**, 3621–3624. 3, 9, 72

Cadle, R.D. (1980). Some effects of the emissions of explosive volcanoes on the stratosphere. *Journal of Geophysical Research: Oceans*, **85**, 4495–4498. 37

Carazzo, G., Kaminski, E. & Tait, S. (2008). On the rise of turbulent plumes: Quantitative effects of variable entrainment for submarine hydrothermal vents, terrestrial and extra terrestrial explosive volcanism. *Journal of Geophysical Research: Solid Earth*, **113**, n/a–n/a. 71, 72, 90, 100

Carey, S. & Sigurdsson, H. (1987). Temporal variations in column height and magmadischarge rate during the 79 a.d. eruption of vesuvius. *Geological Society of Amercian Bulletin*, **99**, 303314. 29

Carlsen, H.K., Hauksdottir, A., Valdimarsdottir, U.A., Gslason, T., Einarsdottir, G., Runolfsson, H., Briem, H., Finnbjornsdottir, R.G., Gudmundsson, S., Kolbeinsson, T.B., Thorsteinsson, T. & Ptursdttir,

G. (2012). Health effects following the eyjafjallajkull volcanic eruption: a cohort study. *BMJ Open*, **2**. 32

Carn, S.A., Krotkov, N.A., Yang, K. & Krueger, A. (2013). Measuring global volcanic degassing withthe ozone monitoring instrument (omi). in: Pyle, d. m., mather ,t.a. and biggs, j. (eds) remote sensing of volcanoes and volcanic processes: Integrating observation and modelling. *Geological Society, London, Special Publications*, **380**. 129, 135

Cas, R. (1987). *Volcanic successions: modern and ancient: a geological approach to processes*. Allen and Union, London. 16, 17

Clarisse, L., Coheur, P.F., Prata, A.J., Hurtmans, D., Razavi, A., Phulpin, T., Hadji-Lazaro, J. & Clerbaux, C. (2008). Tracking and quantifying volcanic so2 with iasi, the september 2007 eruption at jebel at tair. *Atmospheric Chemistry and Physics*, **8**, 7723–7734. 47

Coffey, M.T. (1996). Observations of the impact of volcanic activity on stratospheric chemistry. *Journal of Geophysical Research: Atmospheres*, **101**, 6767–6780. 37

Cohard, J.M. & Pinty, J.P. (2000). A comprehensive two-moment warm microphysical bulk scheme. ii: 2d experiments with a non-hydrostatic model. *Quarterly Journal of the Royal Meteorological Society*, **126**, 1843–1859. 84

Cole, P. & Stinton, A. (2010). Scientific advisory committee on volcanic activity at soufriere hills volcano montserrat. 32

Corradini, S., Merucci, L. & Prata, A.J. (2009). Retrieval of so2 from thermal infrared satellite measurements: correction procedures for the effects of volcanic ash. *Atmospheric Measurement Techniques*, **2**, 177–191. 47

Cuxart, J., Bougeault, P. & Redelsperger, J.L. (2000). A turbulence scheme allowing for mesoscale and large-eddy simulations. *Quarterly Journal of the Royal Meteorological Society*, **126**, 1–30. 65, 66, 84

Dai, A., Trenberth, K. & Qian, T. (2004). A global dataset of palmer drought severity index for 18702002: relationship with soil moisture and effects of surface warming. 31

Davis, F. (1992). *Myths and Legends of Japan*. Dover books on folklore, folk art, and folk song, Dover Publications. 14

Dawson, J.B. (1992). First thin sections of experimentally melted igneous rocks: Sorbys observations on magma crystallization. *Journal of Geology*, **100**, 251–257. 20

de' Michieli Vitturi, M., Neri, A., Esposti Ongaro, T., Lo Savio, S. & Boschi, E. (2010). Lagrangian modeling of large volcanic particles: Application to vulcanian explosions. *Journal of Geophysical Research: Solid Earth*, **115**, n/a–n/a. 54

Degruyter, W. & Bonadonna, C. (2012). Improving on mass flow rate estimates of volcanic eruptions. *Geophysical Research Letters*, **39**, n/a–n/a. 59

Delmelle, P. & Stix, J. (2000). Volcanic gases. in: Encyclopedia of volcanoes. 38

Delmelle, P., Stix, J., Bourque, C.P.A., Baxter, P.J., Garcia-Alvarez, J. & Barquero, J. (2001). Dry deposition and heavy acid loading in the vicinity of masaya volcano, a major sulfur and chlorine source in nicaragua. *Environmental Science and Technology*, **35**, 1289–1293. 46

Delmelle, P., Stix, J., Baxter, P., Garcia-Alvarez, J. & Barquero, J. (2002). Atmospheric dispersion, environmental effects and potential health hazard associated with the low-altitude gas plume of masaya volcano, nicaragua. *Bulletin of Volcanology*, **64**, 423–434. 2, 8, 49, 58, 73

Deshler, T., Adriani, A., Gobbi, G.P., Hofmann, D.J., Di Donfrancesco, G. & Johnson, B.J. (1992). Volcanic aerosol and ozone depletion within the antarctic polar vortex during the austral spring of 1991. *Geophysical Research Letters*, **19**, 1819–1822. 31

Di Muro, A., Neri, A. & Rosi, M. (2004). Contemporaneous convective and collapsing eruptive dynamics: The transitional regime of explosive eruptions. *Geophysical Research Letters*, **31**, n/a–n/a. 54

Dobran, F., Neri, A. & Macedonio, G. (1993). Numerical simulation of collapsing volcanic columns. *Journal of Geophysical Research: Solid Earth*, **98**, 4231–4259. 53

Doiron, S.D., Bluth, G.J.S., Schnetzler, C.C., Krueger, A.J. & Walter, L.S. (1991). Transport of cerro hudson so2 clouds. *Eos, Transactions American Geophysical Union*, **72**, 489–498. 31

Dolske, D.A. (1995). Deposition of atmospheric pollutants to monuments, statues, and buildings. *Science of The Total Environment*, **167**, 15 – 31, the Deterioration of Monuments. 48

Draxler, R. & Hess, G.D. (1997). Description of the hysplit4 modeling system. NOAA Air Resources Laboratory, Silver Spring, MD, nOAA Tech. Memo. ERL ARL-224, NOAA. 56

Dutton, E.G. & Christy, J.R. (1992). Solar radiative forcing at selected locations and evidence for global lower tropospheric cooling following the eruptions of el chichon and pinatubo. *Geophysical Research Letters*, **19**, 2313–2316. 31, 40

Eatough, D., Caka, F. & Farber, R. (1994). The conversion of so2 to sulfate in the atmosphere. *Israel Journal of Chemistry*, **34**, 301–314. 31, 43

EPA (2012). Our nations air, status and trends through 2010. 50

Esposti Ongaro, T., Cavazzoni, C., Erbacci, G., Neri, A. & Salvetti, M.V. (2007). A parallel multiphase flow code for the 3d simulation of explosive volcanic eruptions. *Parallel Comput.*, **33**, 541–560. 54

Farman, J., Gardiner, B. & Shanklin, J. (1985). Large losses of total o3 in atmosphere reveal seasonal clox/nox interaction. 31

FinlaysonPitts, B. & Pitts Jr, J. (1986). *Atmospheric Chemistry: Fundamentals and Experimental Techniques*. John Wiley and Sons, New York. 48

FinlaysonPitts, B. & Pitts Jr., J. (1999). Chemistry of the upper and lower atmosphere,theory, experiments and applications. ed.b.j. finlayson-pitts and j.n. pitts jr. 43

Forsyth, P. (1988). In the wake of etna, 44 b.c. *Classical Antiquity*, **7**, 49–57. 35

Franklin, B. (1784). Meteorological imaginations and conjectures. 35, 38

Gerlach, T.M. (2004). Volcanic sources of tropospheric ozone-depleting trace gases. *Geochemistry, Geophysics, Geosystems*, **5**, n/a–n/a. 38

Giacomelli, L., Perrotta, A., Scandone, R. & Scarpati, C. (2003). The eruption of vesuvius of 79 ad and its impact on human environment in pompei. 29

Gibb, F. (1974). Supercooling and the crystallization of plagioclase from a basaltic magma. *Mineralogical Magazine*, **39**, 641–653. 20

Gilbert, J. & Sparks, R. (1998). *The Physics of Explosive Volcanic Eruptions*. Geological Society London: Geological Society special publication, Geological Society. 53

Glaze, L.S. & Baloga, S.M. (1996). Sensitivity of buoyant plume heights to ambient atmospheric conditions: Implications for volcanic eruption columns. *Journal of Geophysical Research: Atmospheres*, **101**, 1529–1540. 3, 9, 55, 72

Glaze, L.S., Baloga, S.M. & Wilson, L. (1997). Transport of atmospheric water vapor by volcanic eruption columns. *Journal of Geophysical Research: Atmospheres*, **102**, 6099–6108. 55, 90

Gonnermann, H.M. & Manga, M. (2007). The fluid mechanics inside a volcano. *Annual Review of Fluid Mechanics*, **39**, 321–356. 80

Gorham, E., Bayley, S.E. & Schindler, D.W. (1984). Ecological effects of acid deposition upon peatlands: A neglected field in acid-rain research. *Canadian Journal of Fisheries and Aquatic Sciences*, **41**, 1256–1268. 48

Graf, H.F., Feichter, J. & Langmann, B. (1997). Volcanic sulfur emissions: Estimates of source strength and its contribution to the global sulfate distribution. *Journal of Geophysical Research: Atmospheres*, **102**, 10727–10738. 43, 44, 55

Graf, H.F., Langmann, B. & Feichter, J. (1998). The contribution of earth degassing to the atmospheric sulfur budget. *Chemical Geology*, **147**, 131 – 145. 45

Graf, H.F., Herzog, M., Oberhuber, J.M. & Textor, C. (1999). Effect of environmental conditions on volcanic plume rise. *Journal of Geophysical Research: Atmospheres*, **104**, 24309–24320. 3, 9, 72, 90

Grattan, J., Durand, M. & Taylor, S. (2003). Illness and elevated human mortality in europe coincident with the laki fissure eruption. in: 'volcanic degassing: Geological society, special publication 213', oppenheimer, c., pyle, d.m. and barclay, j. (eds). *Geological Society, London, Special Publications*, 410–414. 30, 46

Grell, G.A., Peckham, S.E., Schmitz, R., McKeen, A.A., Frost, G., Skamarock, W.C. & Eder, B. (2005). Fully coupled 'online' chemistry in the wrf model. *Atmos. Environ*, **39**, 6957–6976. 55

Gudmundsson, M., Thordarson, T., Hoskuldsson, A., Larsen, G., Bjornsson, H., Prata, F.J., Oddsson, B., Magnsson, E., Hognadttir, T., Petersen, G.N., Hayward, C.L., Stevenson, J.A. & Jonsdottir, I. (2012). Ash generation and distribution from the april-may 2010 eruption of eyjafjallajokull, iceland. *Science*. 33

Hansen, J., Lacis, A., Ruedy, R., Sato, M. & Wilson, H. (1993). How sensitive is the world's climate? 31, 40

Harris, E., Sinha, B., Hoppe, P., Crowley, J.N., Ono, S. & Foley, S. (2012). Sulfur isotope fractionation during oxidation of sulfur dioxide: gas-phase oxidation by oh radicals and aqueous oxidation by h2o2, o3 and iron catalysis. *Atmospheric Chemistry and Physics*, **12**, 407–423. 33, 42

Hastenrath, S. (1991). *Climate Dynamics of the Tropics: From Climate and Circulation of the Tropics*. Atmospheric Sciences Library, Kluwer. 86

Herzog, M. & Oberhuber, J.M. (2003). A prognostic turbulence scheme for the nonhydrostatic plume model atham. *Journal of the Atmospheric Sciences*, **60**, 2783–2796. 55

Herzog, M., Graf, H.F., Textor, C. & Oberhuber, J.M. (1998). The effect of phase changes of water on the development of volcanic plumes. *Journal of Volcanology and Geothermal Research*, **87**, 55 – 74. 27, 55

Hobbs, P.V., Tuell, J.P., Hegg, D.A., Radke, L.F. & Eltgroth, M.W. (1982). Particles and gases in the emissions from the 19801981 volcanic eruptions of mt. st. helens. *Journal of Geophysical Research: Oceans*, **87**, 11062–11086. 45

Hofmann, D., Oltmans, S., Harris, J., Solomon, S., Deshler, T. & Johnson, B. (1992). Observation and possible causes of new ozone depletion in antarctica in 1991. *Nature*, **359**, 283 – 287. 31

Hofmann, D.J. & Solomon, S. (1989). Ozone destruction through heterogeneous chemistry following the eruption of el chichn. *Journal of Geophysical Research: Atmospheres*, **94**, 5029–5041. 31

Hofmann, D.J., Rosen, J.M. & Gringel, W. (1985). Delayed production of sulfuric acid condensation nuclei in the polar stratosphere from el chichon volcanic vapors. *Journal of Geophysical Research: Atmospheres*, **90**, 2341–2354. 48

Hofmann, D.J., Oltmans, S.J., Komhyr, W.D., Harris, J.M., Lathrop, J.A., Langford, A.O., Deshler, T., Johnson, B.J., Torres, A. & Matthews, W.A. (1994a). ozone loss in the lower stratosphere over the united states in 19921993: Evidence for heterogeneous chemistry on the pinatubo aerosol. *Geophysical Research Letters*, **21**, 65–68. 31

Holloway, J. (1976). Fluids in the evolution of granitic magmas: Consequences of finite co2 solubility. *Geological Society of America Bulletin*, **87**, 1513–1518. 25

Holloway, J. & J.G, B. (1994). Application of experimental results to c-o-h species in natural melts, in volatiles in magmas. *Mineralogical Society of America Reviews*, **30**, 187–230. 26

Holton, J. (2004). *An Introduction to Dynamic Meteorology*. An Introduction to Dynamic Meteorology, Elsevier Academic Press. 79

Honnert, R., Masson, V. & Couvreux, F. (2011). A diagnostic for evaluating the representation of turbulence in atmospheric models at the kilometric scale. *Journal of atmospheric sciences*, **68**, 31123131. 66

Hourdin, F., Couvreux, F. & Menut, L. (2002). Parameterization of the dry convective boundary layer based on a mass flux representation of thermals. *Journal of the Atmospheric Sciences*, **59**, 1105–1123. 61, 65, 79

Hunt, G. & Kaye, N. (2001). Virtual origin correction for lazy turbulent plumes. *Journal of Fluid Mechanics*, **435**, 377–396. 100

IPCC (2000). Guidelines for national greenhouse gas inventories. 43

Jerram, D. & Petford, N. (2011). *The Field Description of Igneous Rocks*. Geological Field Guide, Wiley. 18, 20, 21

Josse, B., Simon, P. & Peuch, V. (1994). Radon global simulations with the multiscale chemistry and transport model mocage. *Tellus*, **56B**, 339356. 56

Kain, J. & Fritsch, M. (1990). A one-dimensional entraining/detraining plume model and its application in convective parameterization. *J. Atmos. Sci.*, **47**, 27842802. 70

Kaminski, E., Tait, S. & Carazzo, G. (2005). Turbulent entrainment in jets with arbitrary buoyancy. *Journal of Fluid Mechanics*, **526**, 361–376. 71, 72, 90, 100

Kaminski, E., Tait, S., Ferrucci, F., Martet, M., Hirn, B. & Husson, P. (2011). Estimation of ash injection in the atmosphere by basaltic volcanic plumes: The case of the eyjafjallajkull 2010 eruption. *Journal of Geophysical Research: Solid Earth*, **116**, n/a–n/a. 56, 57, 72, 73

Kaufman, Y.J., Tanra, D. & Boucher, O. (2002). A satellite view of aerosols in the climate system. *Nature*, **419**, 215–223. 45

Kellogg, W.W., Cadle, R.D., Allen, E.R., Lazrus, A.L. & Martell, E.A. (1972). The sulfur cycle. *Science*, **175**, 587–596. 44

Kelly, P.J., Kern, C., Roberts, T.J., Lopez, T., Werner, C. & Aiuppa, A. (2013). Rapid chemical evolution of tropospheric volcanic emissions from redoubt volcano, alaska, based on observations of ozone and halogen-containing gases. *Journal of Volcanology and Geothermal Research*, **259**, 317 – 333, the 2009 Eruption of Redoubt Volcano, Alaska. 38

Kern, C., Sihler, H., Vogel, L., Rivera, C., Herrera, M. & Platt, U. (2009). Halogen oxide measurements at masaya volcano, nicaragua using active long path differential optical absorption spectroscopy. *Bulletin of Volcanology*, **71**, 659–670. 37

Kessler, E. (1969). *On Distribution and Continuity of Water Substance in Atmospheric Circulation*. Meteorological Monograph Series, American Meteorological Society. 84, 109

Kjellstrom, E. (1998). A three-dimensional global model study of carbonyl sulfide in the troposphere and the lower stratosphere. *Journal of Atmospheric Chemistry*, **29**, 151–177. 37

Koyaguchi, T. & Tokuno, M. (1993). Origin of the giant eruption cloud of pinatubo, june 15, 1991. *Journal of Volcanology and Geothermal Research*, **55**, 85 – 96. 31

Krug, E.C., Frink, C.R. *et al.* (1983). Acid rain on acid soil: A new perspective. *Science(Washington)*, **217**, 520–525. 48

Kullman, G., Jones, W., Cornwell, R. & Parker, J.E. (1994). Characterization of air contaminants formed by the interaction of lava and sea water. *Environ Health Perspect.*, **102**, 478 – 482. 48, 49

Lacasse, C., Karlsdottir, S., Larsen, G., Soosalu, H., Rose, W. & Ernst, G. (2004). Weather radar observations of the hekla 2000 eruption cloud, iceland. *Bulletin of Volcanology*, **66**, 457–473. 58

Lafore, J.P., Stein, J., Asencio, N., Bougeault, P., Ducrocq, V., Duron, J., Fischer, C., Héreil, P., Mascart, P., Masson, V., Pinty, J.P., Redelsperger, J.L., Richard, E. & Vilà-Guerau de Arellano, J. (1998). The meso-nh atmospheric simulation system. part i: adiabatic formulation and control simulations. *Annales Geophysicae*, **16**, 90–109. 52, 55, 64, 73, 84

Lambert, G., Cloarec, M.F.L. & Pennisi, M. (1988). Volcanic output of so2 and trace metals: A new approach. *Geochimica et Cosmochimica Acta*, **52**, 39 – 42. 44

Langmann, B. (2014). On the role of climate forcing by volcanic sulphate and volcanic ash. *Advances in Meteorology*, **2014**, 1–17. 36, 41, 42, 58

Langmann, B., Hort, M. & Hansteen, T. (2009). Meteorological influence on the seasonal and diurnal variability of the dispersion of volcanic emissions in nicaragua: A numerical model study. *Journal of Volcanology and Geothermal Research*, **182**, 34 – 44. 57

Lenat, J. & Bachelery, P. (1988). Dynamics of magma transfer at piton de la fournaise volcano (runion island, indian ocean). In C.Y. King & R. Scarpa, eds.,

Modeling of Volcanic Processes, Earth Evolution Sciences, 57–72, Vieweg+Teubner Verlag. 2, 8, 73

Lesouëf, D. (2010). Ph. d thesis: Numerical studies of local atmospheric circulations over reunion island: application to the dispersion of pollutants. 2, 8, 45, 50, 51, 52, 60, 85, 111, 118, 119, 122, 126, 132

Lesouëf, D., Gheusi, F., Delmas, R. & Escobar, J. (2011). Numerical simulations of local circulations and pollution transport over reunion island. *Annales Geophysicae*, **29**, 53–69. 85, 118, 119, 122

Li, J. & Sharma, A. (2013). Evaluation of volcanic aerosol impacts on atmospheric water vapor using cmip3 and cmip5 simulations. *Journal of Geophysical Research: Atmospheres*, **118**, 4448–4457. 41

Likens, G.E., Bormann, F.H. & Johnson, N.M. (1972). Acid rain. *Environment: Science and Policy for Sustainable Development*, **14**, 33–40. 48

Lofgren, G. (1980). *Experimental studies on the dynamic crystallization of silicate melts. eds, Hargraves, R.B.*, 487–551. Princeton University Press. 20

Lucas, D.D. & Akimoto, H. (2007). Contributions of anthropogenic and natural sources of sulfur to so2, h2so4 (g) and nanoparticle formation. *Atmospheric Chemistry and Physics Discussions*, **7**, 7679–7721. 43, 44

Macedonio, G., Costa, A. & Longo, A. (2005). A computer model for volcanic ash fallout and assessment of subsequent hazard. *Computers and Geosciences*, **31**, 837 – 845. 57

Mannino, D., Ruben, S., Holschuh, F.C., Holschuh, T.C., Wilson, M.D. & Holschuh, T. (1996). Emergency department visits and hospitalizations for respiratory disease on the island of hawaii, 1981-1991: Annual trends on the island of hawaii and weekly variability in hilo. 46

Masson, V., Le Moigne, P., Martin, E., Faroux, S., Alias, A., Alkama, R., Belamari, S., Barbu, A., Boone, A., Bouyssel, F., Brousseau, P., Brun, E., Calvet, J.C., Carrer, D., Decharme, B., Delire, C., Donier,

S., Essaouini, K., Gibelin, A.L., Giordani, H., Habets, F., Jidane, M., Kerdraon, G., Kourzeneva, E., Lafaysse, M., Lafont, S., Lebeaupin Brossier, C., Lemonsu, A., Mahfouf, J.F., Marguinaud, P., Mokhtari, M., Morin, S., Pigeon, G., Salgado, R., Seity, Y., Taillefer, F., Tanguy, G., Tulet, P., Vincendon, B., Vionnet, V. & Voldoire, A. (2013). The surfexv7.2 land and ocean surface platform for coupled or offline simulation of earth surface variables and fluxes. *Geoscientific Model Development*, **6**, 929–960. 64

Mastin, L., Guffanti, M., Servranckx, R., Webley, P., Barsotti, S., Dean, K., Durant, A., Ewert, J., Neri, A., Rose, W., Schneider, D., Siebert, L., Stunder, B., Swanson, G., Tupper, A., Volentik, A. & Waythomas, C. (2009). A multidisciplinary effort to assign realistic source parameters to models of volcanic ash-cloud transport and dispersion during eruptions. *Journal of Volcanology and Geothermal Research*, **186**, 10 – 21, improved Prediction and Tracking of Volcanic Ash Clouds. 33, 56, 57, 60

Mather, T., Pyle, D. & Oppenheimer, C. (2003). *Tropospheric Volcanic Aerosol*, 189–212. American Geophysical Union. 2, 3, 8, 37, 43, 44, 45, 58, 73

Matulka, A., López, P., Redondo, J.M. & Tarquis, A. (2014). On the entrainment coefficient in a forced plume: quantitative effects of source parameters. *Nonlinear Processes in Geophysics*, **21**, 269–278. 71, 100

McCormick, B.T., Edmonds, M., Mather, T.A., Campion, R., Hayer, C.S.L., Thomas, H. & Carn, S.A. (2013). Volcano monitoring applications of the ozone monitoring instrument (omi). in: Pyle, d. m., mather ,t.a. and biggs , j. (eds) remote sensing of volcanoes and volcanic processes: Inte- grating observation and modelling. *Geological Society, London, Special Publications*, **380**. 129, 135

McGonigle, A.J.S., Delmelle, P., Oppenheimer, C., Tsanev, V.I., Delfosse, T., Williams-Jones, G., Horton, K. & Mather, T.A. (2004). So2 depletion in tropospheric volcanic plumes. *Geophysical Research Letters*, **31**, n/a–n/a. 121

MEDDTL (2011). Les enjeux atmospheriques etat des lieux france-region pour l'elaboration des schemas regionaux climat, air, energie(srcae), la reunion. 50, 51

Meeker, K., Chuang, R., Kyle, P. & Palais, J. (1991). Emission of elemental gold particles from mount erebus, ross island, antarctica. *Geophysical Research Letters*, **18**, 1405–1408. 38

Melnik, O. & Sparks, R.S.J. (1999). Nonlinear dynamics of lava dome extrusion. *Nature*, **402**, 37–41. 4, 9

Mitchell, J.M. (1961). Recent secular changes of global temperature. *Annals of the New York Academy of Sciences*, **95**, 235–250. 38

Mlawer, E.J., Taubman, S.J., Brown, P.D., Iacono, M.J. & Clough, S.A. (1997). Radiative transfer for inhomogeneous atmospheres: Rrtm, a validated correlated-k model for the longwave. *Journal of Geophysical Research: Atmospheres*, **102**, 16663–16682. 64

Montroty, R., Rabier, F., Westrelin, S., Faure, G. & Viltard, N. (2008). Impact of wind bogus and cloud- and rain-affected ssm/i data on tropical cyclone analyses and forecasts. *Quarterly Journal of the Royal Meteorological Society*, **134**, 1673–1699. 85

Morton, B., Taylor, G. & Turner, J. (1956). Turbulent gravitational convection from maintained and instantaneous sources. *Proceedings of the Royal Society London*, **234**, 1–23. 55, 59, 71, 100

Neri, A. & Macedonio, G. (1996). Numerical simulation of collapsing volcanic columns with particles of two sizes. *Journal of Geophysical Research: Solid Earth*, **101**, 8153–8174. 4, 9, 53

Neri, A., Muro, A.D. & Rosi, M. (2002). Mass partition during collapsing and transitional columns by using numerical simulations. *Journal of Volcanology and Geothermal Research*, **115**, 1 – 18. 54

Neri, A., Esposti Ongaro, T., Macedonio, G. & Gidaspow, D. (2003). Multiparticle simulation of collapsing volcanic columns and pyroclastic flow. *Journal of Geophysical Research: Solid Earth*, **108**, n/a–n/a. 53, 54

Neri, A., Esposti Ongaro, T., Menconi, G., De'Michieli Vitturi, M., Cavazzoni, C., Erbacci, G. & Baxter, P.J. (2007). 4d simulation of explosive eruption dynamics at vesuvius. *Geophysical Research Letters*, **34**, n/a–n/a. 54

Newhall, C.G. & Self, S. (1982). The volcanic explosivity index (vei) an estimate of explosive magnitude for historical volcanism. *Journal of Geophysical Research: Oceans*, **87**, 1231–1238. 17

Noilhan, J. & Mahfouf, J.F. (1996). The isba land surface parameterisation scheme. *Global and Planetary Change*, **13**, 145 – 159, soil Moisture Simulation. 65, 84

Novak, M.M., Watson, I., Delgado-Granados, H., Rose, W., Crdenas-Gonzlez, L. & Realmuto, V. (2008). Volcanic emissions from popocatpetl volcano, mexico, quantified using moderate resolution imaging spectroradiometer (modis) infrared data: A case study of the december 2000january 2001 emissions. *Journal of Volcanology and Geothermal Research*, **170**, 76 – 85, the 1994-Present eruption of Popocatpetl: Background, current activity, and impacts. 47

Oberhuber, J.M., Herzog, M., Graf, H.F. & Schwanke, K. (1998). Volcanic plume simulation on large scales. *Journal of Volcanology and Geothermal Research*, **87**, 29 – 53. 55

Oman, L., Robock, A., Stenchikov, G.L. & Thordarson, T. (2006). High-latitude eruptions cast shadow over the african monsoon and the flow of the nile. *Geophysical Research Letters*, **33**, n/a–n/a. 30

Oppenheimer, C. (2003a). Climatic, environmental and human consequences of the largest known historic eruption: Tambora volcano (indonesia) 1815. *Progress in Physical Geography*, **27**, 230–259. 30, 31

Oppenheimer, C. (2006). Bro formation in volcanic plumes. *Geochim Cosmochim Acta.*, **70**, 29352941. 37

Oppenheimer, C., Pyle, D. & Barclay, J. (2003b). Volcanic degassing, oppenheimer, c and d. m. pyle, and j. barclay (eds.). 43

Oxlade, C. (2012). *Igneous Rock*. Let's Rock, Pearson Education. 18, 20

Papale, P. & Polacci, M. (1999). Role of carbon dioxide in the dynamics of magma ascent in explosive eruptions. *Bulletin of Volcanology*, **60**, 583–594. 25, 26

Papale, P., Neri, A. & Macedonio, G. (1998). The role of magma composition and water content in explosive eruptions: 1. conduit ascent dynamics. *Journal of Volcanology and Geothermal Research*, **87**, 75 – 93. 25

Parfitt, L. & Wilson, L. (2009). *Fundamentals of Physical Volcanology*. Wiley. 22, 23

Patra, A., Bursik, M., Dehn, J., Jones, M., Pavolonis, M., Pitman, E., Singh, T., Singla, P. & Webley, P. (2012). A {DDDAS} framework for volcanic ash propagation and hazard analysis. *Procedia Computer Science*, **9**, 1090 – 1099, proceedings of the International Conference on Computational Science, {ICCS} 2012. 58, 59

Pattantyus, A. & Businger, S. (2014). On the interaction of tropical cyclone flossie and emissions from hawaii's kilauea volcano. *Geophysical Research Letters*, **41**, 4082–4089. 48

Peltier, A., Staudacher, T., Bachlery, P. & Cayol, V. (2009). Formation of the april 2007 caldera collapse at piton de la fournaise volcano: Insights from {GPS} data. *Journal of Volcanology and Geothermal Research*, **184**, 152 – 163, recent advances on the geodynamics of Piton de la Fournaise volcano. 2, 8, 73

Pergaud, J., Masson, V., Malardel, S. & Couvreux, F. (2009). A parameterization of dry thermals and shallow cumuli for mesoscale numerical weather prediction. *Boundary-Layer Meteorology*, **132**, 83–106. 65, 66, 68, 69, 70, 72, 74, 75, 77, 79, 80, 81, 84, 100, 108, 126, 132

Petersen, G.N., Bjornsson, H. & Arason, P. (2012). The impact of the atmosphere on the eyjafjallajkull 2010 eruption plume. *Journal of Geophysical Research: Atmospheres*, **117**, n/a–n/a. 33, 76

Petersen, J., Sack, D. & Gabler, R. (2010). *Fundamentals of Physical Geography*. Cengage Learning. 14, 15

Pfister, C. (1992). The years without a summer in switzerland: 1628 and 1816. 41

Pham, M., Muller, J.F., Brasseur, G.P., Granier, C. & Megie, G. (1995). A three-dimensional study of the tropospheric sulfur cycle. *Journal of Geophysical Research: Atmospheres*, **100**, 26061–26092. 42

Pietruczuk, A., Krzyscin, J.W., Jarosawski, J., Podgorski, J., Sobolewski, P. & Wink, J. (2010). Eyjafjallajokull volcano ash observed over belsk (52 n, 21 e), poland, in april 2010. *International Journal of Remote Sensing*, **31**, 39813986. 33

Pinty, J. & Jabouille, P. (1998). A mixed-phase cloud parameterization for use in a mesoscale non-hydrostatic model: simulations of a squall line and of orographic precipitations. in: Tenth ams cloud physics conference. 65

Porter, J.N., Horton, K.A., Mouginis-Mark, P.J., Lienert, B., Sharma, S.K., Lau, E., Sutton, A.J., Elias, T. & Oppenheimer, C. (2002). Sun photometer and lidar measurements of the plume from the hawaii kilauea volcano pu'u o'o vent: Aerosol flux and so2 lifetime. *Geophysical Research Letters*, **29**, 30–1–30–4. 48

Prather, M. (1992). Catastrophic loss of stratospheric ozone in dense volcanic clouds. *Journal of Geophysical Research: Atmospheres*, **97**, 10187–10191. 31

Pyle, D. (1989). The thickness, volume and grainsize of tephra fall deposits. *Bulletin of Volcanology*, **51**, 1–15. 59

Ramanathan, V., Crutzen, P.J., Kiehl, J.T. & Rosenfeld, D. (2001). Aerosols, climate, and the hydrological cycle. *Science*, **294**, 2119–2124. 41, 58

Randall, D.A., Albrecht, B., Cox, S.K., Minnis, P., Rossow, W. & Starr, D. (1996). On fire at ten. *Adv. Geophys*, **38**, 37–177. 75

Resing, J.A. & Sansone, F.J. (1999). The chemical signature of lava-seawater interactions: The generation of acidity. 48

Resing, J.A., Embley, R., Rubin, K.H., Lupton, J., Baker, E., Baumberger, T., Buck, N.J., Butterfield, D., Caress, D., Clague, D., Cowen, J., Davis, R., Dziak, R., Huber, J., Keller, N., Lilley, M., Merle, S., Michael, P., Reysenbach, A.L., Shank, T., Soule, A., Thomas, H. & Walker, S. (2002).

An active submarine boninite eruption at west mata volcano in the ne lau basin, accessed: 10/09/2014. *NOAA*, 1–16. 49

Rio, C., Hourdin, F. & Chédin, A. (2010). Numerical simulation of tropospheric injection of biomass burning products by pyro-thermal plumes. *Atmospheric Chemistry and Physics*, **10**, 3463–3478. 90, 92, 96, 97, 98, 99, 137

Ripepe, M., Bonadonna, C., Folch, A., Donne, D.D., Lacanna, G., Marchetti, E. & Hskuldsson, A. (2013). Ash-plume dynamics and eruption source parameters by infrasound and thermal imagery: The 2010 eyjafjallajkull eruption. *Earth and Planetary Science Letters*, **366**, 112 – 121. 59

Rix, M., Valks, P., Hao, N., Loyola, D., Schlager, H., Huntrieser, H., Flemming, J., Koehler, U., Schumann, U. & Inness, A. (2012). Volcanic so2, bro and plume height estimations using gome-2 satellite measurements during the eruption of eyjafjallajkull in may 2010. *Journal of Geophysical Research: Atmospheres*, **117**, n/a–n/a. 47

Robock & Oppenheimer (2003). Volcanism and the earth's atmosphere. in: Robock, a. and oppenheimer, c. (eds). 59

Robock, A. (2000). Volcanic eruptions and climate. *Reviews of Geophysics*, **38**, 191–219. 2, 8, 37, 38, 39, 40, 41, 58, 59, 73

Robock, A. & Mass, C. (1982). The mount st. helens volcanic eruption of 18 may 1980: large short-term surface temperature effects. *Science*, **216**, 628–630. 38

Robock, A. & Matson, M. (1983). Circumglobal transport of the el chichon volcanic dust cloud. 38

Robock, A., Adams, T., Moore, M., Oman, L. & Stenchikov, G. (2007). Southern hemisphere atmospheric circulation effects of the 1991 mount pinatubo eruption. *Geophysical Research Letters*, **34**, n/a–n/a. 31

Rose, W., Gu, Y., Watson, I., Yu, T., Blut, G., Prata, A., Krueger, A., Krotkov, N., Carn, S., Fromm, M., Hunton, D., Ernst, G., Viggiano, A., Miller, T., Ballenthin, J., Reeves, J., Wilson, J., Anderson, B. &

Flittner, D. (2013). *The FebruaryMarch 2000 Eruption of Hekla, Iceland from a Satellite Perspective*, 107–132. American Geophysical Union. 58

Roult, G., Peltier, A., Taisne, B., Staudacher, T., Ferrazzini, V. & Muro, A.D. (2012). A new comprehensive classification of the piton de la fournaise activity spanning the 19852010 period. search and analysis of short-term precursors from a broad-band seismological station. *Journal of Volcanology and Geothermal Research*, **241242**, 78 – 104. 75, 76

Schlesinger, W. & Bernhardt, E. (2013). *Biogeochemistry: An Analysis of Global Change*. Academic Press, Academic Press. 37

Schmidt, A. (2013). *Modelling Tropospheric Volcanic Aerosol: From Aerosol Microphysical Processes to Earth System Impacts*. Springer Theses, Springer. 42, 43

Schmidt, A., Carslaw, K.S., Mann, G.W., Rap, A., Pringle, K.J., Spracklen, D.V., Wilson, M. & Forster, P.M. (2012). Importance of tropospheric volcanic aerosol for indirect radiative forcing of climate. *Atmospheric Chemistry and Physics*, **12**, 7321–7339. 41, 44, 58

Schmincke, H. (1993). *Geological Field Guide of Gran Canaria*. Pluto Press. 37

Schumann, U., Weinzierl, B., Reitebuch, O., Schlager, H., Minikin, A., Forster, C., Baumann, R., Sailer, T., Graf, K., Mannstein, H., Voigt, C., Rahm, S., Simmet, R., Scheibe, M., Lichtenstern, M., Stock, P., Rüba, H., Schäuble, D., Tafferner, A., Rautenhaus, M., Gerz, T., Ziereis, H., Krautstrunk, M., Mallaun, C., Gayet, J.F., Lieke, K., Kandler, K., Ebert, M., Weinbruch, S., Stohl, A., Gasteiger, J., Gross, S., Freudenthaler, V., Wiegner, M., Ansmann, A., Tesche, M., Olafsson, H. & Sturm, K. (2011). Airborne observations of the eyjafjalla volcano ash cloud over europe during air space closure in april and may 2010. *Atmospheric Chemistry and Physics*, **11**, 2245–2279. 33

Schwaiger, H.F., Denlinger, R.P. & Mastin, L.G. (2012). Ash3d: A finite-volume, conservative numerical model for ash transport and tephra deposition. *Journal of Geophysical Research: Solid Earth*, **117**, n/a–n/a. 57, 58

Self, S., Rampino, M.R., Newton, M.S. & Wolff, J.A. (1984). Volcanological study of the great tambora eruption of 1815. 30, 31

Self, S., Zhao, J.X., Holasek, R., Torres, R. & King, A. (1998). The atmospheric impact of the 1991 mount pinatubo eruption. in newhall, c.g., punongbayan, r.s. fire and mud, eruptions and lahars of mount pinatubo, philippines. 31

Sen, G. (2013). *Petrology: Principles and Practice*. SpringerLink : Bücher, Springer Berlin Heidelberg. 17, 18, 22

Shindell, D.T., Schmidt, G.A., Mann, M.E. & Faluvegi, G. (2004). Dynamic winter climate response to large tropical volcanic eruptions since 1600. *Journal of Geophysical Research: Atmospheres*, **109**, n/a–n/a. 40

Siebesma, A. (1998). Shallow cumulus convection. In E. Plate, E. Fedorovich, D. Viegas & J. Wyngaard, eds., *Buoyant Convection in Geophysical Flows*, vol. 513 of *NATO ASI Series*, 441–486, Springer Netherlands. 68

Siebesma, A.P. & Teixeira, J. (2000). An advection-diffusion scheme for the convective boundary layer: description and 1d-results, in: Proc. 14th symposium on boundary layers and turbulence. *American Meteorological Society*, 133–136. 79

Siebesma, A.P., Soares, P.M.M. & Teixeira, J. (2007). A combined eddy-diffusivity mass-flux approach for the convective boundary layer. *Journal of the Atmospheric Sciences*, **64**, 1230–1248. 65, 79

Siebesma, A.P., Bretherton, C.S., Brown, A., Chlond, A., Cuxart, J., Duynkerke, P.G., Jiang, H., Khairoutdinov, M., Lewellen, D., Moeng, C.H., Sanchez, E., Stevens, B. & Stevens, D.E. (2013). A large eddy simulation intercomparison study of shallow cumulus convection. *Journal of the Atmospheric Sciences*, **60**, 1201–1219. 75

Sigurdsson, H. (1999). Melting the earth: the history of ideas on volcanic eruptions. 14

Sigurdsson, H. & Houghton, B. (2000). *Encyclopedia of Volcanoes*. Academic Press. 30, 31

Simpson, J. & Wiggert, V. (1969). Models of precipitating cumulus towers. *Monthly Weather Review*, **97**, 471–489. 70, 79

Smithsonian, I. (2014). Frequently asked questions: Smithsonian institution: Global volcanism program. 14

Soares, P.M.M., Miranda, P.M.A., Siebesma, A.P. & Teixeira, J. (2004). An eddy-diffusivity/mass-flux parametrization for dry and shallow cumulus convection. *Quarterly Journal of the Royal Meteorological Society*, **130**, 3365–3383. 65, 79

Soden, B.J., Wetherald, R.T., Stenchikov, G.L. & Robock, A. (2002). Global cooling after the eruption of mount pinatubo: A test of climate feedback by water vapor. *Science*, **296**, 727–730. 31, 41

Sparks, R. (1986). The dimensions and dynamics of volcanic eruption columns. *Bulletin of Volcanology*, **48**, 3–15. 26, 76

Sparks, R. (2003a). Dynamics of magma degassing. *Geological Society, London, Special Publications*, **213**, 5–22. 23

Sparks, R. (2003b). Forecasting volcanic eruptions. *Earth and Planetary Science Letters*, **210**, 1 – 15. 4, 9

Sparks, R.J., Bursik, M., Carey, S., Gilbert, J., Glaze, L., H., S. & Woods, A.W. (1997). Volcanic plumes. 28, 33

Sparks, R.S.J. & Aspinall, W.P. (2013). *Volcanic Activity: Frontiers and Challenges in Forecasting, Prediction and Risk Assessment*, 359–373. American Geophysical Union. 4, 9

Sparks, R.S.J. & Young, S.R. (2002). The eruption of soufrire hills volcano, montserrat (1995-1999): overview of scientific results. 32

Steele, J., Thorpe, S. & Turekian, K. (2009). *Elements of Physical Oceanography: A derivative of the Encyclopedia of Ocean Sciences*. Elsevier Science. 37

Steingrímsson, J. & Kunz, K. (1998). *Fires of the earth: the Laki eruption, 1783-1784*. Nordic Volcanological Institute. 30

Stenchikov, G., Robock, A., Ramaswamy, V., Schwarzkopf, M.D., Hamilton, K. & Ramachandran, S. (2002). Arctic oscillation response to the 1991 mount pinatubo eruption: Effects of volcanic aerosols and ozone depletion. *Journal of Geophysical Research: Atmospheres*, **107**, ACL 28–1–ACL 28–16. 31

Stevenson, D.S., Johnson, C., Collins, W. & Derwent, R.G. (2003). *The tropospheric sulphur cycle and the role of volcanic SO2*, 295–305. Geological Society of London, Special Publication. 45

Stevenson, D.S., Johnson, C.E., Highwood, E.J., Gauci, V., Collins, W.J. & Derwent, R.G. (2003a). Atmospheric impact of the 17831784 laki eruption: Part i chemistry modelling. *Atmospheric Chemistry and Physics*, **3**, 487–507. 48

Stockwell, W.R., Middleton, P., Chang, J.S. & Tang, X. (1990). The second generation regional acid deposition model chemical mechanism for regional air quality modeling. *Journal of Geophysical Research: Atmospheres*, **95**, 16343–16367. 42

Stohl, A., Prata, A.J., Eckhardt, S., Clarisse, L., Durant, A., Henne, S., Kristiansen, N.I., Minikin, A., Schumann, U., Seibert, P., Stebel, K., Thomas, H.E., Thorsteinsson, T., Tørseth, K. & Weinzierl, B. (2011). Determination of time- and height-resolved volcanic ash emissions and their use for quantitative ash dispersion modeling: the 2010 eyjafjallajkull eruption. *Atmospheric Chemistry and Physics*, **11**, 4333–4351. 33

Stommel, H. & Stommel, E. (1983). *Volcano weather: the story of 1816, the year without a summer*. Seven Seas Press. 31

Stothers, R.B. (1984). The great tambora eruption in 1815 and its aftermath. *Science*, **224**, 1191–1198. 30, 31

Stothers, R.B. (1996). The great dry fog of 1783. *Climatic Change*, **32**, 79–89. 30

Strada, S., Mari, C., Filippi, J. & Bosseur, F. (2012a). Wildfire and the atmosphere: Modelling the chemical and dynamic interactions at the regional scale. *Atmospheric Environment*, **51**, 234 – 249. 65, 73

Sturges, W.T., Penkett, S.A., Barnola, J.M., Chappellaz, J., Atlas, E. & Stroud, V. (2001). A long-term record of carbonyl sulfide (cos) in two hemispheres from firn air measurements. *Geophysical Research Letters*, **28**, 4095–4098. 37

Sutton, J., Elias, T., Hendley, J. & Stauffer, P. (2000). Volcanic air pollution-a hazard in hawaii. 48

Suzuki, Y.J. & Koyaguchi, T. (2010). Numerical determination of the efficiency of entrainment in volcanic eruption columns. *Geophysical Research Letters*, **37**, n/a–n/a. 81

Suzuki, Y.J., Koyaguchi, T., Ogawa, M. & Hachisu, I. (2005). A numerical study of turbulent mixing in eruption clouds using a three-dimensional fluid dynamics model. *Journal of geophyscial research*, **110**. 73

Symons, G.J. (1888). The eruption of krakatoa, and subsequent phenomena, trbner, london, england. 38

Tabazadeh, A. & Turco, R.P. (1993). Stratospheric chlorine injection by volcanic eruptions: Hci scavenging and implications for ozone. *Science*, **260**, 1082–1086. 55

Tate, P. (2002). *The Rise and Dilution of Buoyant Jets and Their Behaviour in an Internal Wave Field*. University of New South Wales. 100

Taupin, F.G., Bessafi, M., Baldy, S. & Bremaud, P.J. (1999). Tropospheric ozone above the southwestern indian ocean is strongly linked to dynamical conditions prevailing in the tropics. *Journal of Geophysical Research: Atmospheres*, **104**, 8057–8066. 85

Textor, C., Graf, H., Timmreck, C. & Robock, A. (2004). *Chapter 7: Emissions from volcanoes. eds.Granier, C., Artaxo, P., Reeves, C.*, 269–303. Kluwer, Dordrecht. 37, 38, 44

Textor, C., Graf, H., Longo, A., Neri, A., Ongaro, T.E., Papale, P., Timmreck, C. & Ernst, G.G.J. (2005). Numerical simulation of explosive volcanic eruptions from the conduit flow to global atmospheric scales. *Annals of Geophysics*, **48**. 25, 26, 52, 53, 54, 55, 56, 58

Theys, N., Van Roozendael, M., Dils, B., Hendrick, F., Hao, N. & De Mazire, M. (2009). First satellite detection of volcanic bromine monoxide emission after the kasatochi eruption. *Geophysical Research Letters*, **36**, n/a–n/a. 37

Theys, N., Campion, R., Clarisse, L., Brenot, H., van Gent, J., Dils, B., Corradini, S., Merucci, L., Coheur, P.F., Van Roozendael, M., Hurtmans, D., Clerbaux, C., Tait, S. & Ferrucci, F. (2013). Volcanic so2 fluxes derived from satellite data: a survey using omi, gome-2, iasi and modis. *Atmospheric Chemistry and Physics*, **13**, 5945–5968. 46, 47

Thorarinsson, S. (1979). *On the damage caused by volcanic eruptions, with special reference to tephra and gases.In:sheets P.D. and GRAYSON, D. K. (eds) Volcanic Activity and Human Ecology*. Academic Press New York. 30

Thorarinsson, S. (1981). Greetings from iceland. ash-falls and volcanic aerosols in scandinavia. *Geografiska Annaler. Series A, Physical Geography*, **63**, 109–118. 30

Thordarson, T. & Self, S. (2003). Atmospheric and environmental effects of the 17831784 laki eruption: A review and reassessment. *Journal of Geophysical Research: Atmospheres*, **108**, AAC 7–1–AAC 7–29. 29, 30

Trenberth, K.E. & Dai, A. (2007). Effects of mount pinatubo volcanic eruption on the hydrological cycle as an analog of geoengineering. *Geophysical Research Letters*, **34**, n/a–n/a. 31, 32, 41

Trigo, R.M., Vaquero, J.M., Alcoforado, M.J., Barriendos, M., Taborda, J., Garca-Herrera, R. & Luterbacher, J. (2009). Iberia in 1816, the year without a summer. *International Journal of Climatology*, **29**, 99–115. 41

Tulet, P. & Villeneuve, N. (2011). Large scale modeling of the transport, chemical transformation and mass budget of the sulfur emitted during the april 2007 eruption of piton de la fournaise. *Atmospheric Chemistry and Physics*, **11**, 4533–4546. 49, 50, 73

Tulet, P., Crassier, V., Solmon, F., Guedalia, D. & Rosset, R. (2003). Description of the mesoscale nonhydrostatic chemistry model and application to a transboundary pollution episode between northern france and southern england. *Journal of Geophysical Research: Atmospheres*, **108**, ACH 5–1–ACH 5–11. 55

Tulet, P., Crassier, V., Cousin, F., Suhre, K. & Rosset, R. (2005). Orilam, a three-moment lognormal aerosol scheme for mesoscale atmospheric model: Online coupling into the meso-nh-c model and validation on the escompte campaign. *Journal of Geophysical Research: Atmospheres*, **110**, n/a–n/a. 55

Tulet, P., Grini, A., Griffin, R.J. & Petitcol, S. (2006). Orilam-soa: A computationally efficient model for predicting secondary organic aerosols in three-dimensional atmospheric models. *Journal of Geophysical Research: Atmospheres*, **111**, n/a–n/a. 55

Tupper, A., Kinoshita, K., Kanagaki, C., Iino, N. & Kamada, Y. (2003). Observations of volcanic cloud heights and ash-atmosphere interactions. 58

Tupper, A., Textor, C., Herzog, M., Graf, H.F. & Richards, M. (2009). Tall clouds from small eruptions: the sensitivity of eruption height and fine ash content to tropospheric instability. *Natural Hazards*, **51**, 375–401. 3, 9, 59, 72

Urai, M. (2004). Sulfur dioxide flux estimation from volcanoes using advanced space-borne thermal emission and reflection radiometer: a case study of miyakejima volcano, japan. *J. Volcanol. Geotherm. Res.*, **1**, 1–13. 47

Valentine, G. (1997). Eruption column physics. 27

Valentine, G.A. & Wohletz, K.H. (1989). Numerical models of plinian eruption columns and pyroclastic flows. *Journal of Geophysical Research: Solid Earth*, **94**, 1867–1887. 53

VANHEIM (2013). (volcanic and atmospheric near- to far-field analysis of plumes helping interpretation and modelling - vanaheim - newsletter. 59

Viane, C., Bhugwant, B., C.and Sieja, Staudacher, T. & Demoly, P. (2009). Etude comparative des emissions de gaz volcanique du piton de la fournaise et des hospitalisations pour asthme de la population reunionnaise de 2005 a 2007. *Revue Franaise d'Allergologie*, **49**, 346 – 351. 3, 9, 73, 118

von Glasow, R. (2010). Atmospheric chemistry in volcanic plumes. *Proc Natl Acad Sci*, **107**, 65946599. 37, 38

von Glasow, R., Bobrowski, N. & Kern, C. (2009). The effects of volcanic eruptions on atmospheric chemistry. *Chemical Geology*, **263**, 131 – 142, halogens in Volcanic Systems and Their Environmental Impacts. 38

Walker, G. (1981). Plinian eruptions and their products. *Bulletin Volcanologique*, **44**, 223–240. 26

Wegmann, M. (2012). *Impacts of explosive volcanic eruptions on large-scale climate variability in model ensemble data for the last 400 years*. Master's thesis, Faculty of Sciences, University of Bern. 35, 38, 39, 40, 41

White, J. & Houghton, B. (2000). *Surtseyan and related phreatomagmatic eruptions, In: H. Sigurdsson, B. Houghton, S. R. McNutt, H. Rymar, and J. Stix (eds), Encyclopedia of volcanoes*. Academic Press, San Diego. 16

Wicander, R. & Monroe, J. (2005). *Essentials of Geology*. Cengage Learning. 18, 20, 21, 22

Wilson, L., Sparks, R.S.J., Huang, T.C. & Watkins, N.D. (1978). The control of volcanic column heights by eruption energetics and dynamics. *Journal of Geophysical Research: Solid Earth*, **83**, 1829–1836. 33, 55

Wilson, L., Sparks, R.S.J. & Walker, G.P.L. (1980). Explosive volcanic eruptions iv. the control of magma properties and conduit geometry on eruption column behaviour. *Geophysical Journal of the Royal Astronomical Society*, **63**, 117–148. 25

Witek, M.L., Teixeira, J. & Matheou, G. (2011). An eddy diffusivitymass flux approach to the vertical transport of turbulent kinetic energy in convective boundary layers. *Journal of the Atmospheric Sciences*, **68**, 2385–2394. 79

Wohletz, K.H., McGetchin, T.R., Sandford, M.T. & Jones, E.M. (1984). Hydrodynamic aspects of caldera-forming eruptions: Numerical models. *Journal of Geophysical Research: Solid Earth*, **89**, 8269–8285. 53

Wolff, E.W. & Mulvaney, R. (1991). Reactions on sulphuric acid aerosol and on polar stratospheric clouds in the antarctic stratosphere. *Geophysical Research Letters*, **18**, 1007–1010. 31

Woods, A. (1988). The fluid dynamics and thermodynamics of eruption columns. *Bulletin of Volcanology*, **50**, 169–193. 27, 28, 55, 81, 90

Wright, S. (1984). Buoyant jets in density-stratified cross flow. *Journal of Hydraulic Engineering*, **110**, 643–656. 100

Yang, K., Krotkov, N.A., Krueger, A.J., Carn, S.A., Bhartia, P. & Levelt, P. (2007). Retrieval of large volcanic so2 columns fromthe aura ozone monitoring instrument: Comparison and limitations. *Journal of Geophysical Research-Atmospheres*, **112**, 24. 47

Yuan, T., Remer, L.A. & Yu, H. (2011). Microphysical, macrophysical and radiative signatures of volcanic aerosols in trade wind cumulus observed by the a-train. *Atmospheric Chemistry and Physics*, **11**, 7119–7132. 41, 58

Zeilinga de Boer, J. & Sanders, D.T. (2004). Volcanoes in human history: The far-reaching effects of major eruptions. 13, 14

Abstract

Piton de la Fournaise a volcano of altitude 2600 m a.s.l is located in Reunion Island in the Indian Ocean. With an average of on eruption every eight months, its amongst one of the world's most active volcano. Volcanic ejecta, a mixture of tephra and gases are known to have considerable impact on the safety of air traffic and on human health. Acidic pollution created by the eruptions can be transported by wind over large distances. Uncertainties in modelling such transport demands continuous improvements in modelling techniques. This study aims to take a first step toward the development of a new volcano emissions alert notification system with a first application on the Piton de La Fournaise volcano.

A critical factor in successfully monitoring and forecasting the dispersion of volcanic ash and gases relies on a correct identification of the height reached by eruption clouds. The objective of this study is to parameterise a volcanic convection in a mesoscale model ($\sim$ 1 km resolution) initialised by heat sources prescribed at the ground. This is achieved by modifying a current shallow convection scheme used in a mesoscale model, Meso−NH. This modified parameterisation is validated by LES simulation considered as a reference. Having fulfilled the primary objective of this study, the modified scheme is tested as a first application in a 3D real−case environment.

Keywords: numerical modelling, parameterisation, convection, volcanic plumes, injection height, sub-grid processes, Piton de la Fournaise

Résumé

Le Piton de la Fournaise est un volcan situé sur l'Ile de la Réunion, dans l'Océan Indien, à 2600 m d'altitude. Avec une éruption tous les huit mois en moyenne, le Piton de la Fournaise est un des volcans les plus actifs du monde. Les débris volcaniques, un mélange de téphra et de gaz sont connus pour avoir un impact considérable sur l'atmosphère et la santé humaine. La pollution acide créée par les éruptions peut être transportée par les vent sur de grandes distances. Les incertitudes dans la modélisation de tels transports exigent des améliorations continues des techniques de modélisation. Cette étude est un premier pas vers le développement d'un nouveau système d'alerte à la pollution par les émissions volcaniques avec une première application sur le Piton de la Fournaise.

Un facteur critique pour le succès de la surveillance et de la prévision de la dispersion des cendres et des gaz volcaniques repose sur une identification correcte de la hauteur atteinte par les nuages éruptifs. L'objectif de cette étude est de paramétriser la convection atmosphérique induite par le volcan dans un modèle mésoéchelle ($\sim$1 km de résolution) initialisé par des sources de chaleur prescrites en surface. Le choix a été fait de modifier un schéma de convection peu profonde utilisé dans le modèle mésoéchelle Méso-NH. Cette paramétrisation est validée par une simulation LES considérée comme une référence. Cet objectif initial atteint, le schéma modifié est testé dans la version tri-dimensionnelle du modèle sur un cas réel.

Mots-clés: modélisation numérique, paramétrisation, convection, panache volcanique, hauteur d'injection, processus sous-maille, Piton de la Fournaise